NASA/CR-1999-209719

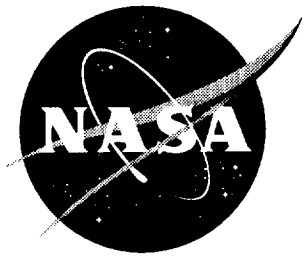

Development of an Empirical Method for Predicting Jet Mixing Noise of Cold Flow Rectangular Jets

James W. Russell
Lockheed Martin Engineering & Sciences, Hampton, Virginia

November 1999

The NASA STI Program Office ... in Profile

Since its founding, NASA has been dedicated to the advancement of aeronautics and space science. The NASA Scientific and Technical Information (STI) Program Office plays a key part in helping NASA maintain this important role.

The NASA STI Program Office is operated by Langley Research Center, the lead center for NASA's scientific and technical information. The NASA STI Program Office provides access to the NASA STI Database, the largest collection of aeronautical and space science STI in the world. The Program Office is also NASA's institutional mechanism for disseminating the results of its research and development activities. These results are published by NASA in the NASA STI Report Series, which includes the following report types:

- TECHNICAL PUBLICATION. Reports of completed research or a major significant phase of research that present the results of NASA programs and include extensive data or theoretical analysis. Includes compilations of significant scientific and technical data and information deemed to be of continuing reference value. NASA counterpart of peer-reviewed formal professional papers, but having less stringent limitations on manuscript length and extent of graphic presentations.

- TECHNICAL MEMORANDUM. Scientific and technical findings that are preliminary or of specialized interest, e.g., quick release reports, working papers, and bibliographies that contain minimal annotation. Does not contain extensive analysis.

- CONTRACTOR REPORT. Scientific and technical findings by NASA-sponsored contractors and grantees.

- CONFERENCE PUBLICATION. Collected papers from scientific and technical conferences, symposia, seminars, or other meetings sponsored or co-sponsored by NASA.

- SPECIAL PUBLICATION. Scientific, technical, or historical information from NASA programs, projects, and missions, often concerned with subjects having substantial public interest.

- TECHNICAL TRANSLATION. English-language translations of foreign scientific and technical material pertinent to NASA's mission.

Specialized services that complement the STI Program Office's diverse offerings include creating custom thesauri, building customized databases, organizing and publishing research results ... even providing videos.

For more information about the NASA STI Program Office, see the following:

- Access the NASA STI Program Home Page at ***http://www.sti.nasa.gov***

- E-mail your question via the Internet to help@sti.nasa.gov

- Fax your question to the NASA STI Help Desk at (301) 621-0134

- Phone the NASA STI Help Desk at (301) 621-0390

- Write to:
  NASA STI Help Desk
  NASA Center for AeroSpace Information
  7121 Standard Drive
  Hanover, MD 21076-1320

NASA/CR-1999-209719

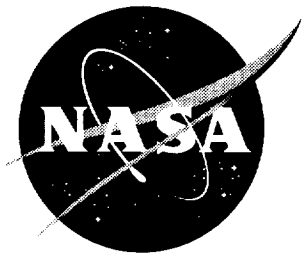

Development of an Empirical Method for Predicting Jet Mixing Noise of Cold Flow Rectangular Jets

James W. Russell
Lockheed Martin Engineering & Sciences, Hampton, Virginia

National Aeronautics and
Space Administration

Langley Research Center
Hampton, Virginia 23681-2199

Prepared for Langley Research Center
under Contract NAS1-96014

November 1999

Available from:

NASA Center for AeroSpace Information (CASI)
7121 Standard Drive
Hanover, MD 21076-1320
(301) 621-0390

National Technical Information Service (NTIS)
5285 Port Royal Road
Springfield, VA 22161-2171
(703) 605-6000

DEVELOPMENT OF AN EMPIRICAL METHOD FOR PREDICTING JET MIXING NOISE OF COLD FLOW RECTANGULAR JETS

James W. Russell
Lockheed Martin Engineering & Sciences
Hampton, Virginia

November 1999

ABSTRACT

This report presents an empirical method for predicting the jet mixing noise levels of cold flow rectangular jets. The report presents a detailed analysis of the methodology used in development of the prediction method. The empirical correlations used are based on narrow band acoustic data for cold flow rectangular model nozzle tests conducted in the NASA Langley Jet Noise Laboratory. There were 20 separate nozzle test operating conditions. For each operating condition 60 Hz bandwidth microphone measurements were made over a frequency range from 0 to 60,000 Hz. Measurements were performed at 16 polar directivity angles ranging from 45 degrees to 157.5 degrees in 7.5 degree increments. At each polar directivity angle, measurements were made at 9 azimuth directivity angles including 0, 15, 30, 45, 60, 75, 90, 180, and 270 degrees. The report shows the methods employed to remove screech tones and shock noise from the data in order to obtain the jet mixing noise component. The data reduction is predicated on the jet mixing noise spectra characteristics being similar to the spectra characteristics of a circular jet.

For each test point, the jet mixing noise was defined in terms of one third octave band spectral content, polar and azimuth directivity, and overall power level. Empirical correlations were performed over the range of test conditions to define each of these jet mixing noise terms as a function of aspect ratio, jet velocity, and polar and azimuth directivity angles. The report presents the method for predicting the overall power level, the average polar directivity, the azimuth directivity, and the location and shape of the spectra for jet mixing noise of cold flow rectangular jets.

It is recommended that this study be extended to include higher temperature rectangular jets and that additional tests be performed to obtain jet mixing noise data for higher temperature rectangular jets.

ACKNOWLEDGEMENTS

This work was performed at NASA Langley Research Center as part of contract NAS1-96014 under the guidance of Mr. Robert A. Golub, Mr. Donald P. Garber, and Mr. John S. Preisser of the Aeroacoustics Branch. The author thanks Dr. John M. Seiner and Mr. Bernard J. Jansen of the Aeroacoustics Branch for their technical expertise and assistance in providing the data. The author also thanks Mr. John W. Rawls of Lockheed Martin Engineering & Sciences for his technical expertise and assistance.

TABLE OF CONTENTS

INTRODUCTION

Current high speed research aircraft concepts may employ rectangular designed exit nozzles. To determine the Effective Perceived Noise Levels associated with jet mixing noise during takeoff and landing operations, it is necessary to know the spectra content of the jet mixing noise of rectangular jets at each polar directivity angle and azimuth directivity angle.

This report presents a method for predicting the jet mixing noise characteristics of cold flow rectangular jets. The rectangular jet mixing noise characteristics consist of defining the overall power levels, the average polar directivity, the azimuth directivity, and then the spectral content. Although this method is applicable to cold flow jets, it demonstrates that a rectangular jet mixing noise method could readily be developed for hot jets.

The method was empirically derived from cold flow rectangular jet model tests performed in the NASA Langley Jet Noise Laboratory. The measured jet noise levels include screech tones and shock noise in addition to the jet mixing noise. Included in this report are the data reduction methods employed to obtain only the jet mixing noise component.

TEST DESCRIPTION

The test description includes a description of the rectangular jet nozzle configurations, the test measurements, and the nozzle operating conditions.

Description of Nozzle Configurations

The width of both the nozzle throat and nozzle exit for all four rectangular nozzles were 4.00 inches. Nozzle 1 has a design exit Mach number of 1.66. The throat height was 2 inches and the exit height was 2.60 inches. Nozzles 3, 4, and 5 have a design exit Mach number of 1.35. For nozzle 3 the throat height was 1.081 inches and the exit height was 1.177 inches. Nozzle 4 has a throat height of 0.690 inches and an exit height of 0.751 inches. Nozzle 5 had a throat height of 0.526 inches and an exit height of 0.573 inches. Thus the exit plane aspect ratios for nozzles 1, 3, 4, and 5 were 1.538, 3.397, 5.324, and 6.985 respectively. Since the nozzles were operated at various exit pressure ratios, both the exit area and the associated aspect ratio of the fully expanded jet varied from the nozzle design values. The computed aspect ratios are predicated on two dimensional expansion, and assume the width of the jet exit flow will be maintained at 4.00 inches even for the under expanded nozzle flow conditions. It should be noted that the walls of these nozzles were not contoured and that the exhaust velocity along the upper and lower surfaces was at an angle and not perpendicular to the nozzle exit plane. Figure 1 shows a sketch of a typical

rectangular nozzle and the dimensions of the nozzles. The nozzle descriptions are taken from the test data report [ref 1].

Figure 1 also shows the polar directivity angles and the azimuth directivity angle. The line connecting the center of the throat plane and the exit plane is the directivity reference line. The azimuth is referenced from the line that bisects the top and bottom walls of the exit plane. At 0 degrees azimuth angle, the 90-degree polar directivity angle point is directly above the center of the nozzle exit area. Similarly, at 90 degrees azimuth angle, the 90-degree polar directivity angle point is on the line that bisects the right and left sides of the exit plane.

Acoustic Test Measurements

For each test, microphone data were taken at a distance of 12 feet from the center of the nozzle exit plane at 16 polar directivity angles ranging from 45 degrees to 157.5 degrees in increments of 7.5 degrees. The polar directivity angles are measured in an arc starting with the nozzle inlet being at 0 degrees, and the nozzle exit being at 180 degrees. The azimuth directivity angles varied from 0 degrees to 90 degrees in 15-degree increments. Also microphones were placed at azimuth directivity angles of 180 degrees and 270 degrees, making a total of 9 azimuth directivity angles. Thus for each test, there were 144 microphone positions.

The microphone data at the 12-foot radius at each azimuth directivity angle and polar directivity angle consisted of 1 Hz average power spectral densities (PSDs) for each 60 Hz frequency bandwidth over the frequency range from 0 to 61,380 Hz. Thus for each test, there were 1024 PSDs at each of the 144 microphone positions. Again the test data report [ref 1] describes the microphone positions and the spectra measurements.

Nozzle Operating Conditions

The nozzles were tested at a range of operating pressure ratios from under expansion, to over expansion. The ratios of the exit pressure of the jet to the free stream ambient pressure, if the flow were allowed to expand to the nozzle exit, were varied from 0.65 to 1.45 and include 0.65, 0.85, 1.0, 1.25, and 1.45. The tests consist entirely of cold flow jet data, where the ratio of the jet total temperature to the ambient temperature was near 1.00.

A test point consists of a particular nozzle and nozzle pressure ratio. There are 20 test points in this study. At each microphone position of each test point there is a corresponding set of flow conditions consisting of total pressure, P_{Tjet}, ambient pressure, P_∞, jet total temperature, T_{Tjet}, ambient temperature, T_∞, and

fully expanded jet flow area, A_J.

From the ambient temperature and the ambient pressure, the ambient speed of sound, C_∞, and the ambient density, ρ_∞ , were computed as follows:

$$C_\infty = (\gamma g R T_\infty)^{0.5} \quad (1)$$

where γ is the ratio of specific heat for air,
R is the gas constant for air
and g is the gravitational constant.

$$\rho_\infty = P_\infty / (g R T_\infty) \quad (2)$$

The jet Mach number is computed from the ratio of the jet total pressure, P_{Tjet} , to the ambient pressure,P_∞ , as follows:

$$M_J = \{ [(P_{Tjet} / P_\infty)^{[(\gamma-1.0)/\gamma]} - 1.0] * 2.0 / (\gamma -1.0) \}^{0.5} \quad (3)$$

The jet static temperature, T_J, is defined from the jet total temperature, T_{Tjet} , and the jet mach number, M_J, as follows:

$$T_J = T_{Tjet} / \{ 1.0 + [(\gamma - 1.0)/2.0] * M_J^2 \} \quad (4)$$

The jet velocity, V_J, and the jet density, ρ_J, are defined from the jet temperature, T_J, and the jet Mach number as follows:

$$V_J = M_J * (\gamma g R T_J)^{0.5} \quad (5)$$

$$\rho_J = P_{Tjet} / (g R T_J) \quad (6)$$

The fully expanded jet exit area, A_J, is computed from the nozzle throat area, A_{th}, and the jet Mach number, M_J , as follows:

$$A_J = A_{th} / M_J * \{ [2.0 + (\gamma - 1.0) * M_J^2] / (\gamma + 1.0) \}^{\{ (\gamma + 1.0) / [2.0* (\gamma - 1.0)] \}} \quad (7)$$

The equivalent circular jet diameter, D_J, is computed from the jet area, A_J, as follows:

$$D_J = (4.0 * A_J / \pi)^{0.5} \quad (8)$$

It should be noted that for each test point, measurements were often performed over a period of time, so that there were variations in the nozzle flow properties associated with each test.. Each of these properties were averaged over the 16 polar directivity angles, θ, associated with each azimuth directivity angle, ϕ, to obtain the average flow properties for each azimuth directivity angle for each test point. These resultant flow properties were again averaged over the 9 azimuth directivity angles to obtain the overall average flow properties for each test point. Table I presents the flow properties at each azimuth directivity angle and the average flow properties for each test point. The flow properties listed in Table I include total temperature, total pressure, ambient pressure, and the ambient temperature. The overall average operating flow conditions at each test point were used for predicting the circular jet noise and the shock noise characteristics for that test point.

REDUCTION OF DATA TO OBTAIN ONE-THIRD OCTAVE BAND JET MIXING NOISE LEVELS

There are several steps involved in converting the measured data to one-third octave band jet mixing noise data. The measured data includes screech tones and shock noise as well as jet mixing noise. The first step is to convert the 1 Hz bandwidth PSDs to 60 Hz bandwidth Sound Pressure Levels (SPLs). The second step is remove the screech tones from the narrow band SPL data. The third step is to convert the 60 Hz bandwidth SPLs to one-third octave band SPLs. The fourth step involves messaging the measured data to remove the shock noise. These steps should provide the jet mixing noise levels at each test point.

Conversion of Measured Data to Sound Pressure Levels

For each test point at each microphone position, the 1 Hz bandwidth PSDs were converted to 60 Hz bandwidth by increasing the PSD value by the 60 Hz bandwidth as follows:

$$SPL(test,\theta,\phi, f) = PSD(test,\theta,\phi,f) + 10.0 * \log_{10}(60) \quad (9)$$

Spectral plots were generated for each of the nozzle test conditions at each frequency, freq, and azimuth directivity angle, ϕ. Figures 2a through 2d show typical spectral plots at azimuth directivity angles of 0 degrees. Each figure contains spectral plots at 16 polar directivity angles ranging from 45 degrees to 157.5 degrees.

Figures 2a and 2b show the narrow band spectral distribution for the fully expanded jet ($P_{Tjet}/P_{\infty} = 1.00$) for nozzle 1 and nozzle 5 respectively. Figure 2c

presents the narrow band spectra distribution for nozzle 4 at a nozzle jet pressure ratio of 0.85. Figure 2d shows the narrow band spectra distribution for nozzle 5 at a nozzle jet pressure ratio of 1.45. Figures 2b through 2d show that there are numerous tones in the narrow band spectra. It is thought that these are screech tones associated with the fact that the flow is supersonic.

Removal of Screech Tones

A review of the narrow band spectral distribution plots of each test point showed that for the five different operating pressure ratios, there were no screech tones associated with the low aspect ratio nozzle, nozzle 1. This was true even at the very high nozzle pressure ratio ($P_{Tjet} / P_{\infty} = 1.45$). Also at the lowest operating pressure ratio ($P_{Tjet} / P_{\infty} = 0.65$), there were no screech tones for any of the four different nozzle configurations. This is probably due to the fact that the fully expanded jet Mach number is very close to 1.0. Table II presents a range in the number of tones associated with each azimuth directivity angle for each test point.

Associated with each azimuth directivity angle are 16 polar directivity angles. A review of Figures 2b through 2d show that as directivity angle is increased, the number and intensity of the screech tones decreases. This is also representative of all the other test points where screech tones exist. Table II shows that for the four highest nozzle operating pressure ratios, as the nozzle number increased and thus the nozzle aspect ratio increased, the number of screech tones increased. Table II also shows that as azimuth directivity angle increased the number of screech tones decreased. The nozzle exit is narrowest at 0 degrees azimuth angle, and the nozzle exit is widest at the 90 degrees azimuth angle. If these nozzles were truly two- dimensional, the number of screech tones at each azimuth angle should have very little variance.

In order to obtain the jet mixing noise, it was necessary to remove the screech tones. A program was developed to search out and remove the screech tones. This was accomplished by dividing the data at each microphone position into groups of 10 narrow band SPL values and then fitting a quadratic curve to each group. The quadratic curve points were then compared with the data and a standard deviation was computed. If the standard deviation of the curve fit was less than 0.60 dB, then it was assumed that there was no screech tone in that group. However if the standard deviation was greater than 0.60 dB, then a search was performed on both that group of 10 SPLs and the next group of 10 SPLs to find the peak screech tone SPL and the associated frequency. Thus the search covered 20 SPLs of 60 Hz bandwidth or a total bandwidth of 1200 Hz. Once the peak frequency was determined, a quadratic curve was fit through 10 SPL values on each side of the peak. However, the peak SPL and four adjacent

SPL values on each side of the peak were eliminated from the quadratic fit. This allowed the peak to be replaced with a smooth curve fit. The eliminated SPL values were replaced by SPL values obtained from the quadratic curve fit using the associated frequency of the eliminated points. Figures 3a through 3d show the smoothed narrow band data for the same test points at 0° azimuth angle that are presented in Figures 2a through 2d.

Conversion to One-Third Octave Band Data

The 1024 smoothed 60 Hz bandwidth SPLs were fit into thirty-four (34) one-third octave bands (OTOB) with the center band frequencies ranging from 31.5 Hz to 50,000 Hz. This was done by converting the 60 Hz bandwidth SPLs to mean square pressures, and then proportioning the mean square pressure value by the ratio of the frequency range that was applicable to a particular OTOB frequency range. These mean square pressure values were then summed over the OTOB frequency range, and the summed mean square pressure was converted to an OTOB SPL value. In addition to converting the data to OTOB SPLs, the data were corrected to obtain lossless data by removing atmospheric attenuation effects. The atmospheric attenuation was computed in accordance with the ANSI method [ref 2].

To account for the different test point flow conditions, the OTOB center band frequencies were converted to Strouhal Number, ST, which is defined from the OTOB center band frequency, f, the fully expanded equivalent circular jet diameter, D_J, and the fully expanded jet velocity, V_J, as follows:

$$ST = f * D_J / V_J \qquad (10)$$

To plot the data in equal OTOB intervals, the logarithm of the Strouhal Number, logST, was used as the X-axis. Figures 4a through 4e show the OTOB SPLs over logST range from −1.5 to +1.0 for five selected test points at 0° azimuth directivity angle. Figures 4a and 4b each show 16 spectral plots for the 16 directivity angles for nozzle 3 at nozzle exit pressure ratios of 0.65 and 0.85 respectively. Figure 4c and 4d shows the 16 spectral plots for nozzle 4 operating at nozzle exit pressure ratios of 1.00 and 1.45 respectively. Figure 4e shows the 16 spectral plots for nozzle 1 operating at a nozzle exit pressure ratio of 1.25.

Also shown on Figures 4a through 4e are the SAE predicted jet noise levels [ref 3] and the combination of the SAE predicted jet noise level and Tam predicted shock noise level for rectangular jets [ref 4]. For each test point, the average flow properties from Table I were used to predict the SAE circular jet noise and the Tam shock noise. The SAE method is for circular jets and therefore does not vary with azimuth directivity angle. However, the Tam shock noise for rectangular jets does vary with azimuth directivity angle.

A review of Figure 4a shows that the contribution of shock noise is minimal. This is because the jet exit flow Mach number is 1.015, which is near sonic flow. Since the exit area of the nozzle is larger than the fully expanded jet and the shock is very weak, the shock noise will probably not exist beyond the nozzle walls. Figure 4b shows that for nozzle 3 operating at a nozzle pressure ratio of 0.85, there is evidence of shock noise. This can be seen by the sharp rise in the SPL levels at a logST value near 0.0 at polar directivity angles below 120 degrees. Figures 4c through 4e also show a significant increase in the SPL values at logST values near 0.0 for polar directivity angles below 120 degrees. These sharp increases in the SPL levels are very near the Tam predicted shock noise levels [ref 4]. Also the data in Figures 4a through 4e show that at the higher polar directivity angles, the spectral shape of the measured data is similar to the spectral shape of the SAE predicted circular jet noise [ref 3].

It should be noted that the Strouhal number is based on the equivalent circular jet diameter, rather than the hydraulic diameter of the rectangular nozzle. This is because the peak frequencies of the derived jet noise data are close to the peak frequencies of the SAE circular jet noise predictions. If the hydraulic diameter were to be used for the measured jet noise, the Strouhal Number would be significantly reduced and the data would not be in as good agreement with SAE predicted jet noise levels.

Removal of Shock Noise

To remove the shock noise component from the data, the measured spectral shape at each test point and each azimuth directivity angle and polar directivity angle was individually evaluated to determine what portion of the spectral shape was solely jet mixing noise. Both low frequency and high frequency measured jet noise data were edited. The high frequency data of each particular case was evaluated, and the portion of the spectra not attributed to jet mixing noise was removed and replaced with the profile of the SAE circular jet prediction. In many cases, the actual measured data was used as representative of the jet mixing noise. Figures 5a through 5e show the measured spectra, the predicted SAE circular jet spectra, and the data fit that was used to represent the measured jet mixing noise component for the same test points and azimuth directivity angles as the data presented in Figures 4a through 4e.

Figures 5a through 5e show for the X axis, the logST values range from –2.0 to +1.0, whereas Figures 4a through 4e showed the logST values range from –1.5 to +1.0. Figures 5a through 5e show that at the very low frequencies the measured SPL levels decrease as the logST value increases from –2.0 to –1.8 at all directivity angles. These measurements are not representative of the jet mixing noise component, and therefore were not included as part of the jet

mixing noise. Thus, at the low frequency end of the spectra, these removed measured data points were replaced by extrapolated values that were derived by fitting a straight line through the low frequency measured jet noise data. Figures 5a through 5e show the dashed line at the low end of the spectra for all the polar directivity angles. These dashed lines represent the low frequency jet mixing noise levels associated with the measured data.

Figure 5a shows that at the high frequency end of the spectra, the measured data were used, since there was not an abrupt shift in the data. Figures 5b through 5d show that at the low polar directivity angles, there is a shift in the spectra and that the high frequency jet mixing noise was estimated by using a shifted SAE predicted curve that is represented by the dashed line on the figures. At the high polar directivity angles, Figures 5b through 5e show that the measured data spreads out, which may be attributed to shock noise. Therefore, the SAE predicted profile was shifted to pass through the high frequency data prior to spreading out. The dashed lines shown in figures 5a through 5e represent the jet mixing noise that was used in the analyses.

The measured data presented in Figures 4a through 4e and 5a through 5e are reasonably smooth and the separation of the jet mixing noise from the shock noise is not unreasonably difficult. However there are other test points where the separation of the jet mixing noise from the shock noise is not very well defined. Figures 6a through 6d show measured test data for four different test points at 0° azimuth directivity angle. Figures 6a and 6b show the data for a nozzle pressure ratio of 0.85 for nozzle 4 and nozzle 5 respectively. Figures 6c and 6d show the data for a nozzle pressure ratio of 1.25 for nozzle 4 and nozzle 5 respectively. Also shown on these figures are the predicted SAE circular jet noise levels and the combined SAE jet noise and Tam rectangular shock noise prediction. These figures show that the scatter of the measured data over the frequency range, makes it very difficult to separate the jet mixing noise component from the shock noise. This is true at both the high polar directivity angles and the low polar directivity angles. Therefore considerable engineering judgment went into defining the jet mixing noise characteristics of these particular data points.

Figures 7a through 7d show the estimated jet mixing noise levels used in the analyses for the same four test points of Figures 6a through 6d. Also shown on Figures 7a through 7d are the predicted SAE circular jet noise levels. As previously stated the shape of the SAE predicted jet noise levels at the high frequency end were used to define the high frequency jet mixing noise levels. There is probably considerable discrepancy between the actual jet mixing noise levels of these four test points and the estimated jet noise levels used in the analyses.

The jet noise profiles employed in this study are modeled after the predicted SAE jet noise [ref 3] profiles. It should be pointed out that Tam, Golebiowski, and Seiner [ref 5] found that the jet noise spectrum was made up of two independent noise components; the large turbulent/instability waves and the fine-scale turbulent noise. The large turbulence/instability wave noise has a relatively sharp peak, whereas the fine-scale turbulent noise component has a very broad peak and rolls off gradually. Thus, to obtain the jet noise component, overlaying the two jet noise components of Tam, et al [ref 5] would probably be more representative than the SAE prediction method profile [ref 3].

The other significant item presented by Tam [ref 5] is that under certain jet operating conditions, the screech tones of an imperfectly expanded jet can be very intense. When this happens, the jet flow is drastically changed and the turbulence level is greatly increased. This results in broadband amplification of fine-scale turbulence noise. This amplification could easily result from the screech tones associated with several of the test points including those presented in Figures 2b through 2d.

ANALYSIS OF JET MIXING NOISE

The jet mixing noise analysis involves deriving the overall power level and the polar directivities, the azimuth directivities, and the spectra content for each test point. To obtain the polar directivities, for each test point at each azimuth directivity angle and each polar directivity angle, the derived jet mixing noise spectra were adjusted such that the summation of the spectra over all the frequencies was equal to 1.0. The overall sound pressure levels at each azimuth directivity angle and each polar directivity angle were adjusted to compensate for the corrections to the spectra. These corrected overall sound pressure levels were then employed to obtain the overall power level and the associated directivities.

Adjustment of Spectral Distribution

At each azimuth directivity angle and each polar directivity angle at each frequency, there is a measured spectral distribution factor, F_m, that is computed as the difference between the measured overall sound pressure level, $OASPL_m$, and the measured one-third octave band jet noise sound pressure level, SPL_m.

$$F_m(f,\theta,\phi) = SPL_m(f,\theta,\phi) - OASPL_m(\theta,\phi) \qquad (11)$$

For each azimuth angle, these spectral distributions at each one-third octave center band frequency were smoothed over the range of directivity angles using

second order polynomial least squares fits. The second order polynomial equations were then used to obtain a revised spectral distribution function,

$F_R (f,\theta,\phi)$, for each frequency at directivity angles ranging from 60 degrees to 160 degrees in 10 degree increments.

For each aspect ratio nozzle, a jet velocity was defined as that velocity that corresponds to a Strouhal Number of 0.01 and a frequency of 50 Hz and the equivalent jet diameter of the particular nozzle. The arbitrary jet velocity was defined as follows:

$$V_{Jnew} = 50 * D_{jet} * 0.01 \qquad (12)$$

This new jet velocity was then used to define the Strouhal Numbers that correspond to the 29 one-third octave center band frequencies ranging from 50 Hz to 31,500 Hz. An interpolation was performed on the logST values to define a revised spectral distribution function, $F_R (f, \theta,\phi)$ at each of the specified frequencies. The revised spectral distribution functions were then summed over the 29 frequencies at each polar directivity angle for each azimuth directivity angle to obtain a spectral summation, $F_{sum}(\theta,\phi)$.

$$F_{sum}(\theta,\phi) = \sum_{f} 10.0^{[F_R (f,\theta,\phi) / 10.0]} \qquad (13)$$

For any prediction method, the spectral summation must be equal to unity. However, the spectral summations of the measured data for the 11 polar directivity angles and 9 azimuth directivity angles of the 20 test points ranged from 0.825 to 1.356. Typically, however the summations ranged between 0.90 and 1.10. Table III shows the spectral summations for the same 4 test points that were presented in Figures 2a through 2d at each azimuth directivity angle and each polar directivity angle. Table III shows that at the polar directivity angle of 160 degrees there is a larger spread in the summations. This is because the measured data was extrapolated from the polar directivity angle of 157.5 degrees.

The spectral distribution values for each frequency were corrected by the reciprocal of the spectral summation value corresponding to the polar directivity angle and azimuth directivity angle as follows:

$$F_{new} (f,\theta,\phi) = F_R (f, \theta,\phi) - 10.0 * \log_{10} [F_{sum}(\theta,\phi)] \qquad (14)$$

To compensate for the changes in the spectral distribution values, the F_{sum} values were applied to the particular overall sound pressure level value, $OASPL(\theta,\phi)$, in accordance with equation 8 below. Thus, the sum of the directivity value and spectral distribution factor at a particular frequency and polar directivity angle result in the same total as the uncorrected sum of the directivity and spectral distribution factor.

Computation of Overall Sound Pressure Levels

The measured overall sound pressure level, $OASPL_m(\theta,\phi)$, at each of the 16 polar directivity angles and nine azimuth directivity angles was obtained by summing the derived measured jet noise spectra, $SPL_m(f,\theta,\phi)$ over the frequency range.

$$OASPL_m(\theta,\phi) = \sum_f SPL_m(f,\theta,\phi) \qquad (15)$$

At each azimuth directivity angle, ϕ, the $OASPL_m(\theta,\phi)$ values were curve fit in terms of polar directivity angle using a second order polynomial in a least squares sense to obtain smoothed OASPL values. The second order polynomials were then used to obtain revised measured overall sound pressure levels, $OASPL_R(\theta,\phi)$, at directivity angles ranging from 60 degrees to 160 degrees at each azimuth directivity angle. Table IV lists the $OASPL_R(\theta,\phi)$ values as a function of polar directivity angle and azimuth directivity angle for each of the four test points presented in Figures 2a through 2d.

As previously stated, the $OASPL_R(\theta,\phi)$ values were adjusted by the changes in the summation of the spectral distribution factors at each polar directivity angle at each azimuth directivity angle to obtain corrected overall sound pressure levels, $OASPL_c(\theta,\phi)$.

$$OASPL_c(\theta,\phi) = OASPL_R(\theta,\phi) + 10.0 * \log_{10}[F_{sum}(\theta,\phi)] \qquad (16)$$

Table V lists the $OASPL_c(\theta,\phi)$ values as a function of polar directivity angle and azimuth directivity angle for each of the four test points presented in Figures 2a through 2d.

Computation of Overall Power Levels

The next step in the process is the computation of the overall power level, OAPWL. The overall power level is the integration of the intensity level over the surface area of the sphere. Since the measured data only exists at directivity angles between 60 degrees and 160 degrees, an overall power level was computed for only that portion of the sphere. The measured overall power level was computed from the intensity levels associated with the measured overall sound pressure levels, $OASPL_m(\theta,\phi)$, and the associated areas. The measured intensity level, IL_m, is computed from the overall sound pressure level as follows:

$$IL_m(\theta,\phi) = p_{ref}^2 / (2 * \rho_\infty * C_\infty) * 10.0^{[OASPL_m(\theta,\phi) / 10.0]} \quad (17)$$

For a sphere of radius r, the area associated with a particular polar directivity angle, θ_J, and azimuth directivity angle, ϕ_I, is defined by:

$$A(\theta_J,\phi_I) = 4r^2 * [(\phi_{I+1} - \phi_{I-1})/2] * [\cos ((\theta_J + \theta_{J-1}) /2) - \cos ((\theta_J + \theta_{J+1}) /2)] \quad (18)$$

The measured overall power level, $OAPWL_m$, is then computed from the sum of the products of the intensity levels and the areas as follows:

$$OAPWL_m = \sum_{\phi} \sum_{\theta} IL_m(\theta_J,\phi_I) * A(\theta_J,\phi_I) \quad (19)$$

The overall power level in decibels, $OAPWL_{dB}$, is defined from the OAPWL and the reference power level, $OAPWL_{ref}$, as follows:

$$OAPWL_{dB} = 10.0 * \log_{10} [OAPWL_m / OAPWL_{ref}] \quad (20)$$

In addition to the $OAPWL_m$, the corrected overall power level, $OAPWL_c$, was computed using the $OASPL_c(\theta,\phi)$ values. Also a predicted overall power level, $OAPWL_p$, was computed for the same range of polar and azimuth directivity angles using predicted overall sound pressure levels from the SAE circular jet prediction method [ref 3]. All these OAPWLs are based on that portion of the sphere for polar directivity angles ranging from 60° to 160°. Table VI lists these OAPWL values for the 20 test points corresponding to the five operating pressure ratios for each of the four rectangular nozzles.

The SAE prediction method was used to predict OASPLs over the range of directivity angles from 0° to 180°. These OASPLs were then used to predict an overall power level, $OAPWL_{ptot}$, over the entire twelve (12) foot radius spherical area rather than the spherical area between 60° and 160. The $OAPWL_{ptot}$ values are presented in Table VI and are greater than the $OAPWL_p$ values for the partial sphere.. Table VI presents the difference between the predicted partial sphere and predicted total sphere values of OAPWL for each of the 20 test points.

These differences in predicted OAPWLs between the partial sphere and total sphere were applied to the corrected measured data to obtain corrected total overall power levels, $OAPWL_{ctot}$, for the total sphere in accordance with equation 13 as follows:

$$OAPWL_{ctot} = OAPWL_c + (OAPWL_{ptot} - OAPWL_p) \quad (21)$$

These values are also presented in Table VI for each of the 20 test points.

The spherical surface area for the range of polar directivity angles, θ_1 and θ_2, is computed as follows:

$$A_s = 2 \pi r^2 * [\cos(\theta_1) - \cos(\theta_2)] \quad (22)$$

Associated with each of the OAPWL values is an average overall sound pressure level, $OASPL_{avg}$, that is computed from the ambient conditions and the spherical surface area, A_s, as follows:

$$OASPL_{avg} = 10.0 * \log_{10} [OAPWL * (2 * \rho_\infty * C_\infty) / (A_s * p_{ref}^2)] \quad (23)$$

Also presented in Table VI are the associated average overall sound pressure levels, $OASPL_{ctot}$, corresponding to the corrected overall power level, $OAPWL_{ctot}$.

The SAE predicted overall power level of the circular jet, $OAPWL_{circ\ jet}$, is defined in reference 3 as a function of the ratio of the jet density to the ambient density, (ρ_J*), the ratio of the jet velocity to the ambient speed of sound, (V_J*), and the ambient density, (ρ_∞), the ambient speed of sound, (C_∞), and the jet exit area, (A_J) as follows:

$$OAPWL_{circ\ jet} = 6.67*10^{-5} * (\rho_J^*)^\omega * (V_J^*)^8 * P(V_J^*) * \rho_\infty C_\infty^3 * A_J \quad (24)$$

where the parameters ω and P (V_J^*) are tabulated as functions of V_J^* in the SAE circular jet prediction method [ref 3].

The OAPWL values for the whole sphere obtained from the OAPWL equation from the SAE prediction method [ref 3] are 2 to 3 dB greater than the OAPWL values computed from the product of the predicted intensity levels and areas in accordance with equations 19 and 20 above. Table VI shows the SAE predicted overall power level values using equation 24. Also shown are the differences between these $OAPWL_{circ\ jet}$ values and the total corrected overall power levels for the rectangular jets, $OAPWL_{ctot}$. This difference is defined as ΔOAPWL.

DEVELOPMENT OF PREDICTION METHOD

The development of the prediction method consists of the same approach as the SAE method for circular jets [ref 3]. That is correlations are made for the overall power level first, then for the polar directivity angle, then the azimuth directivity angle, and lastly the spectra distribution. The correlations were obtained by using the particular parameter such as frequency, f, azimuth directivity angle,θ, and polar directivity angle,ϕ, where applicable. In addition two other parameters were used, the nozzle exit fully expanded aspect ratio, AR, and the normalized jet velocity, V_J^*. The coefficients for the pertinent parameters used in each of the correlations were obtained using Data Desk statistical software program [ref 6].

Correlation of Overall Power Level

The measured difference in overall power level, $\Delta OAPWL_m$, between the overall power level of the circular jet, $OAPWL_{circ\ jet}$, and the corrected overall power level of the rectangular jet, $OAPWL_{ctot}$, was thought to be a function of both aspect ratio, AR, and the logarithm of the normalized jet velocity, $\log_{10}(V_J^*)$, where V_J^* is the ratio of the jet velocity, V_J, to the ambient speed of sound, C_∞. The correlation was performed using a constant term, an AR term, an AR^2 term, a $\log_{10}(V_J^*)$, a $[\log_{10}(V_J^*)]^2$, and the cross products of these terms as follows:

$$\Delta OAPWL_m = \text{function (AR, AR2, } \log_{10}(V_J^*),\ [\log_{10}(V_J^*)]^2) + \text{constant} \qquad (25)$$

The resultant statistical correlation performed with Data Desk [ref 6] showed that the jet velocity had very little effect on the $\Delta OAPWL_m$. For the twenty test points,

the least squares fit for the predicted difference in overall power level, $\Delta OAPWL_p$ is defined as follows:

$$\Delta OAPWL_p = 4.8902 + AR * (0.1025*AR - 1.4020) \quad (26)$$

Table VII also shows for each of the 20 test points, the nozzle number, the pressure ratio, the aspect ratio, the velocity term, the measured ΔOAPWL value, $\Delta OAPWL_m$, the predicted ΔOAPWL value, $\Delta OAPWL_p$, from equation 26, and the difference between the two values. Table VII shows that the test point corresponding to nozzle 5 at a pressure ratio of 0.85 had a very large discrepancy between the measured ΔOAPWL value and the predicted ΔOAPWL value. This is one of the cases presented in the section on shock removal, that was difficult to ascertain where shock noise existed and where jet noise existed. It was decided to rerun the correlation using the other 19 test points. For the 19 test points the least squares fit of the difference in overall power level is defined as follows:

$$\Delta OAPWL_p = 5.7716 + AR * (0.20156*AR - 2.0699) \quad (27)$$

The result of this fit is presented in Table VIII. The standard deviation of 1.10 dB for the fit presented in Table VIII is considerably less than the standard deviation of 1.44 dB presented in Table VII. Figure 8 shows the plot of the ΔOAPWL against aspect ratio along with the least square fits of the data for both the 20 test point cases and the 19 test point cases.

The OAPWL for the rectangular jet is as follows:

$$OAPWL_{rect\ jet} = OAPWL_{circ\ jet} + 0.20156 * AR^2 - 2.0699 * AR + 5.7716 \quad (28)$$

Computation of Directivities

The directivity function, $D(\theta,\phi)$, is defined from the difference between the average overall sound pressure level over the total spherical area, $OASPL_{avg}$, and the overall sound pressure level at a particular polar directivity angle and azimuth directivity angle, $OASPL(\theta,\phi)$.

$$D(\theta,\phi) = OASPL(\theta,\phi) - OASPL_{avg} \quad (29)$$

For this study, the directivity function was divided into an average polar directivity function, $D(\theta)_{avg}$, and then applying an azimuth directivity correction, $D(\theta,\phi)_c$, to

it. Note that the azimuth directivity correction varies with polar directivity angle. Thus the directivity is defined as follows:

$$D(\theta,\phi) = D(\theta)_{avg} + D(\theta,\phi)_c \tag{30}$$

For each test point, the average overall sound pressure level at each polar directivity angle, $OASPL(\theta)_{avg}$, was obtained by averaging the corrected $OASPL_c(\theta,\phi)$ over the range of azimuth angles at each polar directivity angle as follows:

$$OASPL(\theta)_{avg} = [\,\Sigma\, OASPL_c(\theta,\phi)\,] / 7 \tag{31}$$

There are 7 azimuth angles, 0, 15, 30, 45, 60, 75, and 90 degrees. The $OASPL_c(\theta,0)$ is an average of the $OASPL_c(\theta,0)$ and $OASPL_c(\theta,180)$. Similarily, the $OASPL_c(\theta,90)$ is an average of the $OASPL_c(\theta,90)$ and the $OASPL_c(\theta,270)$. The $D(\theta)_{avg}$ term is then defined from the average corrected $OASPL_{avg}$ of the total sphere and the $OASPL(\theta)_{avg}$ as follows:

$$D(\theta)_{avg} = OASPL_{avg} - OASPL(\theta)_{avg} \tag{32}$$

Similarly, the azimuth directivity correction is determined from the average polar overall sound pressure level, $OASPL(\theta)_{avg}$,and the overall sound pressure level at a particular polar directivity angle and azimuth directivity angle, $OASPL_c(\theta,\phi)$ as follows:

$$D(\theta,\phi)_c = OASPL(\theta)_{avg} - OASPL_c(\theta,\phi) \tag{33}$$

Table VI lists the values of $OASPL_{avg}$ for all 20 test points, and Table V lists the values of $OASPL_c(\theta,\phi)$ for the same four test points as shown in Table II. Table IX lists the average polar directivities, $D(\theta)_{avg}$, and the azimuth directivity corrections, $D(\theta,\phi)_c$, for the same four test points that were presented in Table II. At each directivity angle over the range from 60 degrees to 160 degrees, the average polar directivity was evaluated for those 19 test points of Table VIII that were used for curve fitting the overall power levels.

Correlation of Average Polar Directivity

The average polar directivities, $D(\theta)_{avg}$, were correlated against the aspect ratio, AR, the log of the normalized jet velocity, $\log_{10}(V_J^*)$, and the polar directivity angle, θ, as well as the square of these terms and the cross products of all these terms and their squares. The least squares fit of all these terms was made against polar directivity angles ranging from 60 degrees to 160 degrees using the Data Desk program [ref 6]. The polar directivity equation was defined as follows:

$$D(\theta)_{avg} = \text{function } \{\theta, \theta^2, AR, AR^2, , \log_{10}(V_J^*), [\log_{10}(V_J^*)]^2\} + C \qquad (34)$$

The initial least squares fit for the range of directivity angles from 60 degrees to 160 degrees resulted in a standard deviation that was significantly greater than 1.0 dB. Therefore, the directivity fit was divided into two parts. A least squares fit was performed over the range of polar directivity angles from 60 degrees to 150 degrees. This least squares fit was applied to polar directivity angles from 60 degrees to 140 degrees and is written as follows:

$$D(\theta)_1 = -11.89 + AR^*(1.089 - 0.0646^*AR) + \theta^{2*}(2.325 - 0.009022 * AR^2) \qquad (35)$$

where AR is the aspect ratio of rectangular jet and θ is the polar directivity angle in radians as measured from the jet inlet. It should be noted that the jet velocity term, $\log_{10}(V_J^*)$, was not a significant contributor to the polar directivity for directivity angles between 60 degrees and 140 degrees. The standard deviation for the polar directivity of equation 35 is 1.00 dB.

A second least squares fit was applied to polar directivity angles from 150 degrees to 160 degrees. This least squares fit is as follows:

$$D(\theta)_2 = -19.13 + AR^* \{3.315^*\theta - 49.60 * [\log_{10}(V_J^*)]^2\} + \theta^{2*} \{4.000 - 1.513^* \log_{10}(V_J^*) + AR^* \{0.0107 - 1.407^*AR)\} \qquad (36)$$

where AR is the aspect ratio of rectangular jet, θ is the polar directivity angle in radians as measured from the jet inlet, and V_J^* is the normalized fully expanded jet velocity as referenced to the ambient speed of sound. The standard deviation of the polar directivity obtained with equation 36 is 1.17 dB. For polar directivity angles between 140 degrees and 150 degrees, the polar directivity is obtained by interpolation between equation 35 and equation 36 as follows.

$$D(\theta)_3 = D(\theta)_1 + [D(\theta)_2 - D(\theta)_1] * (\theta * 180 / \pi - 140°) / 10.0 \qquad (37)$$

The average overall OASPL at a particular directivity angle is obtained by applying the directivity correction to the average OASPL values obtained from the overall power level. Thus equation 32 can be rewritten as follows:

$$OASPL(\theta)_{avg} = OASPL_{avg} + D(\theta) \quad (38)$$

The overall sound pressure level at a particular polar directivity angle and azimuth directivity angle also depends on the azimuth directivity.

Correlation of Azimuth Directivities

The azimuth directivity, $D(\phi)$, was correlated against a corrected azimuth angle, ϕ_c, the polar directivity angle, θ, the aspect ratio, AR, and the logarithm of the normalized jet velocity, $\log_{10}(V_J^*)$, and the squares of all these parameters as follows:

$$D(\phi) = \text{function } \{\phi_c, \phi_c^2, \theta, \theta^2, AR, AR^2, \log_{10}(V_J^*), [\log_{10}(V_J^*)]^2\} \quad (39)$$

Where the corrected azimuth angle, ϕ_c, is the difference between the azimuth angle as measured from the center of the nozzle exit as shown in Figure 1, and the azimuth angle of the corner, ϕ_{corn}, where ϕ_{corn} is derived from the aspect ratio. The equations for the corrected azimuth angle and the corner azimuth angle are as follows:

$$\phi_c = \phi - \phi_{corn} \quad (40)$$

$$\phi_{corn} = \arctan (1 / AR) \quad (41)$$

As in the case of the polar directivity, the azimuth directivity was correlated against all these terms and the cross products of these terms using Data Desk program [ref 6]. As in the case of the polar directivity, the azimuth directivity correlation was made for two different ranges of polar directivity angles. The first azimuth directivity, $D(\phi)_1$, is applicable to polar directivity angles from 60 degrees to 140 degrees, and is defined as follows:

$$D(\phi)_1 = \phi_c^* \{2.352 - \theta * (3.397 - 1.084*\theta) - \phi_c * (1.507 - 0.7904*\theta - 0.0490*AR)\} + AR * [0.3955 - \theta * (0.4559 - 0.1163*\theta)] \quad (42)$$

It should be noted that like the polar directivity, the azimuth directivity for polar directivity angles from 60 degrees to 140 degrees is not dependent on the jet velocity. The standard deviation in azimuth directivity for polar directivity angles from 60 degrees to 140 degrees is 0.21 dB.

For polar directivity angles between 150 and 160 degrees the azimuth directivity is defined from the corrected azimuth directivity angle, the polar directivity angle, the aspect ratio, and the fully expanded jet velocity as follows:

$$D(\phi)_2 = \phi_c^* \{3.624^*\theta - 8.493 - 0.3159^*AR - \phi_c^* (0.3169^*AR + 0.9787^*\phi_c) \} + AR^*(0.3893^*\theta - 1.028) + \log_{10}(V_J^*) * (8.478 + 14.62^*\phi_c) + [\log_{10}(V_J^*)]^2 * (10.85 * AR - 51.73) \quad (43)$$

At polar directivity angles between 150 degrees and 160 degrees, the jet velocity term is included in equation 43. The standard deviation is 0.44 dB for the azimuth directivity at polar directivity angles from 150 degrees to 160 degrees.

For polar directivity angles between 140 degrees and 150 degrees, the azimuth directivity is obtained by interpolation between method 1 and method 2 as follows.

$$D(\phi) = D(\phi)_1 + [D(\phi)_2 - D(\phi)_1] * (\theta - 140°) / 10.0 \quad (44)$$

At a particular directivity angle, θ, and azimuth angle, ϕ, he overall sound pressure level, OASPL(θ,ϕ), is obtained by correcting the average sound pressure level associated with the overall power level, $OASPL_{avg}$, for the polar directivity term, $D(\theta)$, and the azimuth directivity term, $D(\phi)$, as follows:

$$OASPL(\theta,\phi) = OASPL_{avg} + D(\theta) + D(\phi) \quad (45)$$

The jet mixing noise at a particular directivity angle, azimuth angle, and frequency is computed by applying a spectral term to the overall sound pressure level term.

Correlation of Spectra Function

The spectral distribution consists of defining the frequency in terms of Strouhal Number, St_{peak}, and magnitude of the spectral peak relative to the overall sound pressure level, ΔSPL_{peak}, at each polar directivity angle and azimuth directivity angle. The spectral shape relative to the spectral peak is then defined by dividing

the spectra into four segments. Figure 9 shows the various segments used to define the spectral shape.

The location of the peak frequency is defined in terms of the logarithm of the peak Strouhal Number, $\log_{10}(St_{peak})$. The location and magnitude of the spectral peaks were defined at each polar directivity angle and azimuth directivity angle for each of the 20 test points. This data was then correlated against azimuth directivity angle, ϕ_c , the polar directivity angle, θ ,the aspect ratio, AR, and the normalized jet velocity, $\log_{10}(V_J^*)$ and the squares of these parameters using the Data Desk software package [ref 6] to obtain correlations. Unlike the directivity correlations, the spectra correlations were defined using one equation over the range of polar directivity angles from 60 degrees to 160 degrees.

The location of the peak Strouhal number, $\log_{10}(St_{peak})$, is defined as a function of the corrected azimuth directivity angle, ϕ_c , the polar directivity angle, θ ,the aspect ratio, AR, and the normalized jet velocity, $\log_{10}(V_J^*)$, as follows:

$$\log_{10}(St_{peak}) = -0.9383 + 0.0217 * \phi_c + \theta * (1.437 - 0.4761*\theta) - 0.0129 * AR - \log_{10}(V_J^*) * [2.195 - 10.13 * \log_{10}(V_J^*)] \quad (46)$$

The magnitude of the peak sound pressure level relative to the overall sound pressure level, ΔSPL_{peak} , relative to the overall sound pressure level at a particular directivity angle and azimuth angle is defined as follows:

$$\Delta SPL_{peak} = 5.034 + \theta * (6.988 - 2.190*\theta) + AR * (0.3014 - 0.0405*AR) - \log_{10}(V_J^*) * [5.425 - 64.47 * \log_{10}(V_J^*)] \quad (47)$$

Equation 47 shows that the relative peak SPL value, ΔSPL_{peak}, is independent of azimuth angle, ϕ. For a particular test point at a particular polar directivity angle and azimuth directivity angle, the peak SPL value, $SPL_{peak}(\theta, \phi)$ is defined from the overall sound pressure level, $OASPL(\theta, \phi)$, and the relative peak sound pressure level, ΔSPL_{peak}, as follows:

$$SPL_{peak}(\theta, \phi) = , OASPL(\theta, \phi) - \Delta SPL_{peak} \quad (48)$$

Once the peak is located the shape of the spectral distribution about the peak can be ascertained. The spectral shape was divided into four segments as shown in Figure 9. Two segments for frequencies that are less than the peak frequency, and two segments for frequencies that are greater than the peak frequency. The first segment is a circular segment that ranges from the spectral peak to four one-third octave bands below the spectral peak as shown on Figure 9. The radius of this arc is defined by performing a least squares fit using the Data Desk program [ref 6] of the spectra data for each of the azimuth angles and directivity angles for each of the 20 test points. The results of the fit show that the radius of the curve, C, is defined as follows:

$$C = 55.93 - \theta * (58.91 - 20.25*\theta) - AR * (5.039 - 0.8248*AR) + \log_{10}(V_J^*) * [179.5 - 1511.0 * \log_{10}(V_J^*)] \quad (49)$$

Equation 49 shows that the radius of curvature is not affected by the azimuth angle,ϕ. For logarithm of the Strouhal number, $\log_{10}(St)$, ranging from $[\log_{10}(St_{peak}) - 0.4]$ to $\log_{10}(St_{peak})$ the SPL value is defined as follows:

$$SPL(St,\theta,\phi) = SPL_{peak}(\theta,\phi) - C * [\log_{10}(St) - \log_{10}(St_{peak})]^2 \quad (50)$$

The second segment is for frequencies corresponding to Strouhal numbers that have logarithms less than $[\log_{10}(St_{peak}) - 0.4]$. The spectral shape is defined by a straight line that has a slope,E, and an intercept, F. Like the radius of curvature, C, the E and F parameters shown on Figure 9 are functions of the corrected azimuth angle, ϕ_c , the polar directivity angle, θ ,the aspect ratio, AR, and the normalized jet velocity, $\log_{10}(V_J^*)$, and the squares of these parameters as follows:

$$E = -19.34 + \phi_c * (0.9042 + 0.3920*\phi_c) + \theta * (15.65 - 5.654*\theta) - AR * (3.136 - 0.2594*AR) - \log_{10}(V_J^*) * [50.08 - 109.5 * \log_{10}(V_J^*)] \quad (51)$$

and

$$F = 3.182 - 0.2162 * \phi_c - \theta * (7.574 - 2.414*\theta) - AR * (2.361 - 0.2602*AR) + \log_{10}(V_J^*) * [7.123 - 200.0* \log_{10}(V_J^*)] \quad (52)$$

The second segment equation for the sound pressure levels, $SPL(St,\theta,\phi)$, at the low end of the spectra, $\{ \log_{10}(St) < [\log_{10}(St_{peak}) - 0.4] \}$, is defined from the slope E and the intercept F as follows:

$$SPL(St,\theta,\phi) = SPL_{peak}(\theta,\phi) - E * [\log_{10}(St) - \log_{10}(St_{peak})] - F \quad (53)$$

The third segment is a circular segment that ranges from the spectral peak to four one-third octave bands above the spectral peak as shown on Figure 9. The radius of this arc is defined by performing a least squares fit using the Data Desk program [ref 6] of the spectra data for each of the azimuth angles and directivity angles for each of the 20 test points. The results of the fit show that the radius of the curve, D, is defined as follows:

$$D = 71.34 - \theta * (70.86 - 21.60*\theta) - AR * (3.207 - 0.3976*AR) + \log_{10}(V_J^*) * [47.01 - 600.5*\log_{10}(V_J^*)] \quad (54)$$

Equation 54 shows that the radius of curvature is not affected by the azimuth angle,ϕ. For logarithm of the Strouhal number, $\log_{10}(St)$, ranging from $\log_{10}(St_{peak})$ to $[\log_{10}(St_{peak}) + 0.4]$ the SPL value is defined as follows:

$$SPL(St,\theta,\phi) = SPL_{peak}(\theta,\phi) - C * [\log_{10}(St) - \log_{10}(St_{peak})]^2 \quad (55)$$

The fourth segment is for frequencies corresponding to Strouhal numbers that have logarithms greater than $[\log_{10}(St_{peak}) + 0.4]$. The spectral shape is defined by a straight line that has a slope,G, and an intercept, H. The G and H parameters shown on Figure 9 are functions of the corrected azimuth angle, ϕ_c , the polar directivity angle, θ ,the aspect ratio, AR, and the normalized jet velocity, $\log_{10}(V_J^*)$, and the squares of these parameters as follows:

$$G = 20.61 + 0.8340 * \phi_c - \theta * (18.58 - 5.587*\theta) + AR * (0.8998 - 0.1061*AR) + 37.58 * \log_{10}(V_J^*) \quad (56)$$

and

$$H = 3.906 - 0.2297 * \phi_c - \theta * (4.228 - 1.246*\theta) - AR * (0.9532 - 0.1022*AR) - 64.11 * \log_{10}(V_J^*) \quad (57)$$

The fourth segment equation for the sound pressure levels, $SPL(St,\theta,\phi)$, at the high end of the spectra, $\{ < [\log_{10}(St_{peak}) + 0.4] < \log_{10}(St) \}$, is defined from the slope G and the intercept H as follows:

$$SPL(St,\theta,\phi) = SPL_{peak}(\theta,\phi) - G * [\log_{10}(St) - \log_{10}(St_{peak})] - H \quad (58)$$

It should be noted that sometimes there are disjoints between the segments. Because of time constraints, a smoothing was not applied to these disjoints. The disjoints are especially pronounced between segments 1 and 2.

RESULTS

The empirical prediction method that was developed provides a method for computation of jet mixing noise for cold flow rectangular jets. The method was applied to all the test cases in the database and the results appear to be satisfactory. Comparisons of the predicted and derived jet mixing noise levels for a few of the test points are discussed.

Prediction Method

The overall power level for rectangular jets was defined by computing the overall power level of circular jets using the SAE method [ref 3] and then applying a correction factor that is a function of aspect ratio. From the overall power level, the average overall sound pressure level over a sphere of a specified radius can be computed. Next a polar directivity correction is applied to the average overall sound pressure level to obtain an average overall sound pressure level at a particular polar directivity angle. This polar directivity is a function of polar directivity angle and aspect ratio. Also at directivity angles above 140 degrees, the polar directivity is dependent on the normalized jet velocity. The overall sound pressure level at particular azimuth directivity is obtained by adding an azimuth directivity correction to the average overall sound pressure level at a particular polar directivity angle. This azimuth directivity angle was found to be a function of aspect ratio, normalized jet velocity, polar directivity angle, and azimuth directivity angle. The last step in the process is defining the spectra shape. The spectra shape was broken down into four specific regions. First the frequency location and sound pressure level magnitude of the spectra peak were defined. Next the spectra content relative to the peak point were defined. Thus the sound pressure level at a particular frequency is determined by correcting the overall sound pressure level at a particular polar and azimuth directivity for the peak magnitude and then adding the correction for the spectra magnitude at a particular frequency relative to the peak.

Comparison of Predicted and Derived Jet Mixing Noise Levels

For the same five test points presented in Figures 4 and 5, Figures 10a through 10e show comparisons of the predicted jet mixing sound pressure levels with the sound pressure levels of the jet mixing noise that were derived from the data, and the measured data that includes shock noise. The figures present the comparisons of the predicted SPL values with the derived SPL values at 14 polar directivity angles ranging from 60 degrees to 157.5 degrees at 0-degree azimuth

angle. The test points include nozzle 3 at a nozzle exit pressure ratio of 0.65, nozzle 3 at a nozzle exit pressure of 0.85, nozzle 4 at nozzle exit pressure of 1.00, nozzle 4 at a nozzle exit pressure of 1.45, and nozzle 1 at a nozzle exit pressure of 1.25.

Figure 10a is for an aspect ratio 3.70 nozzle with a jet exit Mach Number of 1.015, thus there is virtually no shock noise present. The figure shows that in the forward arc, polar directivity angles below 120 degrees, the location and magnitude of the predicted peak Strouhal number compares very well with the data. At frequencies below the peak frequency, the fairing of the initial slope with the circular arc around the peak needs to be corrected. In the aft arc, the predicted peak is generally higher than the measured jet mixing noise levels, and this is attributed to the fact that this empirical method is not going to fit all the data exactly.

Figure 10b is for an aspect ratio 3.56 nozzle with a jet exit Mach Number of 1.230. In the forward arc and at polar directivity angles up to 150 degrees, the predicted jet noise levels are below the derived jet noise levels. Again the location of the peak frequency is predicted reasonably well. At the directivity angle of 157.5 degrees, the predicted peak noise level is greater than the derived jet mixing noise level.

Figure 10c shows an aspect ratio 5.32 nozzle with a jet exit Mach Number of 1.350. In the forward arc, the predicted peak jet mixing noise levels are approximately 5 dB greater than the derived jet mixing noise levels. In the aft arc, the predicted jet mixing noise levels are slightly below the derived jet mixing noise levels. At polar directivity angles above 150 degrees, the predicted values are as much as 3 dB below the derived values. Again the predicted location of the peak Strouhal Number compares very well with the data over the range of directivity angles.

Figure 10d is for an aspect ratio 1.38 nozzle operating at a jet exit Mach Number of 1.807. In the forward arc, at polar directivity angles up to 135 degrees, the predicted jet mixing noise levels are 1 dB to 3 dB greater than the derived jet mixing noise levels. At the higher polar directivity angles, the predicted values are very close to the derived jet mixing noise values.

Figure 10e shows the comparison of the predicted and derived jet mixing noise levels for an aspect ratio 4.61 nozzle operating at a Mach Number of 1.608. At the very low directivity angles the predicted and derived jet mixing noise levels compare within 1 dB. At polar directivity angles from 80 degrees to 120 degrees, the predicted jet mixing noise levels range from 1 dB to 2.5 dB above the derived jet mixing noise levels. At the higher directivity levels, the predicted jet mixing noise levels compare reasonably well with the derived jet mixing noise levels.

For all the cases presented in Figures 10a through 10e, the location of the peak Strouhal Number was predicted very well over the range of directivity angles. The data is often not extremely well behaved, and this report shows that deriving the jet mixing noise from the measured data is an art. Thus there are some discrepancies in the derived data. The prediction method does not seem to be affected by jet exit Mach Number, but is affected by aspect ratio. At low aspect ratios, the method predicts the jet mixing noise component better than at the high aspect ratios.

Figures 11a through 11e show comparisons of predicted jet mixing noise levels with derived measured jet mixing noise levels for the same four cases as shown in Figures 5 and 6, where it was difficult to separate out the shock noise. The four cases shown in Figure 11 are for nozzles 4 and 5 operating at nozzle exit pressure ratios of 0.85 and 1.25 respectively. The aspect ratios vary from 4.909 to 7.314 and the jet exit Mach Number varies from 1.230 to 1.507.

Figure 11a shows that the predicted jet mixing noise levels are generally 2 dB less than the derived values at polar directivity angles below 140 degrees. Figure 11b also show that at all directivity angles, the predicted levels are considerably less than the derived jet mixing noise levels. However, the derived jet noise levels may contain shock noise, and the predicted levels are indicative of jet mixing noise only. Figure 11c shows that at the very low polar directivity angles, the predicted mixing noise levels are 5 dB less than the derived jet mixing noise levels. At polar directivity angles from 75 degrees to 135 degrees, the predicted noise values are generally 2 dB less than the derived jet mixing noise levels. At polar directivities above 140 degrees, the predicted values are larger than the derived jet mixing noise levels. Figure 11d shows that at polar directivity angles from 60 degrees to 135 degrees, the predicted values are about 2 dB less than the derived jet mixing noise levels. At the high directivity angles, the derived jet mixing noise levels are about the same as the predicted values, although the predicted peak Strouhal Numbers are generally higher than the derived peak Strouhal Numbers.

Although Figure 11 shows discrepancies between the predicted and derived jet mixing noise levels, the predicted jet noise levels can give some insight as to the characteristics of the data. For example, what was thought to be shock noise is really jet mixing noise, and what was thought to be jet mixing noise in the data, may really be shock noise. Thus the prediction method may provide more insight to allow a more scientific method of defining and removing the shock noise component from the total jet noise.

Both Figures 10 and 11 show that there are discrepancies between the derived and predicted jet mixing noise levels at polar directivity angles of 157.5 degrees,

whereas at polar directivity angles of 150 degrees, the discrepancies between the predicted and derived values are minimized. This is due to the fact that in many of the tests there are significant differences between the measured data at a polar directivity angle of 150 degrees and the measured data at polar directivity angle of 157.5 degrees. At measurement distances of 36 to 80 nozzle diameters, it is anticipated, that the sound waves at adjacent polar directivity angles would experience some interaction, thus reducing the differences at adjacent polar directivity angles. The fact that the prediction method does involve curve fitting, allows for this interaction, and may actually be more representative of the jet mixing noise characteristics than the data measurements that have been corrected for shock noise and screech tones.

Figures 10 and 11 show disjoints between segments 1 and 2 in the prediction. These disjoints are due to the fact that because of time constraints no attempts were made to perform a smoothing between segments. It is recommended that the spectral prediction method be modified to incorporate a smoothing method for merging segments.

CONCLUSIONS AND RECOMMENDATIONS

This report presents an empirical method for predicting the jet mixing noise characteristics for rectangular jets operating at cold flow conditions. The jet mixing noise prediction involves computing the overall power level first, and then obtaining an average overall sound pressure level based on the spherical radius. The overall sound pressure level at a particular directivity is then defined by adding terms adding terms for the average polar directivity and the azimuth directivity to the average overall sound pressure level. To obtain the sound pressure level at a particular frequency, the spectra content of the jet mixing noise is defined and the spectra term is added to the overall sound pressure level at the particular directivity. Each of these noise component parameters is defined as a function of the rectangular jet aspect ratio, the normalized jet velocity, the polar directivity, and azimuth directivity. Of course the overall power level is not dependent on the directivities. Similarly, the average polar directivity is not dependent on the azimuth directivity angle. Because of the existence of disjoints between segments in the prediction of the spectra shape, it is recommended that the spectra shape prediction be modified to incorporate a smoothing function in the area where two segments merge.

The correlations are predicated on the jet noise spectra characteristics being similar to the spectra characteristics of the circular jet. A recent analysis of the data by Tam etal [ref 5] indicated that the jet mixing noise may have two spectral components, the large turbulent/ instability waves, and the fine-scale turbulent noise. However, the jet noise spectra shapes do appear to resemble the SAE predicted circular jet spectral shape [ref 3]. Therefore the empirical

prediction method is predicated on the SAE circular jet prediction method in terms of spectra shape as well as overall power level.

It is recommended that the study be continued to incorporate temperature effects. This can be accomplished initially by incorporating temperature correction tables from the SAE circular jet prediction method into the polar directivity and into the spectra. Also there is limited high temperature rectangular jet data available that could be used to ascertain the validity of the temperature corrections. Finally it is recommended that additional model tests be conducted with contoured rectangular jet nozzles to minimize the shock noise and to establish a high temperature database for rectangular jet mixing noise.

REFERENCES

1. Ponton, M. K., Manning, J. C., and Seiner, J. M.: "Far-Field Acoustics of Supersonic Rectangular Nozzles With Various Throat Aspect Ratios, " NASA TM 89002, Nasa Langley Research Center, December 1986.

2. Sutherland, Louis C.: "Review of Experimental Data in Support of a Proposed New Method for Computing Atmospheric Absorption Losses," DOT-TST-75-87, U.S. Department of Transportation, May 1975.

3. "Gas Turbine Jet Exhaust Noise Prediction," ARP 876, Society of Automotive Engineers, March 1978.

4. Tam, C. K. W.: "Broadband Shock-Associated Noise of Supersonic Jets Measured By a Ground Observer," AIAA Paper 92-0502, Florida State University, Tallahassee, FL, January 1992.

5. Tam, C.K.W., Golebiowski,M., and Seiner, J.M.,: "On the Two Components of Turbulent Mixing Noise from Supersonic Jets," AIAA Paper 96-1716, Florida State University, Tallahassee Fl, May 1996.

6. Velleman, Paul F.: "Data Desk Version 6.0," Data Description Inc., Ithaca NY, 1997

TABLE I. Rectangular Jet Flow Properties

NOZZLE	PRESSURE RATIO	AZIMUTH ANGLE	PTOTAL PSIA	TTOTAL DEG R	MACH NUMBER	VJET FT/S	JET AREA SQ FT	JET DIAM FT	ASPECT RATIO	C AMB FT/S	RHO JET LB/CU FT	RHO AMB LB/CU FT	T AMB DEG R
1	0.65	0	41.16	532.73	1.3057	1275.73	0.05937	0.2749	1.8714	1135.43	0.100135	0.074154	536.48
1	0.65	15	41.26	533.88	1.3051	1276.67	0.05936	0.2749	1.8719	1135.71	0.100236	0.074368	536.75
1	0.65	30	41.15	534.43	1.3042	1276.73	0.05934	0.2749	1.8725	1135.76	0.099940	0.074242	536.79
1	0.65	45	41.16	535.91	1.3048	1278.88	0.05935	0.2749	1.8721	1138.85	0.099643	0.073808	539.72
1	0.65	60	40.92	546.04	1.3047	1290.90	0.05935	0.2749	1.8721	1139.43	0.097217	0.073299	540.27
1	0.65	75	40.97	539.66	1.3059	1284.19	0.05938	0.275	1.8712	1140.38	0.098390	0.073162	541.17
1	0.65	90	40.93	535.89	1.3041	1278.40	0.05934	0.2749	1.8726	1136.56	0.099148	0.073755	537.55
1	0.65	180	41.01	545.42	1.3036	1289.31	0.05932	0.2748	1.8730	1140.64	0.097660	0.073427	541.42
1	0.65	270	41.08	542.77	1.3052	1287.36	0.05936	0.2749	1.8717	1143.77	0.098133	0.072977	544.39
AVERAGE	VALUES		41.07	538.53	1.3048	1282.02	0.05935	0.2749	1.8721	1138.50	0.098945	0.073688	539.39
STANDARD	DEVIATION		0.11	4.82	0.0008	5.59				2.74	0.001065		2.54

NOZZLE	PRESSURE RATIO	AZIMUTH ANGLE	PTOTAL PSIA	TTOTAL DEG R	MACH NUMBER	VJET FT/S	JET AREA SQ FT	JET DIAM FT	ASPECT RATIO	C AMB FT/S	RHO JET LB/CU FT	RHO AMB LB/CU FT	T AMB DEG R
1	0.85	0	58.13	531.98	1.5499	1440.25	0.06731	0.2927	1.6509	1134.93	0.110582	0.074134	536.01
1	0.85	15	58.41	535.92	1.5495	1445.30	0.06729	0.2927	1.6513	1136.38	0.110350	0.074350	537.38
1	0.85	30	58.22	533.04	1.5497	1441.57	0.0673	0.2927	1.6510	1135.70	0.110560	0.074171	536.74
1	0.85	45	58.08	537.84	1.5483	1447.18	0.06724	0.2926	1.6524	1139.17	0.109472	0.073695	540.02
1	0.85	60	57.99	543.60	1.5508	1456.46	0.06734	0.2928	1.6500	1139.07	0.107862	0.073328	539.92
1	0.85	75	57.73	539.01	1.5480	1448.55	0.06723	0.2926	1.6527	1140.55	0.108613	0.073109	541.33
1	0.85	90	58.01	535.12	1.5506	1444.91	0.06733	0.2928	1.6502	1136.05	0.109632	0.073765	537.06
1	0.85	180	58.14	543.05	1.5500	1455.24	0.06731	0.2928	1.6507	1140.38	0.108337	0.073430	541.17
1	0.85	270	57.99	543.51	1.5489	1455.18	0.06727	0.2927	1.6518	1144.35	0.108087	0.072848	544.94
AVERAGE	VALUES		58.08	538.12	1.5495	1448.29	0.06729	0.2927	1.6512	1138.51	0.109277	0.073648	539.40
STANDARD	DEVIATION		0.18	4.24	0.0011	5.68				2.92	0.001022		2.72

NOZZLE	PRESSURE RATIO	AZIMUTH ANGLE	PTOTAL PSIA	TTOTAL DEG R	MACH NUMBER	VJET FT/S	JET AREA SQ FT	JET DIAM FT	ASPECT RATIO	C AMB FT/S	RHO JET LB/CU FT	RHO AMB LB/CU FT	T AMB DEG R
1	1.00	0	68.40	531.11	1.6600	1505.80	0.07228	0.3034	1.5372	1135.07	0.115993	0.074078	536.14
1	1.00	15	68.75	534.79	1.6593	1510.58	0.07224	0.3033	1.5380	1136.42	0.115873	0.074361	537.41
1	1.00	30	68.50	533.07	1.6595	1508.25	0.07225	0.3033	1.5378	1135.88	0.115804	0.074142	536.91
1	1.00	45	68.49	538.40	1.6596	1515.83	0.07226	0.3033	1.5377	1138.83	0.114624	0.073733	539.70
1	1.00	60	68.11	543.07	1.6597	1522.49	0.07227	0.3033	1.5375	1139.28	0.112996	0.073253	540.12
1	1.00	75	68.03	539.76	1.6590	1517.42	0.07223	0.3033	1.5383	1140.75	0.113629	0.073049	541.52
1	1.00	90	68.23	534.35	1.6599	1510.32	0.07227	0.3034	1.5373	1135.87	0.115019	0.073804	536.90
1	1.00	180	68.16	541.52	1.6575	1519.01	0.07216	0.3031	1.5398	1140.50	0.113671	0.073393	541.28
1	1.00	270	68.28	544.44	1.6595	1524.28	0.07226	0.3033	1.5378	1144.91	0.113008	0.072732	545.48
AVERAGE	VALUES		68.33	537.84	1.6593	1514.89	0.07225	0.3033	1.5379	1138.61	0.114513	0.073616	539.50
STANDARD	DEVIATION		0.21	4.45	0.0007	6.10				2.94	0.001155		2.84

Table I Continued. - Rectangular Jet Flow Properties

NOZZLE	PRESSURE RATIO	AZIMUTH ANGLE	PTOTAL PSIA	TTOTAL DEG R	MACH NUMBER	VJET FT/S	JET AREA SQ FT	JET DIAM FT	ASPECT RATIO	C AMB FT/S	RHO JET LB/CU FT	RHO AMB LB/CU FT	T AMB DEG R
1	1.25	0	85.38	531.01	1.8066	1587.42	0.08034	0.3198	1.3829	1135.24	0.123563	0.074024	536.30
1	1.25	15	85.96	534.24	1.8070	1592.47	0.08037	0.3199	1.3825	1136.42	0.123596	0.074326	537.41
1	1.25	30	85.55	533.79	1.8066	1591.58	0.08034	0.3198	1.3829	1136.54	0.123171	0.074006	537.53
1	1.25	45	85.56	537.59	1.8070	1597.42	0.08037	0.3199	1.3826	1138.54	0.122261	0.073711	539.43
1	1.25	60	85.09	541.93	1.8070	1603.90	0.08037	0.3199	1.3825	1139.26	0.120607	0.073206	540.10
1	1.25	75	85.01	540.39	1.8067	1601.44	0.08035	0.3198	1.3828	1140.76	0.120881	0.072982	541.53
1	1.25	90	85.06	533.79	1.8059	1591.20	0.0803	0.3198	1.3837	1135.88	0.122553	0.073743	536.91
1	1.25	180	85.44	540.99	1.8071	1602.54	0.08037	0.3199	1.3824	1140.88	0.121315	0.073297	541.64
1	1.25	270	85.36	543.59	1.8076	1606.66	0.08041	0.32	1.3819	1145.16	0.120542	0.072617	545.72
AVERAGE	VALUES		85.38	537.48	1.8068	1597.18	0.08036	0.3199	1.3827	1138.74	0.122054	0.073546	539.62
STANDARD	DEVIATION		0.29	4.19	0.0008	6.36	0	0	0.0000	3.02	0.001178	0.000000	2.85

NOZZLE	PRESSURE RATIO	AZIMUTH ANGLE	PTOTAL PSIA	TTOTAL DEG R	MACH NUMBER	VJET FT/S	JET AREA SQ FT	JET DIAM FT	ASPECT RATIO	C AMB FT/S	RHO JET LB/CU FT	RHO AMB LB/CU FT	T AMB DEG R
1	1.45	0	99.18	530.39	1.9044	1636.81	0.08671	0.3323	1.2815	1135.42	0.129067	0.073960	536.47
1	1.45	15	99.47	532.53	1.9023	1639.09	0.08657	0.332	1.2836	1136.24	0.129226	0.074309	537.24
1	1.45	30	99.19	533.14	1.9032	1640.46	0.08662	0.3321	1.2827	1136.54	0.128593	0.073962	537.53
1	1.45	45	99.29	533.85	1.9038	1641.84	0.08666	0.3322	1.2821	1138.21	0.128460	0.073748	539.11
1	1.45	60	98.60	537.11	1.9032	1646.55	0.08662	0.3321	1.2827	1139.24	0.126878	0.073171	540.09
1	1.45	75	98.62	540.29	1.9036	1651.61	0.08665	0.3322	1.2823	1141.02	0.126103	0.072915	541.78
1	1.45	90	98.68	532.33	1.9027	1638.97	0.08659	0.332	1.2832	1135.73	0.128182	0.073734	536.76
1	1.45	180	99.00	539.30	1.9034	1650.02	0.08664	0.3321	1.2825	1140.63	0.126844	0.073264	541.41
1	1.45	270	98.93	542.82	1.9039	1655.65	0.08667	0.3322	1.2820	1144.83	0.125866	0.072622	545.40
AVERAGE	VALUES		99.00	535.75	1.9034	1644.56	0.08664	0.3321	1.2825	1138.65	0.127691	0.073520	539.53
STANDARD	DEVIATION		0.30	4.03	0.0000	6.22				2.94	0.001208		2.79

NOZZLE	PRESSURE RATIO	AZIMUTH ANGLE	PTOTAL PSIA	TTOTAL DEG R	MACH NUMBER	VJET FT/S	JET AREA SQ FT	JET DIAM FT	ASPECT RATIO	C AMB FT/S	RHO JET LB/CU FT	RHO AMB LB/CU FT	T AMB DEG
3	0.65	0	28.31	537.12	1.0155	1050.50	0.03004	0.1956	3.6992	1135.66	0.089020	0.073857	536.69
3	0.65	15	28.26	543.57	1.0144	1055.83	0.03004	0.1956	3.6993	1142.21	0.087890	0.072978	542.90
3	0.65	30	28.33	542.17	1.0159	1055.75	0.03004	0.1956	3.6992	1140.63	0.088221	0.073229	541.41
3	0.65	45	28.39	540.45	1.0170	1055.03	0.03004	0.1956	3.6991	1139.46	0.088595	0.073430	540.29
3	0.65	60	28.39	539.17	1.0166	1053.44	0.03004	0.1956	3.6991	1134.54	0.088854	0.074119	535.64
3	0.65	75	28.31	541.66	1.0169	1056.11	0.03004	0.1956	3.6991	1139.80	0.088152	0.073186	540.62
3	0.65	90	28.29	544.67	1.0160	1058.21	0.03004	0.1956	3.6992	1138.62	0.087698	0.073389	539.49
3	0.65	180	28.25	538.75	1.0146	1051.32	0.03004	0.1956	3.6993	1137.99	0.088622	0.073470	538.90
3	0.65	270	28.30	536.15	1.0150	1049.08	0.03004	0.1956	3.6992	1135.67	0.089183	0.073871	536.70
AVERAGE	VALUES		28.32	540.41	1.0158	1053.92	0.03004	0.1956	3.6992	1138.29	0.088471	0.073503	539.18
STANDARD	DEVIATION		0.05	2.72	0.0008	2.83				2.47	0.000482		2.28

Table I Continued. - Rectangular Jet Flow Properties

NOZZLE	PRESSURE RATIO	AZIMUTH ANGLE	PTOTAL PSIA	TTOTAL DEG R	MACH NUMBER	VJET FT/S	JET AREA SQ FT	JET DIAM, FT	ASPECT RATIO	C AMB FT/S	RHO JET LB/CU FT	RHO AMB LB/CU FT	T AMB DEG
3	0.85	0	37.05	538.34	1.2299	1225.72	0.03123	0.1994	3.5583	1135.61	0.095928	0.073879	536.65
3	0.85	15	36.97	544.35	1.2289	1231.77	0.03122	0.1994	3.5595	1142.76	0.094767	0.072907	543.43
3	0.85	30	37.03	543.22	1.2300	1231.36	0.03123	0.1994	3.5581	1140.94	0.095006	0.073140	541.70
3	0.85	45	37.04	541.58	1.2296	1229.13	0.03122	0.1994	3.5587	1139.86	0.095354	0.073338	540.67
3	0.85	60	37.03	540.29	1.2286	1226.93	0.03121	0.1993	3.5598	1138.21	0.095651	0.073632	539.11
3	0.85	75	36.92	542.62	1.2289	1229.81	0.03122	0.1994	3.5594	1139.92	0.094940	0.073171	540.73
3	0.85	90	37.00	544.88	1.2304	1233.50	0.03123	0.1994	3.5578	1138.95	0.094607	0.073302	539.81
3	0.85	180	37.02	539.97	1.2303	1227.87	0.03123	0.1994	3.5578	1138.27	0.095523	0.073433	539.17
3	0.85	270	37.04	537.69	1.2298	1224.89	0.03122	0.1994	3.5584	1135.85	0.096038	0.073848	536.87
AVERAGE	VALUES		37.01	541.44	1.2296	1229.00	0.03122	0.1994	3.5586	1138.93	0.095313	0.073406	539.79
STANDARD	DEVIATION		0.03	2.40	0.0006	2.74				2.21	0.000481		2.03

NOZZLE	PRESSURE RATIO	AZIMUTH ANGLE	PTOTAL PSIA	TTOTAL DEG R	MACH NUMBER	VJET FT/S	JET AREA SQ FT	JET DIAM, FT	ASPECT RATIO	C AMB FT/S	RHO JET LB/CU FT	RHO AMB LB/CU FT	T AMB DEG
3	1.00	0	43.58	538.75	1.3497	1314.79	0.0327	0.2041	3.3979	1135.24	0.100398	0.073924	536.30
3	1.00	15	43.63	541.69	1.3511	1319.37	0.03272	0.2041	3.3958	1136.30	0.099845	0.073739	537.30
3	1.00	30	43.67	543.39	1.3517	1321.88	0.03273	0.2041	3.3948	1141.12	0.099558	0.073117	541.87
3	1.00	45	43.66	541.92	1.3510	1319.60	0.03272	0.2041	3.3959	1139.84	0.099867	0.073332	540.65
3	1.00	60	43.56	540.22	1.3488	1315.97	0.03269	0.204	3.3992	1138.20	0.100167	0.073596	539.10
3	1.00	75	43.41	542.62	1.3490	1318.96	0.03269	0.204	3.3990	1139.88	0.099385	0.073126	540.70
3	1.00	90	43.42	543.99	1.3487	1320.42	0.03268	0.204	3.3995	1139.11	0.099191	0.073275	539.97
3	1.00	180	43.59	540.46	1.3509	1317.71	0.03272	0.2041	3.3961	1138.33	0.099995	0.073426	539.22
3	1.00	270	43.62	537.75	1.3507	1314.28	0.03271	0.2041	3.3964	1135.86	0.100587	0.073815	536.88
AVERAGE	VALUES		43.57	541.20	1.3502	1318.11	0.03271	0.2041	3.3972	1138.21	0.099888	0.073483	539.11
STANDARD	DEVIATION		0.09	1.95	0.0013	2.47				1.90	0.000431		1.79

NOZZLE	PRESSURE RATIO	AZIMUTH ANGLE	PTOTAL PSIA	TTOTAL DEG R	MACH NUMBER	VJET FT/S	JET AREA SQ FT	JET DIAM, FT	ASPECT RATIO	C AMB FT/S	RHO JET LB/CU FT	RHO AMB LB/CU FT	T AMB DEG
3	1.25	0	54.51	538.41	1.5078	1422.02	0.03548	0.2125	3.1316	1134.98	0.107047	0.073911	536.05
3	1.25	15	54.35	542.78	1.5059	1426.49	0.03544	0.2124	3.1351	1134.73	0.106099	0.073943	535.82
3	1.25	30	54.35	543.77	1.5062	1428.04	0.03545	0.2124	3.1345	1141.54	0.105864	0.073022	542.27
3	1.25	45	54.40	542.08	1.5065	1425.98	0.03545	0.2125	3.1340	1140.35	0.106264	0.073216	541.14
3	1.25	60	54.38	539.98	1.5052	1422.40	0.03543	0.2124	3.1363	1138.40	0.106767	0.073567	539.29
3	1.25	75	54.23	542.61	1.5058	1426.22	0.03544	0.2124	3.1353	1140.23	0.105908	0.073079	541.02
3	1.25	90	54.38	542.96	1.5071	1427.56	0.03547	0.2125	3.1328	1138.60	0.105971	0.073337	539.48
3	1.25	180	54.29	540.61	1.5061	1423.76	0.03544	0.2124	3.1348	1138.37	0.106393	0.073374	539.26
3	1.25	270	54.33	537.41	1.5057	1419.34	0.03544	0.2124	3.1354	1135.89	0.107135	0.073779	536.92
AVERAGE	VALUES		54.36	541.18	1.5063	1424.65	0.03545	0.2124	3.1344	1138.12	0.106383	0.073470	539.03
STANDARD	DEVIATION		0.07	2.09	0.0007	2.85				2.29	0.000463		2.20

Table I Continued. - Rectangular Jet Flow Properties

NOZZLE	PRESSURE RATIO	AZIMUTH ANGLE	PTOTAL PSIA	TTOTAL DEG R	MACH NUMBER	VJET FT/S	JET AREA SQ FT	JET DIAM, FT	ASPECT RATIO	C AMB FT/S	RHO JET LB/CU FT	RHO AMB LB/CU FT	T AMB DEG
3	1.45	0	63.07	536.66	1.6072	1482.08	0.03772	0.2192	2.9456	1134.87	0.111969	0.073925	535.95
3	1.45	15	63.08	541.13	1.6078	1488.57	0.03774	0.2192	2.9445	1135.32	0.111000	0.073818	536.38
3	1.45	30	63.11	543.93	1.6082	1492.64	0.03774	0.2192	2.9438	1142.22	0.110441	0.072927	542.91
3	1.45	45	63.13	542.10	1.6078	1489.94	0.03774	0.2192	2.9444	1140.61	0.110872	0.073183	541.38
3	1.45	60	63.09	539.75	1.6065	1485.92	0.0377	0.2191	2.9469	1138.10	0.111442	0.073602	539.01
3	1.45	75	63.17	543.61	1.6081	1492.15	0.03774	0.2192	2.9440	1137.61	0.110627	0.073604	538.54
3	1.45	90	62.94	542.92	1.6072	1490.67	0.03772	0.2192	2.9457	1139.10	0.110453	0.073229	539.96
3	1.45	180	63.09	540.54	1.6084	1488.15	0.03775	0.2192	2.9433	1138.39	0.111069	0.073368	539.28
3	1.45	270	63.02	536.50	1.6072	1481.81	0.03772	0.2192	2.9457	1136.39	0.111922	0.073676	537.39
AVERAGE	VALUES		63.08	540.79	1.6076	1487.99	0.03773	0.2192	2.9449	1138.07	0.111088	0.073481	538.98
STANDARD	DEVIATION		0.06	2.59	0.0007	3.77				2.26	0.000545		2.11

NOZZLE	PRESSURE RATIO	AZIMUTH ANGLE	PTOTAL PSIA	TTOTAL DEG R	MACH NUMBER	VJET FT/S	JET AREA SQ FT	JET DIAM FT	ASPECT RATIO	C AMB FT/S	RHO JET LB/CU FT	RHO AMB LB/CU FT	T AMB DEG R
4	0.65	0	28.59	526.01	1.0172	1041.01	0.01917	0.1562	5.7957	1123.69	0.091673	0.076035	525.44
4	0.65	15	28.66	527.28	1.0187	1043.50	0.01917	0.1562	5.7954	1122.91	0.091540	0.076177	524.71
4	0.65	30	28.23	530.48	1.0135	1042.25	0.01917	0.1562	5.7962	1131.05	0.090030	0.074424	532.35
4	0.65	45	28.38	529.39	1.0172	1044.33	0.01917	0.1562	5.7957	1129.93	0.090412	0.074643	531.29
4	0.65	60	28.42	532.81	1.0181	1048.50	0.01917	0.1562	5.7955	1130.56	0.089899	0.074591	531.89
4	0.65	75	28.38	530.11	1.0157	1043.75	0.01917	0.1562	5.7959	1130.31	0.090405	0.074725	531.65
4	0.65	90	28.37	528.99	1.0143	1041.49	0.01917	0.1562	5.7961	1128.99	0.090660	0.074985	530.41
4	0.65	180	28.37	532.64	1.0143	1045.09	0.01917	0.1562	5.7961	1129.93	0.090038	0.074862	531.29
4	0.65	270	28.32	533.22	1.0138	1045.20	0.01917	0.1562	5.7962	1133.79	0.089822	0.074268	534.93
AVERAGE	VALUES		28.41	530.10	1.0159	1043.90	0.01917	0.1562	5.7959	1129.02	0.090498	0.074968	530.44
STANDARD	DEVIATION		0.13	2.37	0.0019	2.12				3.30	0.000647		3.11

NOZZLE	PRESSURE RATIO	AZIMUTH ANGLE	PTOTAL PSIA	TTOTAL DEG R	MACH NUMBER	VJET FT/S	JET AREA SQ FT	JET DIAM FT	ASPECT RATIO	C AMB FT/S	RHO JET LB/CU FT	RHO AMB LB/CU FT	T AMB DEG R
4	0.85	0	37.36	527.45	1.2306	1213.79	0.01993	0.1593	5.5739	1123.47	0.098669	0.076049	525.24
4	0.85	15	37.43	529.82	1.2315	1217.19	0.01994	0.1593	5.5723	1122.96	0.098325	0.076170	524.76
4	0.85	30	37.03	531.21	1.2300	1217.68	0.01993	0.1593	5.5749	1130.97	0.097153	0.074436	532.27
4	0.85	45	37.06	532.18	1.2300	1218.74	0.01993	0.1593	5.5751	1130.82	0.097065	0.074524	532.14
4	0.85	60	37.00	533.13	1.2284	1218.60	0.01992	0.1593	5.5779	1129.95	0.096875	0.074671	531.32
4	0.85	75	37.07	530.78	1.2288	1216.20	0.01992	0.1593	5.5772	1130.37	0.097451	0.074717	531.71
4	0.85	90	37.11	529.71	1.2290	1215.14	0.01992	0.1593	5.5769	1128.80	0.097726	0.074979	530.23
4	0.85	180	37.22	533.85	1.2310	1221.45	0.01994	0.1593	5.5732	1129.63	0.097072	0.074892	531.01
4	0.85	270	37.08	533.72	1.2290	1219.76	0.01992	0.1593	5.5768	1133.79	0.096922	0.074268	534.93
AVERAGE	VALUES		37.15	531.31	1.2298	1217.62	0.01993	0.1593	5.5754	1128.97	0.097473	0.074967	530.40
STANDARD	DEVIATION		0.14	2.00	0.0009	2.18				3.37	0.000605		3.14

Table I Continued. - Rectangular Jet Flow Properties

NOZZLE	PRESSURE RATIO	AZIMUTH ANGLE	PTOTAL PSIA	TTOTAL DEG R	MACH NUMBER	VJET FT/S	JET AREA SQ FT	JET DIAM FT	ASPECT RATIO	C AMB FT/S	RHO JET LB/CU FT	RHO AMB LB/CU FT	T AMB DEG R
4	1.00	0	43.86	527.78	1.3489	1300.79	0.02086	0.163	5.3257	1123.46	0.103225	0.076050	525.23
4	1.00	15	43.99	528.34	1.3507	1302.74	0.02088	0.163	5.3214	1123.33	0.103257	0.076120	525.10
4	1.00	30	43.58	531.35	1.3503	1306.14	0.02088	0.163	5.3224	1130.81	0.101738	0.074443	532.13
4	1.00	45	43.61	532.46	1.3502	1307.44	0.02088	0.163	5.3227	1130.78	0.101608	0.074511	532.09
4	1.00	60	43.71	532.77	1.3514	1308.66	0.02089	0.1631	5.3198	1129.75	0.101663	0.074695	531.12
4	1.00	75	43.59	531.08	1.3484	1304.48	0.02086	0.163	5.3269	1130.45	0.102009	0.074706	531.79
4	1.00	90	43.56	529.89	1.3474	1302.30	0.02085	0.1629	5.3293	1128.86	0.102267	0.074968	530.29
4	1.00	180	43.76	533.71	1.3504	1309.14	0.02088	0.163	5.3221	1129.26	0.101695	0.074944	530.66
4	1.00	270	43.63	534.00	1.3494	1308.77	0.02087	0.163	5.3246	1133.80	0.101438	0.074229	534.94
AVERAGE	VALUES		43.70	531.27	1.3497	1305.61	0.02087	0.163	5.3239	1128.94	0.102100	0.074963	530.37
STANDARD	DEVIATION		0.14	2.09	0.0012	3.00				3.22	0.000651		3.06

NOZZLE	PRESSURE RATIO	AZIMUTH ANGLE	PTOTAL PSIA	TTOTAL DEG R	MACH NUMBER	VJET FT/S	JET AREA SQ FT	JET DIAM FT	ASPECT RATIO	C AMB FT/S	RHO JET LB/CU FT	RHO AMB LB/CU FT	T AMB DEG R
4	1.25	0	54.75	527.76	1.5053	1406.26	0.02261	0.1697	4.9138	1123.57	0.109985	0.076036	525.33
4	1.25	15	54.96	529.81	1.5075	1410.40	0.02264	0.1698	4.9075	1123.35	0.109734	0.076116	525.13
4	1.25	30	54.41	531.33	1.5069	1412.03	0.02263	0.1698	4.9092	1130.73	0.108382	0.074432	532.05
4	1.25	45	54.49	532.35	1.5072	1413.59	0.02264	0.1698	4.9083	1130.73	0.108312	0.074518	532.05
4	1.25	60	54.45	532.26	1.5062	1412.81	0.02262	0.1697	4.9113	1129.56	0.108358	0.074723	530.94
4	1.25	75	54.63	531.19	1.5079	1412.51	0.02265	0.1698	4.9063	1130.70	0.108728	0.074622	532.02
4	1.25	90	54.67	532.11	1.5076	1413.54	0.02264	0.1698	4.9072	1130.60	0.108674	0.074738	531.92
4	1.25	180	54.64	533.43	1.5072	1415.00	0.02264	0.1698	4.9084	1129.17	0.108394	0.074933	530.58
4	1.25	270	54.48	534.12	1.5061	1415.22	0.02262	0.1697	4.9115	1133.75	0.108052	0.074222	534.89
AVERAGE	VALUES		54.61	531.59	1.5069	1412.37	0.02263	0.1698	4.9093	1129.13	0.108735	0.074927	530.55
STANDARD	DEVIATION		0.17	1.78	0.0007	2.55				3.24	0.000631		3.06

NOZZLE	PRESSURE RATIO	AZIMUTH ANGLE	PTOTAL PSIA	TTOTAL DEG R	MACH NUMBER	VJET FT/S	JET AREA SQ FT	JET DIAM FT	ASPECT RATIO	C AMB FT/S	RHO JET LB/CU FT	RHO AMB LB/CU FT	T AMB DEG R
4	1.45	0	63.63	527.49	1.6077	1469.66	0.02408	0.1751	4.6137	1123.64	0.114871	0.076026	525.40
4	1.45	15	63.69	528.94	1.6081	1471.92	0.02409	0.1751	4.6125	1123.18	0.114608	0.076110	524.97
4	1.45	30	63.22	531.07	1.6092	1475.55	0.02411	0.1752	4.6092	1130.62	0.113176	0.074437	531.95
4	1.45	45	63.08	531.66	1.6069	1474.97	0.02407	0.1751	4.6161	1130.66	0.113082	0.074527	531.98
4	1.45	60	63.14	531.46	1.6073	1474.95	0.02408	0.1751	4.6148	1129.28	0.113185	0.074734	530.68
4	1.45	75	63.24	530.90	1.6077	1474.36	0.02408	0.1751	4.6139	1130.70	0.113435	0.074622	532.02
4	1.45	90	63.22	531.93	1.6066	1475.16	0.02407	0.1751	4.6170	1130.20	0.113318	0.074790	531.55
4	1.45	180	63.38	531.90	1.6083	1476.12	0.02409	0.1751	4.6120	1128.63	0.113405	0.074998	530.08
4	1.45	270	63.20	533.72	1.6073	1478.03	0.02408	0.1751	4.6151	1133.84	0.112816	0.074210	534.98
AVERAGE	VALUES		63.31	531.01	1.6077	1474.52	0.02408	0.1751	4.6138	1128.97	0.113544	0.074939	530.40
STANDARD	DEVIATION		0.20	1.70	0.0007	2.24				3.30	0.000666		3.07

Table I Continued. - Rectangular Jet Flow Properties

NOZZLE	PRESSURE RATIO	AZIMUTH ANGLE	PTOTAL PSIA	TTOTAL DEG R	MACH NUMBER	VJET FT/S	JET AREA SQ FT	JET DIAM FT	ASPECT RATIO	C AMB FT/S	RHO JET LB/CU FT	RHO AMB LB/CU FT	T AMB DEG R
5	0.65	0	28.73	528.78	1.0158	1042.51	0.01461	0.1364	7.6030	1127.99	0.091743	0.075951	529.47
5	0.65	15	28.87	529.44	1.0187	1045.63	0.01462	0.1364	7.6024	1130.82	0.091843	0.075672	532.14
5	0.65	30	28.58	530.12	1.0180	1045.73	0.01462	0.1364	7.6025	1131.92	0.090843	0.074816	533.17
5	0.65	45	28.56	530.80	1.0180	1046.42	0.01462	0.1364	7.6025	1131.68	0.090686	0.074813	532.95
5	0.65	60	28.44	534.49	1.0160	1048.32	0.01461	0.1364	7.6030	1132.87	0.089838	0.074524	534.06
5	0.65	75	28.38	532.48	1.0143	1044.94	0.01461	0.1364	7.6033	1132.72	0.090084	0.074508	533.92
5	0.65	90	28.49	530.40	1.0154	1043.80	0.01461	0.1364	7.6031	1130.76	0.090715	0.074970	532.08
5	0.65	180	28.50	529.75	1.0146	1042.49	0.01461	0.1364	7.6032	1127.48	0.090926	0.075508	529.00
5	0.65	270	28.75	530.71	1.0180	1046.27	0.01462	0.1364	7.6025	1129.88	0.091301	0.075551	531.25
AVERAGE	VALUES		28.59	530.78	1.0165	1045.12	0.01461	0.1364	7.6028	1130.68	0.090886	0.075146	532.00
STANDARD	DEVIATION		0.15	1.60	0.0015	1.80				1.77	0.000635		1.68

NOZZLE	PRESSURE RATIO	AZIMUTH ANGLE	PTOTAL PSIA	TTOTAL DEG R	MACH NUMBER	VJET FT/S	JET AREA SQ FT	JET DIAM FT	ASPECT RATIO	C AMB FT/S	RHO JET LB/CU FT	RHO AMB LB/CU FT	T AMB DEG R
5	0.85	0	37.64	530.65	1.2313	1217.99	0.0152	0.1391	7.3102	1128.07	0.098748	0.075930	529.55
5	0.85	15	37.54	529.19	1.2281	1213.84	0.01518	0.139	7.3178	1129.92	0.099045	0.075793	531.28
5	0.85	30	37.24	530.63	1.2291	1216.30	0.01519	0.1391	7.3153	1132.29	0.097888	0.074767	533.52
5	0.85	45	37.26	531.30	1.2296	1217.46	0.01519	0.1391	7.3141	1131.23	0.097766	0.074895	532.52
5	0.85	60	37.18	534.23	1.2296	1220.79	0.01519	0.1391	7.3142	1132.57	0.097037	0.074570	533.78
5	0.85	75	37.14	533.78	1.2296	1220.31	0.01519	0.1391	7.3141	1133.03	0.097001	0.074417	534.22
5	0.85	90	37.24	531.64	1.2298	1217.95	0.01519	0.1391	7.3138	1131.11	0.097659	0.074873	532.41
5	0.85	180	37.25	530.76	1.2285	1215.99	0.01519	0.1391	7.3167	1127.66	0.097952	0.075468	529.17
5	0.85	270	37.42	531.84	1.2283	1217.09	0.01518	0.1391	7.3172	1130.05	0.098230	0.075522	531.41
AVERAGE	VALUES		37.32	531.56	1.2293	1217.52	0.01519	0.1391	7.3148	1130.66	0.097925	0.075137	531.98
STANDARD	DEVIATION		0.16	1.49	0.0010	2.03				1.87	0.000646		1.65

NOZZLE	PRESSURE RATIO	AZIMUTH ANGLE	PTOTAL PSIA	TTOTAL DEG R	MACH NUMBER	VJET FT/S	JET AREA SQ FT	JET DIAM FT	ASPECT RATIO	C AMB FT/S	RHO JET LB/CU FT	RHO AMB LB/CU FT	T AMB DEG R
5	1.00	0	44.16	531.18	1.3493	1305.22	0.01591	0.1423	6.9851	1128.37	0.103246	0.075880	529.83
5	1.00	15	44.32	528.11	1.3507	1302.43	0.01592	0.1424	6.9807	1129.58	0.104070	0.075838	530.97
5	1.00	30	43.85	530.66	1.3499	1305.02	0.01591	0.1423	6.9831	1132.10	0.102552	0.074783	533.34
5	1.00	45	43.91	531.54	1.3508	1306.76	0.01592	0.1424	6.9802	1131.97	0.102434	0.074810	533.22
5	1.00	60	43.68	533.95	1.3485	1308.05	0.0159	0.1423	6.9875	1132.02	0.101671	0.074652	533.26
5	1.00	75	43.58	534.42	1.3478	1308.15	0.0159	0.1423	6.9896	1133.44	0.101416	0.074364	534.60
5	1.00	90	43.75	532.48	1.3491	1306.72	0.01591	0.1423	6.9855	1131.43	0.102045	0.074780	532.71
5	1.00	180	43.81	530.75	1.3482	1303.96	0.0159	0.1423	6.9883	1127.90	0.102615	0.075449	529.39
5	1.00	270	44.12	532.35	1.3508	1307.70	0.01592	0.1424	6.9805	1130.62	0.102768	0.075350	531.95
AVERAGE	VALUES		43.91	531.72	1.3495	1306.00	0.01591	0.1423	6.9845	1130.83	0.102535	0.075101	532.14
STANDARD	DEVIATION		0.23	1.80	0.0011	1.90				1.73	0.000757		1.66

Table I Continued. - Rectangular Jet Flow Properties

NOZZLE	PRESSURE RATIO	AZIMUTH ANGLE	PTOTAL PSIA	TTOTAL DEG R	MACH NUMBER	VJET FT/S	JET AREA SQ FT	JET DIAM FT	ASPECT RATIO	C AMB FT/S	RHO JET LB/CU FT	RHO AMB LB/CU FT	T AMB DEG R
5	1.25	0	55.13	530.66	1.5054	1410.21	0.01724	0.1481	6.4453	1128.81	0.110129	0.075840	530.25
5	1.25	15	55.37	527.42	1.5072	1407.06	0.01726	0.1482	6.4385	1130.11	0.111075	0.075793	531.46
5	1.25	30	54.88	530.19	1.5083	1411.40	0.01727	0.1483	6.4347	1132.23	0.109394	0.074725	533.46
5	1.25	45	54.76	531.28	1.5063	1411.59	0.01725	0.1482	6.4421	1132.07	0.109154	0.074797	533.31
5	1.25	60	54.69	533.58	1.5067	1414.87	0.01725	0.1482	6.4407	1132.00	0.108508	0.074674	533.24
5	1.25	75	54.49	534.77	1.5053	1415.58	0.01724	0.1481	6.4457	1133.77	0.108032	0.074320	534.91
5	1.25	90	54.67	533.07	1.5063	1413.96	0.01725	0.1482	6.4421	1131.83	0.108627	0.074718	533.08
5	1.25	180	54.78	530.90	1.5057	1410.71	0.01724	0.1482	6.4442	1128.06	0.109336	0.075419	529.54
5	1.25	270	55.04	532.84	1.5066	1413.84	0.01725	0.1482	6.4410	1130.62	0.109362	0.075344	531.95
AVERAGE	VALUES		54.87	531.63	1.5064	1412.14	0.01725	0.1482	6.4416	1131.06	0.109291	0.075070	532.35
STANDARD	DEVIATION		0.25	2.06	0.0008	2.60				1.77	0.000855		1.62

NOZZLE	PRESSURE RATIO	AZIMUTH ANGLE	PTOTAL PSIA	TTOTAL DEG R	MACH NUMBER	VJET FT/S	JET AREA SQ FT	JET DIAM FT	ASPECT RATIO	C AMB FT/S	RHO JET LB/CU FT	RHO AMB LB/CU FT	T AMB DEG R
5	1.45	0	64.06	532.33	1.6082	1476.67	0.01836	0.1529	6.0503	1129.08	0.114542	0.075753	530.49
5	1.45	15	64.23	530.35	1.6081	1473.86	0.01836	0.1529	6.0507	1131.21	0.115283	0.075677	532.50
5	1.45	30	63.54	529.89	1.6081	1473.24	0.01836	0.1529	6.0505	1132.29	0.114144	0.074720	533.52
5	1.45	45	63.66	530.62	1.6089	1474.72	0.01837	0.153	6.0475	1132.22	0.114096	0.074777	533.45
5	1.45	60	63.44	532.83	1.6080	1477.26	0.01836	0.1529	6.0510	1132.14	0.113348	0.074636	533.37
5	1.45	75	63.27	534.77	1.6075	1479.63	0.01836	0.1529	6.0530	1133.86	0.112689	0.074262	534.99
5	1.45	90	63.50	533.31	1.6086	1478.28	0.01837	0.1529	6.0487	1131.97	0.113277	0.074658	533.22
5	1.45	180	63.64	529.98	1.6083	1473.48	0.01837	0.1529	6.0498	1128.41	0.114283	0.075334	529.86
5	1.45	270	64.02	532.89	1.6095	1478.27	0.01838	0.153	6.0450	1130.61	0.114179	0.075345	531.93
AVERAGE	VALUES		63.71	531.88	1.6084	1476.16	0.01837	0.1529	6.0496	1131.31	0.113982	0.075018	532.59
STANDARD	DEVIATION		0.30	1.62	0.0007	2.18				1.54	0.000727		1.51

TABLE II. - Number of Tones in Cold Flow Rectangular Jet Microphone Data

NOZZLE	PRESSURE RATIO	AZIMUTH DIRECTIVITY ANGLE, DEGREES								
		0	15	30	45	60	75	90	180	270
1	0.65	NONE	NONE	NONE	NONE	NONE	NONE	NONE	NONE	NONE
3	0.65	NONE	NONE	NONE	NONE	NONE	NONE	NONE	NONE	NONE
4	0.65	NONE	NONE	NONE	NONE	NONE	NONE	NONE	NONE	NONE
5	0.65	NONE	NONE	NONE	NONE	NONE	NONE	NONE	NONE	NONE
1	0.85	NONE	NONE	NONE	NONE	NONE	NONE	NONE	NONE	NONE
3	0.85	4-6	3-5	3-5	2-4	1-3	1-3	1-2	4-6	1-3
4	0.85	5-10	4-9	3-7	4-6	3-5	2-4	2-4	4-9	2-4
5	0.85	6-9	4-9	5-9	2-6	2-5	2-4	2-5	6-9	3-5
1	1.00	NONE	NONE	NONE	NONE	NONE	NONE	NONE	NONE	NONE
3	1.00	0-2	1-2	0-2	1-2	0-2	0-1	NONE	0-2	0-1
4	1.00	1-3	0-2	0-2	1-3	0-2	0-1	0-1	0-2	0-1
5	1.00	4-11	3-6	2-6	2-4	1-4	1-3	0-3	3-10	2-3
1	1.25	NONE	NONE	NONE	NONE	NONE	NONE	NONE	NONE	NONE
3	1.25	1-6	1-4	1-4	1-3	0-3	0-2	0-3	1-5	0-2
4	1.25	9-13	8-13	6-11	3-7	3-7	2-5	2-5	9-13	2-6
5	1.25	7-12	7-10	5-8	4-6	2-6	2-5	2-5	7-16	2-6
1	1.45	NONE	NONE	NONE	NONE	NONE	NONE	NONE	NONE	NONE
3	1.45	1-8	1-8	1-7	1-7	1-5	1-4	0-4	2-9	1-3
4	1.45	3-12	2-8	2-6	2-5	1-5	1-4	1-4	3-7	0
5	1.45	11-19	10-19	8-19	4-11	4-10	3-6	2-5	11-19	3-6

TABLE III. Spectra Summation Values For Selected Test Points

NOZZLE 1 PRESSURE RATIO = 1.00 ASPECT RATIO = 1.5379

29 ONE-THIRD OCTAVE BAND FREQUENCIES

POLAR DIRECTIVITY ANGLE	AZIMUTH DIRECTIVITY ANGLE, DEGREES								
	0	15	30	45	60	75	90	180	270
60	1.0244	1.0253	1.0253	1.0251	1.0241	1.0247	1.0230	1.0263	1.0253
70	1.0244	1.0260	1.0263	1.0264	1.0255	1.0258	1.0240	1.0269	1.0262
80	1.0254	1.0261	1.0271	1.0276	1.0266	1.0269	1.0260	1.0273	1.0273
90	1.0260	1.0266	1.0267	1.0280	1.0272	1.0267	1.0270	1.0275	1.0278
100	1.0259	1.0262	1.0256	1.0276	1.0265	1.0259	1.0271	1.0272	1.0281
110	1.0259	1.0259	1.0236	1.0269	1.0254	1.0244	1.0257	1.0271	1.0270
120	1.0262	1.0267	1.0216	1.0253	1.0233	1.0237	1.0239	1.0280	1.0261
130	1.0681	1.0540	1.0423	1.0413	1.0590	1.0788	1.0776	1.0781	1.0835
140	0.9574	0.9532	0.9324	0.9285	0.9417	0.9624	0.9628	0.9768	0.9707
150	0.9208	0.9229	0.9132	0.9114	0.9055	0.9001	0.8984	0.9326	0.9027
160	1.1690	1.1703	1.2434	1.2547	1.2686	1.2337	1.2185	1.1324	1.1848

NOZZLE 5 PRESSURE RATIO = 1.00 ASPECT RATIO = 6.9845

29 ONE-THIRD OCTAVE BAND FREQUENCIES

POLAR DIRECTIVITY ANGLE	AZIMUTH DIRECTIVITY ANGLE, DEGREES								
	0	15	30	45	60	75	90	180	270
60	1.1888	1.1908	1.1965	1.1976	1.2076	1.2166	1.2094	1.1934	1.2117
70	1.1875	1.1893	1.1938	1.1948	1.2071	1.2168	1.2089	1.1835	1.2130
80	1.1861	1.1877	1.1924	1.1946	1.2056	1.2118	1.2060	1.1798	1.2096
90	1.1858	1.1862	1.1913	1.1950	1.2034	1.2028	1.2003	1.1823	1.2028
100	1.1921	1.1892	1.1915	1.1977	1.1997	1.1912	1.1922	1.1914	1.1934
110	1.2144	1.2023	1.1968	1.2062	1.1948	1.1797	1.1849	1.2086	1.1845
120	1.2660	1.2358	1.2140	1.2239	1.1885	1.1735	1.1815	1.2371	1.1809
130	1.0792	1.0818	1.0526	1.0085	1.0220	1.0341	1.0038	1.0970	1.0177
140	1.0165	1.0210	1.0252	0.9894	1.0047	1.0221	1.0087	1.0304	1.0219
150	0.9835	0.9813	0.9860	0.9870	0.9845	0.9873	0.9901	0.9878	0.9945
160	1.0727	1.0689	1.0738	1.0193	0.9838	0.9644	0.9703	1.0586	0.9652

TABLE III Continued. - Spectra Summation Values for Selected Test Points

NOZZLE 4 PRESSURE RATIO = 0.85 ASPECT RATIO = 5.5754

29 ONE-THIRD OCTAVE BAND FREQUENCIES

POLAR DIRECTIVITY ANGLE	AZIMUTH DIRECTIVITY ANGLE, DEGREES								
	0	15	30	45	60	75	90	180	270
60	1.0415	1.0405	1.0405	1.0391	1.0383	1.0384	1.0406	1.0407	1.0418
70	1.0483	1.0476	1.0457	1.0407	1.0388	1.0405	1.0427	1.0491	1.0426
80	1.0458	1.0460	1.0442	1.0402	1.0394	1.0421	1.0416	1.0476	1.0410
90	1.0346	1.0367	1.0374	1.0375	1.0396	1.0407	1.0380	1.0361	1.0361
100	1.0197	1.0241	1.0293	1.0345	1.0403	1.0383	1.0331	1.0203	1.0312
110	1.0103	1.0169	1.0258	1.0359	1.0406	1.0358	1.0311	1.0108	1.0299
120	1.0186	1.0252	1.0358	1.0458	1.0420	1.0379	1.0386	1.0250	1.0409
130	0.9296	0.9163	0.9350	0.9419	0.9746	0.9947	1.0114	0.9131	1.0121
140	0.8825	0.8882	0.8976	0.9259	0.9723	0.9790	0.9843	0.8598	0.9841
150	0.9309	0.9420	0.9454	0.9608	0.9802	0.9736	0.9703	0.9269	0.9740
160	1.2364	1.1789	1.2028	1.1293	1.0385	1.0301	1.0230	1.2903	1.0383

NOZZLE 5 PRESSURE RATIO = 1.45 ASPECT RATIO = 6.0496

29 ONE-THIRD OCTAVE BAND FREQUENCIES

POLAR DIRECTIVITY ANGLE	AZIMUTH DIRECTIVITY ANGLE, DEGREES								
	0	15	30	45	60	75	90	180	270
60	1.0365	1.0333	1.0204	1.0094	1.0082	1.0114	1.0110	1.0446	1.0061
70	1.0372	1.0357	1.0245	1.0170	1.0150	1.0158	1.0156	1.0461	1.0120
80	1.0410	1.0402	1.0326	1.0330	1.0279	1.0209	1.0199	1.0482	1.0208
90	1.0445	1.0462	1.0408	1.0495	1.0378	1.0248	1.0230	1.0515	1.0267
100	1.0475	1.0524	1.0463	1.0616	1.0398	1.0258	1.0240	1.0550	1.0284
110	1.0506	1.0577	1.0469	1.0654	1.0340	1.0249	1.0219	1.0589	1.0241
120	1.0524	1.0631	1.0434	1.0612	1.0226	1.0226	1.0187	1.0665	1.0160
130	0.9915	0.9331	1.0215	1.0809	1.1335	1.1097	1.1116	0.9764	1.0905
140	0.9288	0.9185	0.9702	0.9669	1.0141	1.0027	0.9946	0.9384	0.9828
150	0.9412	0.9535	0.9561	0.9318	0.9319	0.9369	0.9245	0.9513	0.9336
160	1.1422	1.1057	1.0911	1.1918	1.1410	1.1713	1.1963	1.0995	1.2140

TABLE IV. Revised Measured Overall Sound Pressure Levels

NOZZLE 1 PRESSURE RATIO = 1.00 ASPECT RATIO = 1.5379

POLAR DIRECTIVITY ANGLE	REVISED OASPL VALUES, dB AZIMUTH DIRECTIVITY ANGLE, DEGREES								
	0	15	30	45	60	75	90	180	270
60	119.39	119.68	119.20	119.12	118.65	118.61	118.43	119.56	118.28
70	119.95	120.03	119.72	119.64	119.27	119.24	119.25	120.13	119.10
80	120.69	120.63	120.46	120.40	120.09	120.03	120.21	120.80	120.02
90	121.58	121.48	121.42	121.37	121.13	121.00	121.30	121.57	121.04
100	122.64	122.58	122.60	122.57	122.37	122.13	122.53	122.44	122.16
110	123.86	123.92	123.99	124.00	123.83	123.43	123.89	123.40	123.38
120	125.25	125.52	125.60	125.65	125.49	124.91	125.39	124.45	124.69
130	127.96	128.21	128.41	128.88	129.34	129.44	129.94	127.81	129.28
140	130.19	130.54	130.80	131.51	132.26	132.62	133.12	130.29	132.61
150	132.35	132.76	132.99	133.96	134.86	135.38	135.86	132.66	135.68
160	134.43	134.88	134.98	136.22	137.15	137.70	138.15	134.92	138.50

NOZZLE 5 PRESSURE RATIO = 1.00 ASPECT RATIO = 6.9845

POLAR DIRECTIVITY ANGLE	REVISED OASPL VALUES, dB AZIMUTH DIRECTIVITY ANGLE, DEGREES								
	0	15	30	45	60	75	90	180	270
60.00	105.20	105.75	106.33	106.56	106.99	107.24	107.32	106.24	107.64
70.00	106.26	106.66	107.06	107.14	107.64	107.96	108.10	107.27	108.49
80.00	107.58	107.80	108.03	108.00	108.47	108.73	108.96	108.43	109.34
90.00	109.14	109.16	109.22	109.16	109.45	109.55	109.89	109.72	110.21
100.00	110.97	110.76	110.66	110.61	110.60	110.41	110.89	111.13	111.08
110.00	113.04	112.59	112.32	112.35	111.92	111.32	111.97	112.68	111.97
120.00	115.37	114.64	114.22	114.39	113.40	112.29	113.12	114.35	112.86
130.00	118.79	118.41	118.19	116.76	116.70	115.98	116.43	118.27	116.53
140.00	120.29	120.05	119.94	118.47	118.32	117.70	117.97	120.00	118.19
150.00	120.51	120.30	120.03	119.43	119.09	118.54	118.61	120.58	118.88
160.00	119.45	119.16	118.46	119.65	118.99	118.48	118.35	120.00	118.59

TABLE IV Continued. - Revised Measured Overall Sound Pressure Levels

NOZZLE 4 PRESSURE RATIO = 0.85 ASPECT RATIO = 5.5754

POLAR DIRECTIVITY ANGLE	REVISED OASPL VALUES, dB AZIMUTH DIRECTIVITY ANGLE, DEGREES								
	0	15	30	45	60	75	90	180	270
60	107.58	107.81	107.11	107.51	107.97	108.55	108.67	107.72	108.72
70	108.73	108.94	108.22	108.41	108.94	109.51	109.66	108.64	109.78
80	110.04	110.21	109.49	109.52	110.00	110.49	110.61	109.81	110.73
90	111.50	111.64	110.93	110.85	111.16	111.48	111.52	111.23	111.57
100	113.12	113.22	112.54	112.39	112.41	112.49	112.41	112.90	112.30
110	114.89	114.95	114.31	114.15	113.75	113.52	113.26	114.81	112.91
120	116.81	116.83	116.25	116.12	115.18	114.56	114.07	116.98	113.41
130	118.44	117.94	117.70	117.57	117.56	117.69	117.44	118.79	116.97
140	118.99	118.57	118.44	118.55	118.89	119.16	118.97	119.34	118.49
150	118.49	118.35	118.33	118.85	119.54	119.75	119.66	118.72	119.15
160	116.92	117.28	117.38	118.47	119.51	119.44	119.51	116.90	118.97

NOZZLE 5 PRESSURE RATIO = 1.45 ASPECT RATIO = 6.0496

POLAR DIRECTIVITY ANGLE	REVISED OASPL VALUES, dB AZIMUTH DIRECTIVITY ANGLE, DEGREES								
	0	15	30	45	60	75	90	180	270
60	118.16	118.24	118.16	117.96	117.72	116.98	116.88	118.03	117.19
70	118.97	119.05	119.13	118.94	118.83	118.08	118.01	119.07	118.17
80	119.91	120.00	120.16	119.96	119.94	119.22	119.18	120.18	119.24
90	120.98	121.06	121.26	121.04	121.03	120.42	120.39	121.36	120.39
100	122.19	122.25	122.42	122.16	122.12	121.65	121.64	122.61	121.64
110	123.54	123.56	123.65	123.33	123.21	122.93	122.93	123.93	122.97
120	125.03	125.00	124.95	124.55	124.29	124.26	124.26	125.31	124.38
130	125.65	125.67	126.01	127.13	127.78	127.85	128.13	125.72	127.94
140	124.73	124.93	125.49	127.02	128.23	128.60	129.00	124.79	128.79
150	122.45	122.94	123.56	125.13	126.82	127.55	128.00	122.54	127.96
160	118.81	119.70	120.21	121.46	123.54	124.71	125.13	118.96	125.44

TABLE V. Corrected Overall Sound Pressure Levels

NOZZLE 1 PRESSURE RATIO = 1.00 ASPECT RATIO = 1.5379

29 ONE-THIRD OCTAVE BAND FREQUENCIES

POLAR DIRECTIVITY ANGLE	REVISED OASPL VALUES, dB AZIMUTH DIRECTIVITY ANGLE, DEGREES								
	0	15	30	45	60	75	90	180	270
60	119.49	119.79	119.31	119.23	118.75	118.72	118.53	119.67	118.39
70	120.05	120.14	119.83	119.75	119.38	119.35	119.35	120.25	119.21
80	120.80	120.74	120.58	120.52	120.20	120.15	120.32	120.92	120.14
90	121.69	121.59	121.53	121.49	121.25	121.11	121.42	121.69	121.16
100	122.75	122.69	122.71	122.69	122.48	122.24	122.65	122.56	122.28
110	123.97	124.03	124.09	124.12	123.94	123.53	124.00	123.52	123.50
120	125.36	125.63	125.69	125.76	125.59	125.01	125.49	124.57	124.80
130	128.25	128.44	128.59	129.06	129.59	129.77	130.26	128.14	129.63
140	130.00	130.33	130.50	131.19	132.00	132.45	132.96	130.19	132.48
150	131.99	132.41	132.60	133.56	134.43	134.92	135.39	132.36	135.24
160	135.11	135.56	135.93	137.21	138.18	138.61	139.01	135.46	139.24

NOZZLE 5 PRESSURE RATIO = 1.00 ASPECT RATIO = 6.9845

29 ONE-THIRD OCTAVE BAND FREQUENCIES

POLAR DIRECTIVITY ANGLE	REVISED OASPL VALUES, dB AZIMUTH DIRECTIVITY ANGLE, DEGREES								
	0	15	30	45	60	75	90	180	270
60.00	105.95	106.51	107.11	107.34	107.81	108.09	108.15	107.01	108.47
70.00	107.01	107.41	107.83	107.91	108.46	108.81	108.92	108.00	109.33
80.00	108.32	108.55	108.79	108.77	109.28	109.56	109.77	109.15	110.17
90.00	109.88	109.90	109.98	109.93	110.25	110.35	110.68	110.45	111.01
100.00	111.73	111.51	111.42	111.39	111.39	111.17	111.65	111.89	111.85
110.00	113.88	113.39	113.10	113.16	112.69	112.04	112.71	113.50	112.71
120.00	116.39	115.56	115.06	115.27	114.15	112.98	113.84	115.27	113.58
130.00	119.12	118.75	118.41	116.80	116.79	116.13	116.45	118.67	116.61
140.00	120.36	120.14	120.05	118.42	118.34	117.79	118.01	120.13	118.28
150.00	120.44	120.22	119.97	119.37	119.02	118.48	118.57	120.53	118.86
160.00	119.75	119.45	118.77	119.73	118.92	118.32	118.22	120.25	118.44

TABLE V Continued. - Corrected Overall Sound Pressure Levels

NOZZLE 4 PRESSURE RATIO = 0.85 ASPECT RATIO = 5.5754

29 0NE-THIRD OCTAVE BAND FREQUENCIES

POLAR DIRECTIVITY ANGLE	REVISED OASPL VALUES, dB AZIMUTH DIRECTIVITY ANGLE, DEGREES								
	0	15	30	45	60	75	90	180	270
60	107.76	107.98	107.28	107.68	108.13	108.71	108.84	107.89	108.90
70	108.94	109.14	108.41	108.58	109.11	109.68	109.84	108.85	109.96
80	110.23	110.41	109.68	109.69	110.17	110.67	110.79	110.01	110.90
90	111.65	111.80	111.09	111.01	111.33	111.65	111.68	111.38	111.72
100	113.20	113.32	112.67	112.54	112.58	112.65	112.55	112.99	112.43
110	114.93	115.02	114.42	114.30	113.92	113.67	113.39	114.86	113.04
120	116.89	116.94	116.40	116.31	115.36	114.72	114.23	117.09	113.58
130	118.12	117.56	117.41	117.31	117.45	117.67	117.49	118.40	117.02
140	118.45	118.06	117.97	118.22	118.77	119.07	118.90	118.68	118.42
150	118.18	118.09	118.09	118.68	119.45	119.63	119.53	118.39	119.04
160	117.84	117.99	118.18	119.00	119.67	119.57	119.61	118.01	119.13

NOZZLE 5 PRESSURE RATIO = 1.45 ASPECT RATIO = 6.0496

29 0NE-THIRD OCTAVE BAND FREQUENCIES

POLAR DIRECTIVITY ANGLE	REVISED OASPL VALUES, dB AZIMUTH DIRECTIVITY ANGLE, DEGREES								
	0	15	30	45	60	75	90	180	270
60	118.32	118.38	118.25	118.32	117.76	117.03	116.93	118.22	117.22
70	119.13	119.20	119.24	119.01	118.89	118.15	118.08	119.27	118.22
80	120.08	120.17	120.30	120.10	120.06	119.31	119.27	120.38	119.33
90	121.17	121.26	121.43	121.25	121.19	120.53	120.49	121.58	120.50
100	122.39	122.47	122.62	122.42	122.29	121.76	121.74	122.84	121.76
110	123.75	123.80	123.85	123.60	123.36	123.04	123.02	124.18	123.07
120	125.25	125.27	125.13	124.81	124.39	124.36	124.34	125.59	124.45
130	125.61	125.37	126.10	127.47	128.32	128.30	128.59	125.62	128.32
140	124.41	124.56	125.36	126.87	128.29	128.61	128.98	124.51	128.71
150	122.19	122.73	123.36	124.82	126.51	127.27	127.66	122.32	127.66
160	119.39	120.14	120.59	122.22	124.11	125.40	125.91	119.37	126.28

TABLE VI. Computation of Overall Power Levels
Pressure Ratio = 0.65

NOZZLE FLOW PROPERTIES				
Rectangular Nozzle	Nozzle 1	Nozzle 3	Nozzle 4	Nozzle 5
Aspect Ratio	1.8721	3.6992	5.7959	7.6028
Jet Velocity, ft/s	1282.02	1053.92	1043.90	1045.12
Jet Exit Area, sq ft	0.05935	0.03004	0.01917	0.01461

OVERALL POWER LEVELS COMPUTED FROM INTEGRATION OF OASPLS				
Computed from Measured OASPL Data at Polar Directivity Angles from 60 to 160 degrees				
Revised Measured $OAPWL_R$, db, partial sphere	136.17	124.41	122.22	121.19
Corrected $OAPWL_C$, db, partial sphere	136.19	124.39	122.30	121.40
Computed from Predicted OASPL Data at Polar Directivity Angles from 60 to 160 degrees				
SAE predicted $OAPWL_{pred}$, db, circular jet	135.46	123.31	121.28	120.12
Computed from Predicted OASPL Data at Polar Directivity Angles from 0 to 160 degrees				
SAE predicted total, $OAPWL_{ptot}$, dB, circular jet	136.14	124.08	122.05	120.90
$OAPWL_{ptot}$ full sphere - $OAPWL_{pred}$ partial sphere	0.68	0.77	0.77	0.78
$OAPWL_{Ctot}$, full sphere = $OAPWL_C$ partial sphere + ($OAPWL_{ptot}$ full sphere - $OAPWL_{pred}$ partial sphere)				
Corrected total $OAPWL_{Ctot}$, db	136.87	125.16	123.07	122.18

Average Overall Sound Pressure Level Associated with Overall total Corrected Power Level				
Average $OASPL_{Ctot}$	117.73	106.00	103.96	103.10

COMPUTATION OF DIFFERENCE BETWEEN CORRECTED OAPWL AND OAPWL FROM SAE FORMULA				
SAE predicted OAPWL [ref 6 equation]	139.13	127.08	125.06	123.90
SAE predicted OAPWL - Corrected total $OAPWL_{Ctot}$	2.26	1.92	1.99	1.72

TABLE VI. Continued - Computation of Overall Power Levels
Pressure Ratio = 0.85

NOZZLE FLOW PROPERTIES				
Rectangular Nozzle	Nozzle 1	Nozzle 3	Nozzle 4	Nozzle 5
Aspect Ratio	1.6512	3.5586	5.5754	7.3148
Jet Velocity, ft/s	1448.29	1229.00	1217.18	1217.52
Jet Exit Area, sq ft	0.06729	0.03122	0.01993	0.01519

OVERALL POWER LEVELS COMPUTED FROM INTEGRATION OF OASPLS				
Computed from Measured OASPL Data at Polar Directivity Angles from 60 to 160 degrees				
Revised Measured $OAPWL_R$, db, partial sphere	142.91	134.43	132.58	133.88
Corrected $OAPWL_C$, db, partial sphere	142.93	134.31	132.56	133.79
Computed from Predicted OASPL Data at Polar Directivity Angles from 60 to 160 degrees				
SAE predicted $OAPWL_{pred}$, db, circular jet	142.50	130.51	128.50	127.28
Computed from Predicted OASPL Data at Polar Directivity Angles from 0 to 180 degrees				
SAE predicted total, $OAPWL_{ptot}$, dB, circular jet	143.13	131.22	129.20	127.98
$OAPWL_{ptot}$ full sphere - $OAPWL_{pred}$ partial sphere	0.63	0.71	0.70	0.70
$OAPWL_{Ctot}$, full sphere = $OAPWL_C$ partial sphere + ($OAPWL_{ptot}$ full sphere - $OAPWL_{pred}$ partial sphere)				
Corrected total $OAPWL_{Ctot}$, db	143.56	135.02	133.26	134.49

Average Overall Sound Pressure Level Associated with Overall total Corrected Power Level				
Average $OASPL_{Ctot}$	124.41	115.86	114.16	115.41

COMPUTATION OF DIFFERENCE BETWEEN CORRECTED OAPWL AND OAPWL FROM SAE FORMULA				
SAE predicted OAPWL [ref 6 equation]	146.13	134.19	132.20	131.00
SAE predicted OAPWL - Corrected total $OAPWL_{Ctot}$	2.57	-0.83	-1.06	-3.49

TABLE VI. Continued - Computation of Overall Power Levels
Pressure Ratio = 1.00

NOZZLE FLOW PROPERTIES				
Rectangular Nozzle	Nozzle 1	Nozzle 3	Nozzle 4	Nozzle 5
Aspect Ratio	1.5379	3.3972	5.3239	6.9845
Jet Velocity, ft/s	1514.89	1318.11	1305.61	1306.00
Jet Exit Area, sq ft	0.07225	0.03271	0.02087	0.01591

OVERALL POWER LEVELS COMPUTED FROM INTEGRATION OF OASPLS				
Computed from Measured OASPL Data at Polar Directivity Angles from 60 to 160 degrees				
Revised Measured $OAPWL_R$, db, partial sphere	145.33	134.74	132.91	132.08
Corrected $OAPWL_C$, db, partial sphere	145.38	134.79	133.05	132.32
Computed from Predicted OASPL Data at Polar Directivity Angles from 60 to 160 degrees				
SAE predicted $OAPWL_{pred}$, db, circular jet	145.37	134.25	132.24	131.02
Computed from Predicted OASPL Data at Polar Directivity Angles from 0 to 180 degrees				
SAE predicted total, $OAPWL_{ptot}$, dB, circular jet	145.99	134.90	132.90	131.69
$OAPWL_{ptot}$ full sphere - $OAPWL_{pred}$ partial sphere	0.62	0.65	0.66	0.67
$OAPWL_{Ctot}$, full sphere = $OAPWL_C$ partial sphere + ($OAPWL_{ptot}$ full sphere - $OAPWL_{pred}$ partial sphere)				
Corrected total $OAPWL_{Ctot}$, db	146.00	135.44	133.71	132.99

Average Overall Sound Pressure Level Associated with Overall total Corrected Power Level				
Average $OASPL_{Ctot}$	126.85	116.29	114.60	113.89

COMPUTATION OF DIFFERENCE BETWEEN CORRECTED OAPWL AND OAPWL FROM SAE FORMULA				
SAE predicted OAPWL [ref 6 equation]	148.97	137.93	135.90	134.70
SAE predicted OAPWL - Corrected total $OAPWL_{Ctot}$	2.97	2.49	2.19	1.71

TABLE VI. Continued - Computation of Overall Power Levels
Pressure Ratio = 1.25

NOZZLE FLOW PROPERTIES				
Rectangular Nozzle	Nozzle 1	Nozzle 3	Nozzle 4	Nozzle 5
Aspect Ratio	1.3827	3.1344	4.9093	6.4416
Jet Velocity, ft/s	1597.18	1424.65	1412.37	1412.14
Jet Exit Area, sq ft	0.08036	0.03545	0.02263	0.01725

OVERALL POWER LEVELS COMPUTED FROM INTEGRATION OF OASPLS				
Computed from Measured OASPL Data at Polar Directivity Angles from 60 to 160 degrees				
Revised Measured $OAPWL_R$, db, partial sphere	148.20	140.89	139.85	138.64
Corrected $OAPWL_C$, db, partial sphere	148.19	140.79	139.87	138.68
Computed from Predicted OASPL Data at Polar Directivity Angles from 60 to 160 degrees				
SAE predicted $OAPWL_{pred}$, db, circular jet	149.00	138.75	136.74	135.51
Computed from Predicted OASPL Data at Polar Directivity Angles from 0 to 180 degrees				
SAE predicted total, $OAPWL_{ptot}$, dB, circular jet	149.60	139.38	137.38	136.16
$OAPWL_{ptot}$ full sphere - $OAPWL_{pred}$ partial sphere	0.60	0.63	0.64	0.65
$OAPWL_{Ctot}$, full sphere = $OAPWL_C$ partial sphere + ($OAPWL_{ptot}$ full sphere - $OAPWL_{pred}$ partial sphere)				
Corrected total $OAPWL_{Ctot}$, db	148.79	141.42	140.51	139.33

Average Overall Sound Pressure Level Associated with Overall total Corrected Power Level				
Average OASPLCtot	129.64	122.27	121.40	120.24

COMPUTATION OF DIFFERENCE BETWEEN CORRECTED OAPWL AND OAPWL FROM SAE FORMULA				
SAE predicted OAPWL [ref 6 equation]	152.56	142.39	140.40	139.18
SAE predicted OAPWL - Corrected total $OAPWL_{Ctot}$	3.77	0.97	-0.11	-0.15

TABLE VI. Continued - Computation of Overall Power Levels
Pressure Ratio = 1.45

NOZZLE FLOW PROPERTIES				
Rectangular Nozzle	Nozzle 1	Nozzle 3	Nozzle 4	Nozzle 5
Aspect Ratio	1.2825	2.9449	4.6138	6.0496
Jet Velocity, ft/s	1644.56	1487.99	1474.52	1476.16
Jet Exit Area, sq ft	0.08664	0.03773	0.02408	0.01837

OVERALL POWER LEVELS COMPUTED FROM INTEGRATION OF OASPLS				
Computed from Measured OASPL Data at Polar Directivity Angles from 60 to 160 degrees				
Revised Measured $OAPWL_R$, db, partial sphere	149.99	143.96	141.00	141.28
Corrected $OAPWL_C$, db, partial sphere	150.03	143.87	140.98	141.32
Computed from Predicted OASPL Data at Polar Directivity Angles from 60 to 160 degrees				
SAE predicted $OAPWL_{pred}$, db, circular jet	151.08	141.44	139.44	138.27
Computed from Predicted OASPL Data at Polar Directivity Angles from 0 to 180 degrees				
SAE predicted total, $OAPWL_{ptot}$, dB, circular jet	151.67	142.05	142.05	138.89
$OAPWL_{ptot}$ full sphere - $OAPWL_{pred}$ partial sphere	0.59	0.61	2.61	0.62
$OAPWL_{Ctot}$, full sphere = $OAPWL_C$ partial sphere + ($OAPWL_{ptot}$ full sphere - $OAPWL_{pred}$ partial sphere)				
Corrected total $OAPWL_{Ctot}$, db	150.62	144.48	143.59	141.94

Average Overall Sound Pressure Level Associated with Overall total Corrected Power Level				
Average $OASPL_{Ctot}$	131.48	125.33	124.49	122.84

COMPUTATION OF DIFFERENCE BETWEEN CORRECTED OAPWL AND OAPWL FROM SAE FORMULA				
SAE predicted OAPWL [ref 6 equation]	154.64	145.08	145.08	141.90
SAE predicted OAPWL - Corrected total $OAPWL_{Ctot}$	4.02	0.60	1.49	-0.04

TABLE VII. Evaluation of Aspect Ratio and Jet Velocity on Derived Overall Power Level Correction for 20 Test Points

DERIVED OAPWL = 0.1025 * AR**2 - 1.4020 * AR + 4.8902

NOZZLE	PRESSURE RATIO	ASPECT RATIO AR	LOG 10 VJ/CA	MEASURED OAPWL DIFF dB	DERIVED OAPWL dB	DELTA OAPWL DIFF dB
1	0.65	1.8721	0.0516	2.26	2.6248	-0.3648
3	0.65	3.6992	-0.0334	1.92	1.1066	0.8134
4	0.65	5.7959	-0.0340	1.99	0.2077	1.7823
5	0.65	7.6028	-0.0342	1.72	0.1559	1.5641
1	0.85	1.6512	0.1045	2.57	2.8547	-0.2847
3	0.85	3.5586	0.0331	-0.83	1.1991	-2.0291
4	0.85	5.5754	0.0328	-1.06	0.2598	-1.3198
5	0.85	7.3148	0.0321	-3.49	0.1193	-3.6093
1	1.00	1.5379	0.1240	2.97	2.9765	-0.0065
3	1.00	3.3972	0.0637	2.49	1.3103	1.1797
4	1.00	5.3239	0.0631	2.19	0.3314	1.8586
5	1.00	6.9845	0.0625	1.71	0.0983	1.6117
1	1.25	1.3827	0.1469	3.57	3.1476	0.4224
3	1.25	3.1344	0.0975	0.87	1.5028	-0.6328
4	1.25	4.9093	0.0972	-0.36	0.4778	-0.8378
5	1.25	6.4416	0.0964	-0.43	0.1123	-0.5423
1	1.45	1.2825	0.1597	4.02	3.2608	0.7592
3	1.45	2.9449	0.1164	0.60	1.6504	-1.0504
4	1.45	4.6138	0.1160	1.49	0.6037	0.8863
5	1.45	6.0496	0.1156	-0.04	0.1600	-0.2000
				STANDARD DEVIATION =		1.4735

TABLE VIII. Evaluation of Aspect Ratio and Jet Velocity on Derived Overall Power Level Correction for 19 Test Points

DERIVED OAPWL = 0.20156 * AR**2 - 2.0699 * AR + 5.7716

NOZZLE	PRESSURE RATIO	ASPECT RATIO AR	LOG 10 VJ/CA	MEASURED OAPWL DIFF dB	DERIVED OAPWL dB	DELTA OAPWL DIFF dB
1	0.65	1.8721	0.0516	2.26	2.6030	-0.3430
3	0.65	3.6992	-0.0334	1.92	0.8729	1.0471
4	0.65	5.7959	-0.0340	1.99	0.5459	1.4441
5	0.65	7.6028	-0.0342	1.72	1.6857	0.0343
1	0.85	1.6512	0.1045	2.57	2.9034	-0.3334
3	0.85	3.5586	0.0331	-0.83	0.9583	-1.7883
4	0.85	5.5754	0.0328	-1.06	0.4969	-1.5569
1	1.00	1.5379	0.1240	2.97	3.0650	-0.0950
3	1.00	3.3972	0.0637	2.49	1.0661	1.4239
4	1.00	5.3239	0.0631	2.19	0.4649	1.7251
5	1.00	6.9845	0.0625	1.71	1.1476	0.5624
1	1.25	1.3827	0.1469	3.57	3.2949	0.2751
3	1.25	3.1344	0.0975	0.87	1.2640	-0.3940
4	1.25	4.9093	0.0972	-0.36	0.4679	-0.8279
5	1.25	6.4416	0.0964	-0.43	0.8021	-1.2321
1	1.45	1.2825	0.1597	4.02	3.4485	0.5715
3	1.45	2.9449	0.1164	0.60	1.4241	-0.8241
4	1.45	4.6138	0.1160	1.49	0.5123	0.9777
5	1.45	6.0496	0.1156	-0.04	0.6265	-0.6665
				STANDARD DEVIATION =		1.0955

TABLE IX. Average Polar Directivities and Azimuthal Directivities

NOZZLE 1 PRESSURE RATIO = 1.00 ASPECT RATIO = 1.5379

DIRECTIVITY ANGLE DEGREES	POLAR DIRECTIVITY dB	AZIMUTH ANGLE, DEGREES						
		0	15	30	45	60	75	90
		AZIMUTH DIRECTIVITY, dB						
60	-7.73	0.46	0.67	0.19	0.11	-0.37	-0.40	-0.66
70	-7.15	0.45	0.44	0.13	0.05	-0.32	-0.35	-0.42
80	-6.38	0.39	0.27	0.11	0.05	-0.27	-0.32	-0.24
90	-5.43	0.27	0.17	0.11	0.07	-0.17	-0.31	-0.13
100	-4.29	0.09	0.13	0.15	0.13	-0.08	-0.32	-0.10
110	-2.96	-0.14	0.14	0.20	0.23	0.05	-0.36	-0.14
120	-1.45	-0.43	0.23	0.29	0.36	0.19	-0.39	-0.25
130	2.23	-0.89	-0.64	-0.49	-0.02	0.51	0.69	0.86
140	4.48	-1.23	-1.00	-0.83	-0.14	0.67	1.12	1.39
150	6.78	-1.45	-1.22	-1.03	-0.07	0.80	1.29	1.69
160	10.28	-1.84	-1.57	-1.20	0.08	1.05	1.48	2.00

NOZZLE 5 PRESSURE RATIO = 1.00 ASPECT RATIO = 6.9845

DIRECTIVITY ANGLE DEGREES	POLAR DIRECTIVITY dB	AZIMUTH ANGLE, DEGREES						
		0	15	30	45	60	75	90
		AZIMUTH DIRECTIVITY, dB						
60.00	-6.51	-0.90	-0.87	-0.27	-0.04	0.43	0.71	0.93
70.00	-5.74	-0.64	-0.74	-0.32	-0.24	0.31	0.66	0.97
80.00	-4.80	-0.36	-0.54	-0.30	-0.32	0.19	0.47	0.88
90.00	-3.69	-0.04	-0.30	-0.22	-0.27	0.05	0.15	0.64
100.00	-2.40	0.32	0.02	-0.07	-0.10	-0.10	-0.32	0.26
110.00	-0.92	0.72	0.42	0.13	0.19	-0.28	-0.93	-0.26
120.00	0.76	1.18	0.91	0.41	0.62	-0.50	-1.67	-0.94
130.00	3.58	1.42	1.28	0.94	-0.67	-0.68	-1.34	-0.94
140.00	5.13	1.23	1.12	1.03	-0.60	-0.68	-1.23	-0.87
150.00	5.58	1.02	0.75	0.50	-0.10	-0.45	-0.99	-0.75
160.00	5.18	0.93	0.38	-0.30	0.66	-0.15	-0.75	-0.74

TABLE IX Continued. - Average Polar Directivities and Azimuthal Directivities

NOZZLE 4 PRESSURE RATIO = 0.85 ASPECT RATIO = 5.5754

DIRECTIVITY ANGLE DEGREES	POLAR DIRECTIVITY dB	AZIMUTH ANGLE, DEGREES 0	15	30	45	60	75	90
		AZIMUTH DIRECTIVITY, dB						
60	-6.09	-0.24	-0.09	-0.79	-0.39	0.06	0.64	0.80
70	-5.06	-0.21	0.04	-0.69	-0.52	0.01	0.58	0.80
80	-3.93	-0.11	0.18	-0.55	-0.54	-0.06	0.44	0.62
90	-2.72	0.07	0.36	-0.35	-0.43	-0.11	0.21	0.26
100	-1.40	0.33	0.56	-0.09	-0.22	-0.18	-0.11	-0.27
110	0.05	0.69	0.81	0.21	0.09	-0.29	-0.54	-0.99
120	1.64	1.19	1.14	0.60	0.51	-0.44	-1.08	-1.90
130	3.40	0.70	0.00	-0.15	-0.25	-0.11	0.11	-0.30
140	4.31	0.09	-0.41	-0.50	-0.25	0.30	0.60	0.19
150	4.63	-0.50	-0.70	-0.70	-0.11	0.66	0.84	0.50
160	4.65	-0.89	-0.83	-0.63	0.19	0.85	0.76	0.55

NOZZLE 5 PRESSURE RATIO = 1.45 ASPECT RATIO = 6.0496

DIRECTIVITY ANGLE DEGREES	POLAR DIRECTIVITY dB	AZIMUTH ANGLE, DEGREES 0	15	30	45	60	75	90
		AZIMUTH DIRECTIVITY, dB						
60.00	-5.02	0.45	0.56	0.43	0.18	-0.06	-0.79	-0.75
70.00	-4.01	0.37	0.37	0.41	0.18	0.06	-0.68	-0.68
80.00	-2.92	0.31	0.25	0.38	0.18	0.14	-0.61	-0.62
90.00	-1.76	0.30	0.18	0.35	0.17	0.11	-0.55	-0.58
100.00	-0.56	0.34	0.20	0.35	0.14	0.02	-0.51	-0.53
110.00	0.68	0.44	0.28	0.33	0.08	-0.16	-0.48	-0.48
120.00	1.99	0.60	0.44	0.30	-0.02	-0.43	-0.46	-0.43
130.00	4.25	-1.47	-1.72	-0.99	0.38	1.23	1.21	1.36
140.00	3.87	-2.25	-2.15	-1.35	0.16	1.58	1.90	2.13
150.00	2.10	-2.69	-2.21	-1.58	-0.12	1.57	2.33	2.72
160.00	-0.28	-3.18	-2.42	-1.97	-0.34	1.55	2.84	3.53

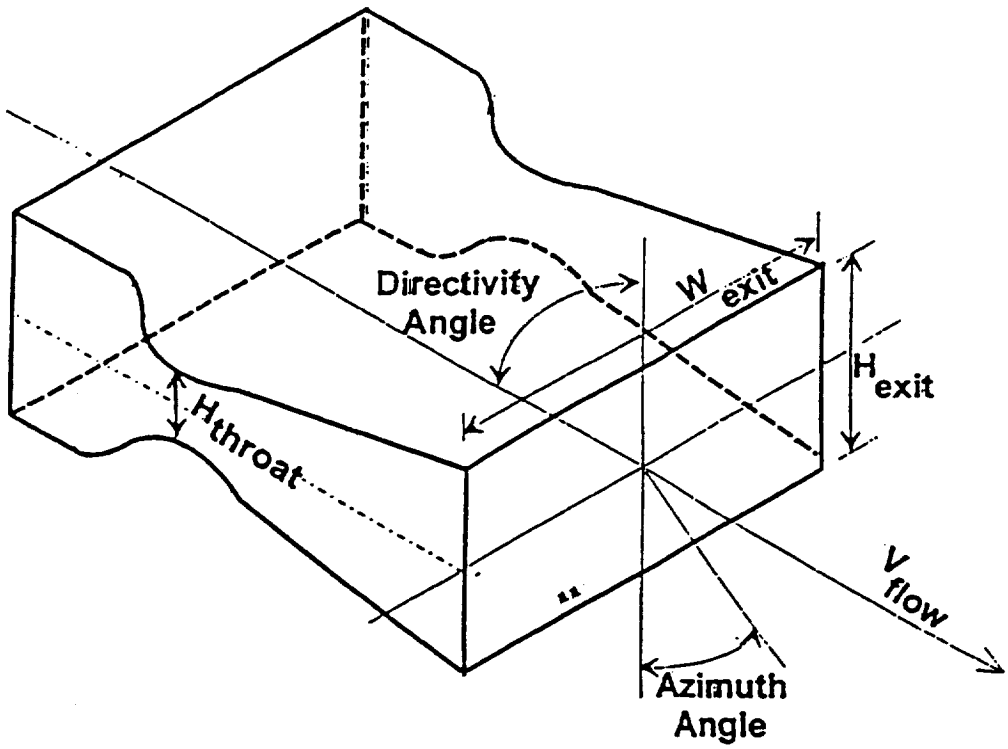

$$\text{Aspect Ratio} = \frac{W_{exit}}{H_{exit}}$$

NOZZLE DIMENSIONS

NOZZLE	W exit in.	H exit in.	H throat in.	Aspect Ratio
1	4.00	2.600	2.000	1.5385
3	4.00	1.177	1.081	3.3985
4	4.00	0.751	0.690	5.3262
5	4.00	0.573	0.527	6.9808

Figure 1. - Rectangular Jet Nozzle Configurations

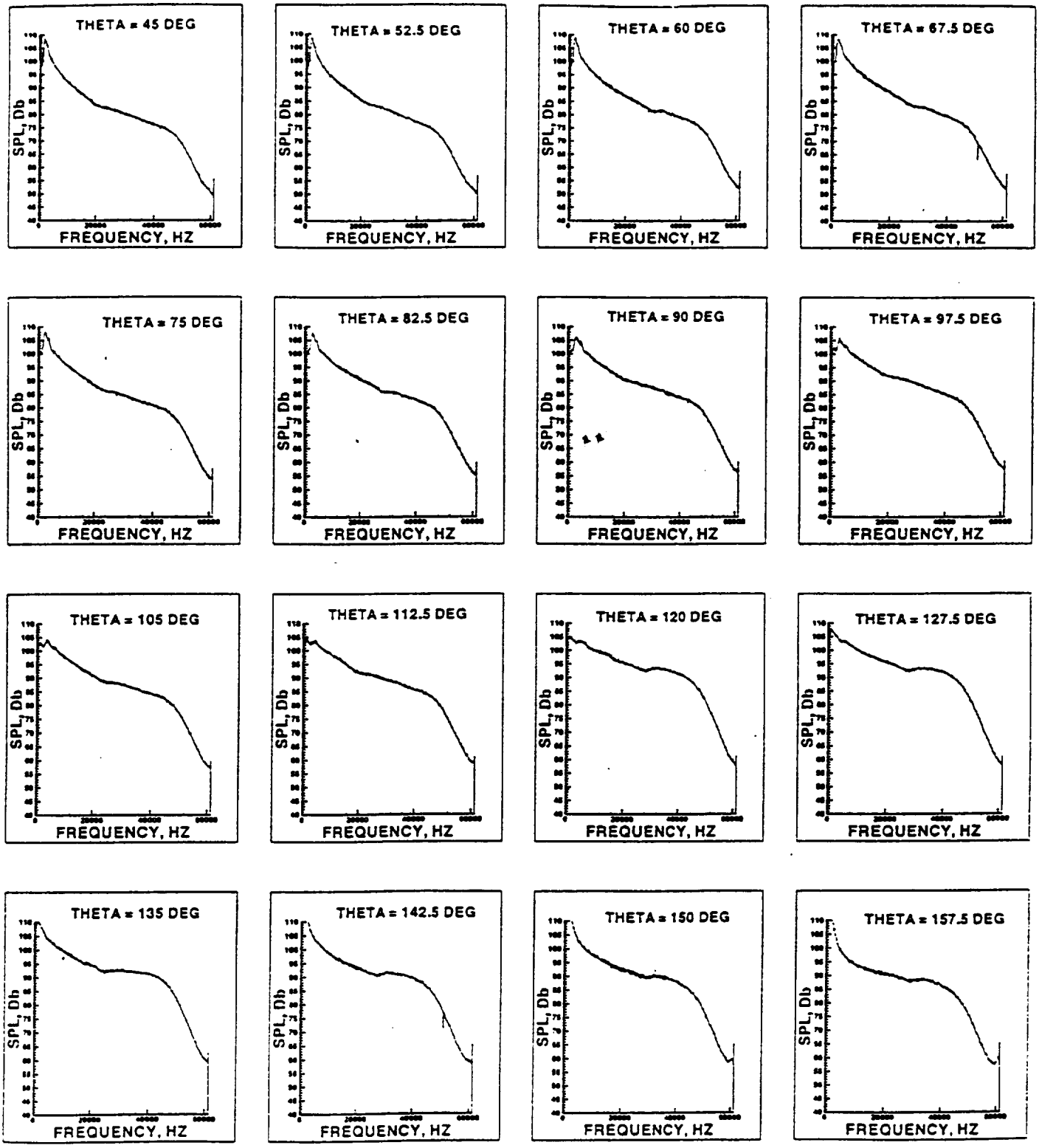

Figure 2. – Measured Narrow Band Spectra at 12 Foot Radius for 0 Degrees Azimuth Angle and 16 Polar Directivity Angles.

a. Nozzle 1, Pexit/Pambient = 1.00

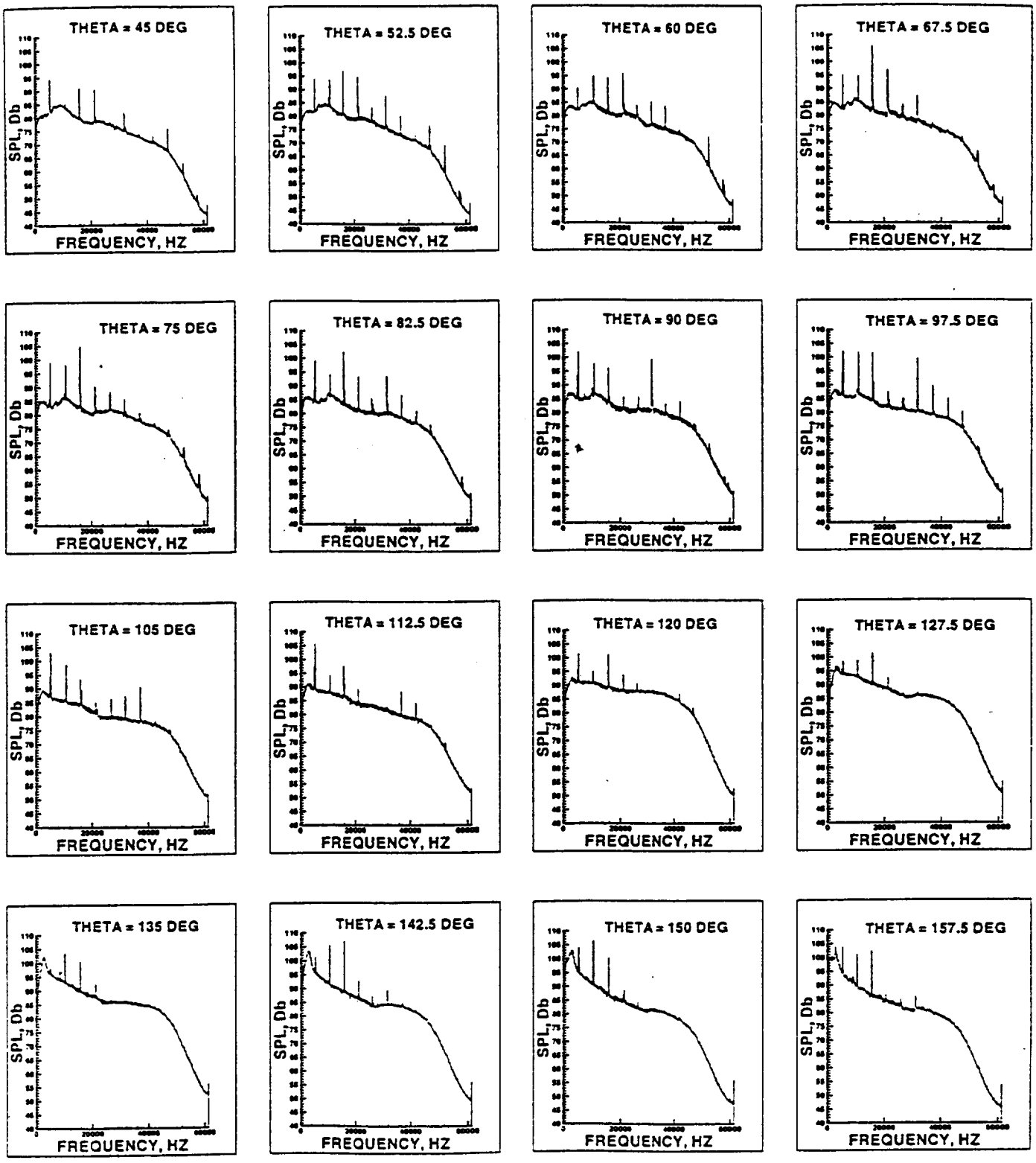

Figure 2 Continued. – Measured Narrow Band Spectra at 12 Foot Radius for 0 Degrees Azimuth Angle and 16 Polar Directivity Angles.

b. Nozzle 5, Pexit/Pambient = 1.00

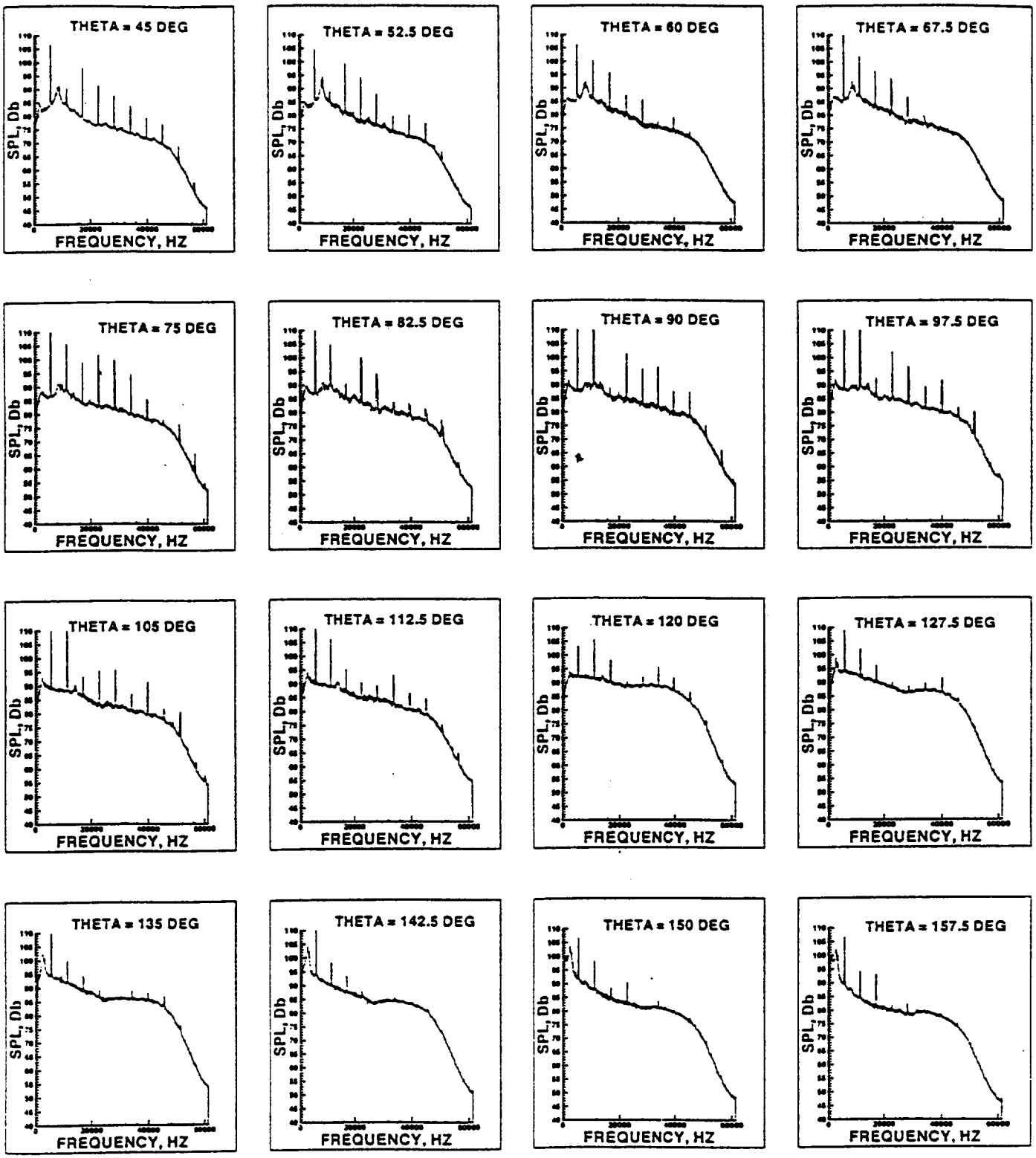

Figure 2 Continued. – Measured Narrow Band Spectra at 12 Foot Radius for 0 Degrees Azimuth Angle and 16 Polar Directivity Angles.

c. Nozzle 4, Pexit/Pambient = 0.85

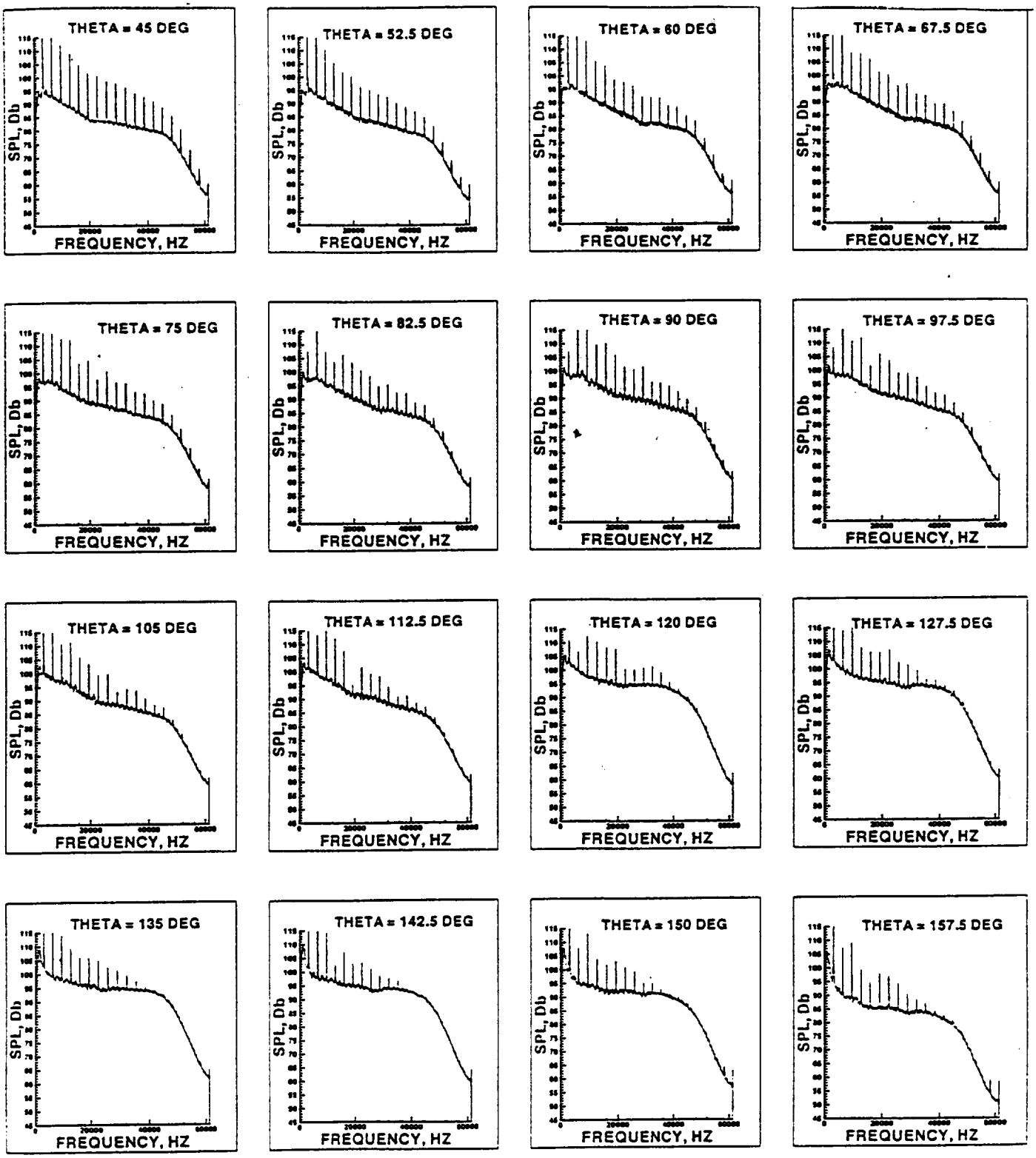

Figure 2 Continued. – Measured Narrow Band Spectra at 12 Foot Radius for 0 Degrees Azimuth Angle and 16 Polar Directivity Angles.

d. Nozzle 5, Pexit/Pambient = 1.45

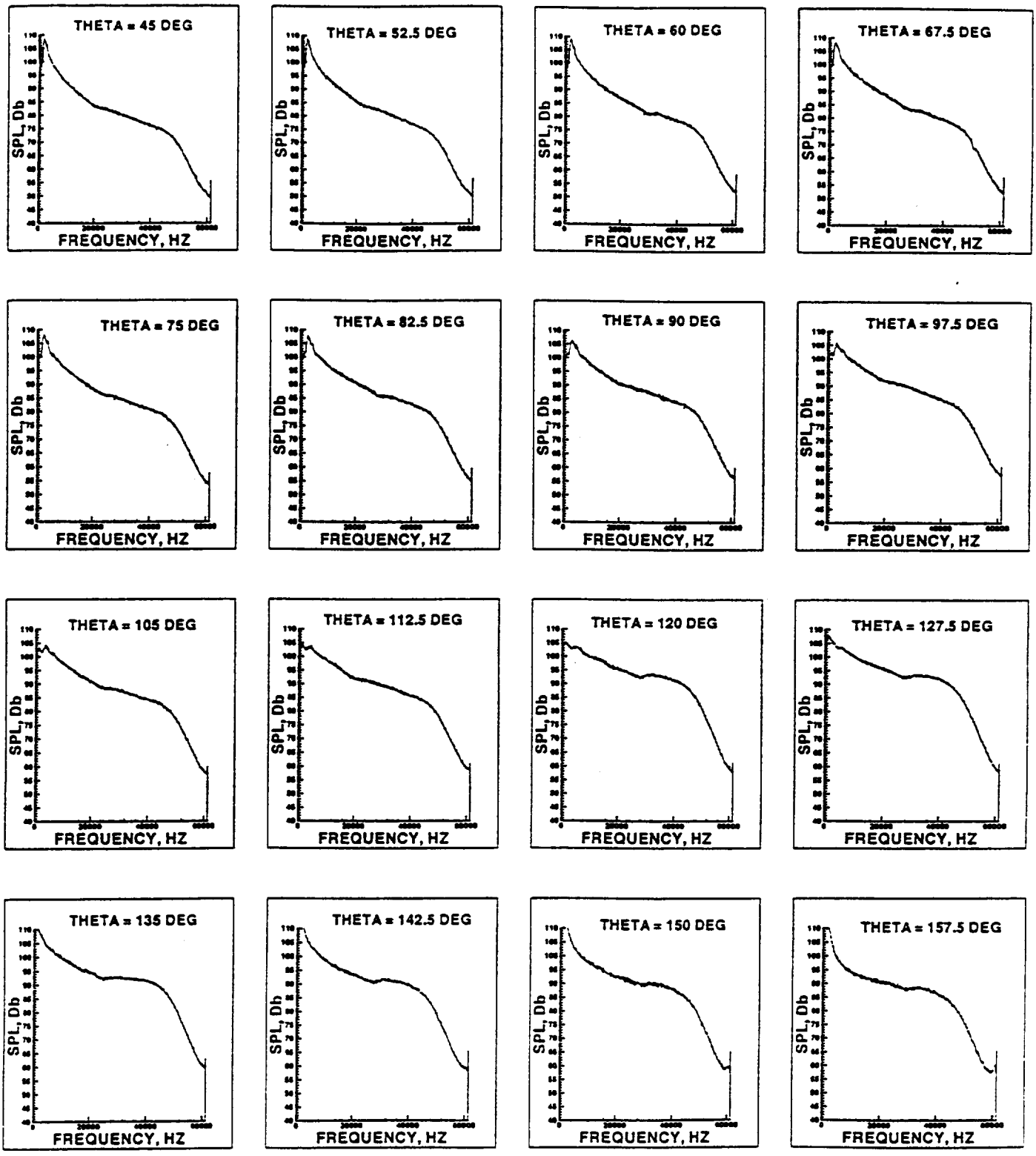

Figure 3. – Smoothed Narrow Band Spectra at 12 Foot Radius for 0 Degrees Azimuth Angle and 16 Polar Directivity Angles.

a. Nozzle 1, Pexit/Pambient = 1.00

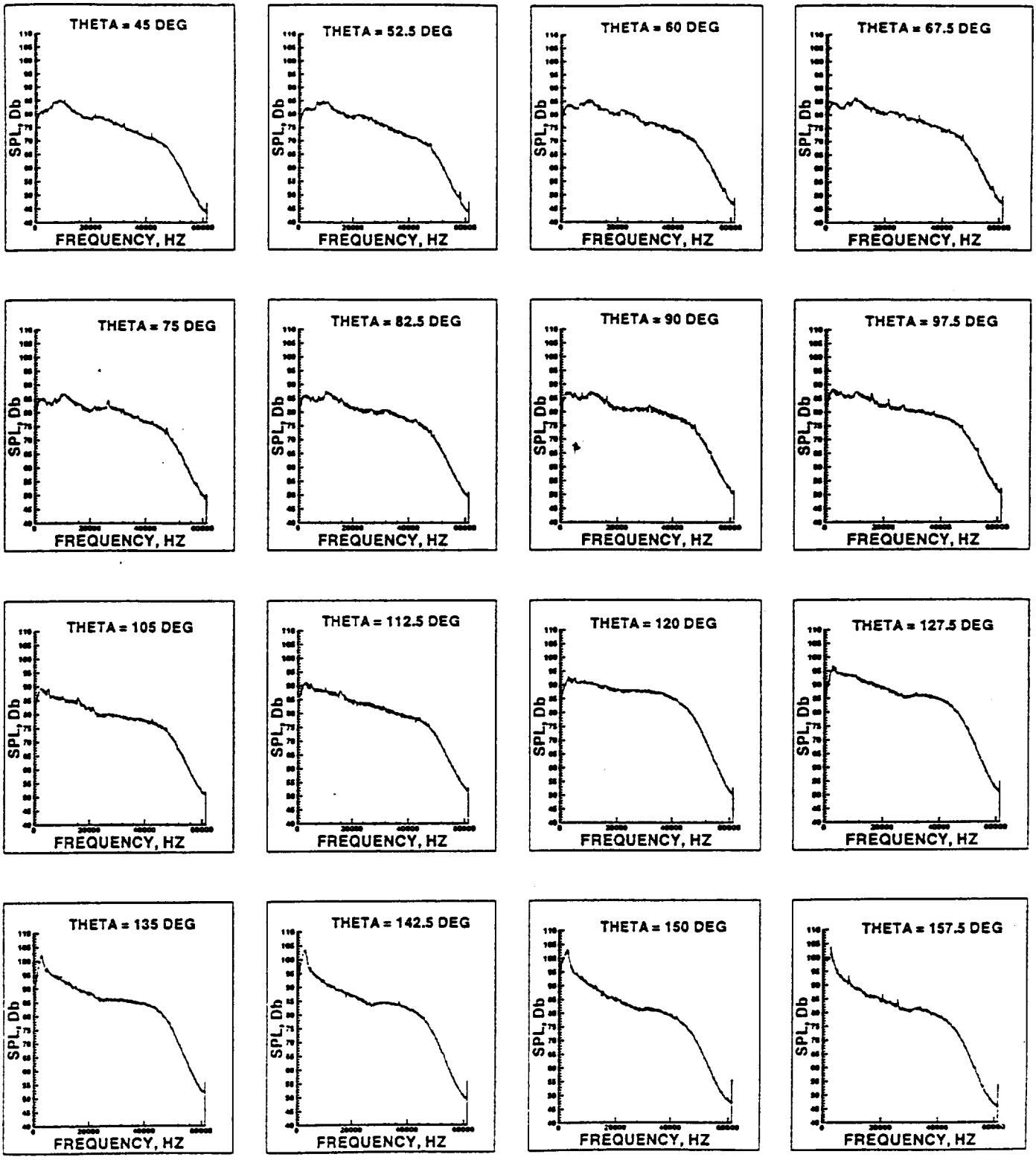

Figure 3 Continued. – Smoothed Narrow Band Spectra at 12 Foot Radius for 0 Degrees Azimuth Angle and 16 Polar Directivity Angles.

b. Nozzle 5, Pexit/Pambient = 1.00

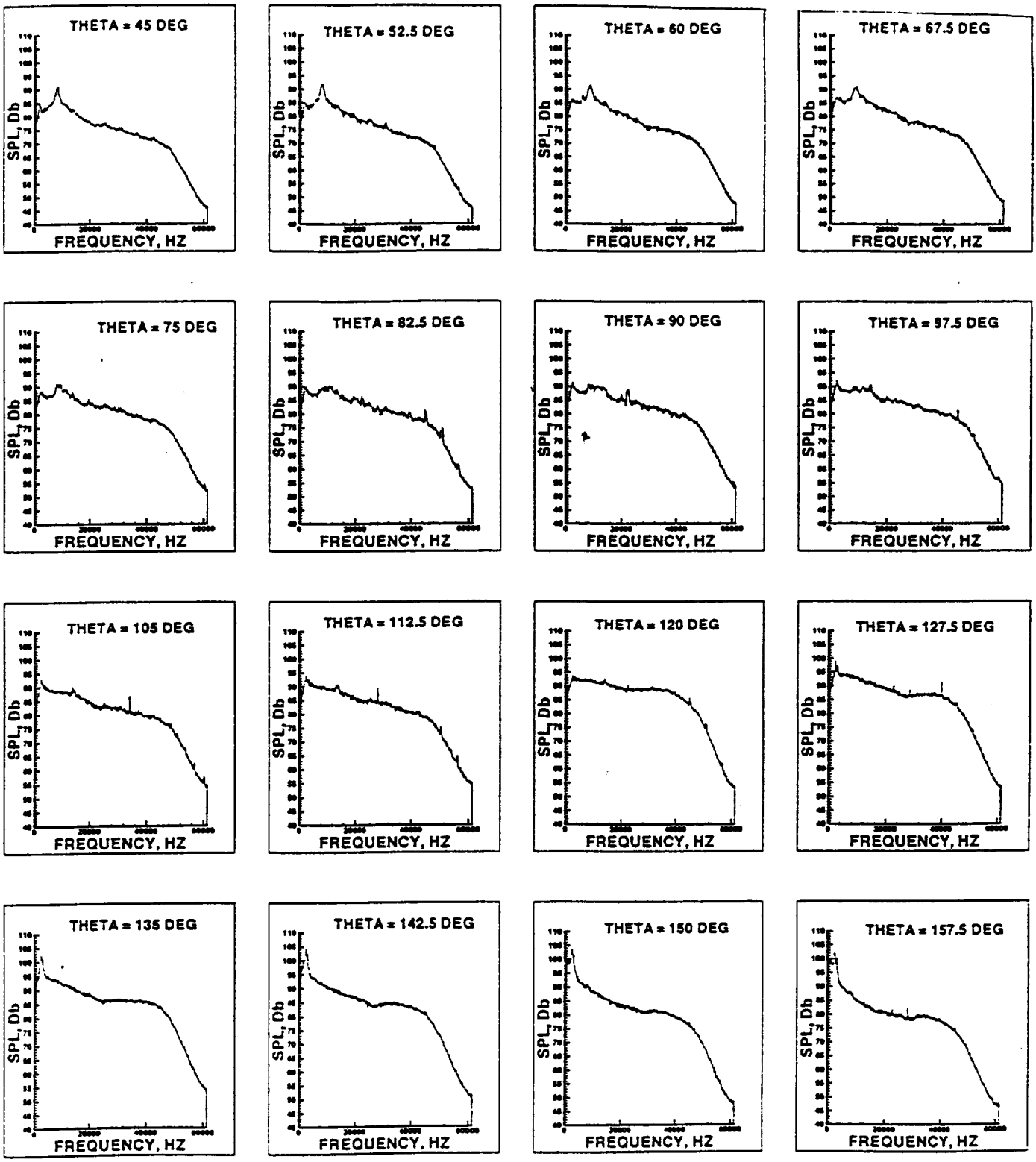

Figure 3 Continued. – Smoothed Narrow Band Spectra at 12 Foot Radius for 0 Degrees Azimuth Angle and 16 Polar Directivity Angles.

c. Nozzle 4, Pexit/Pambient = 0.85

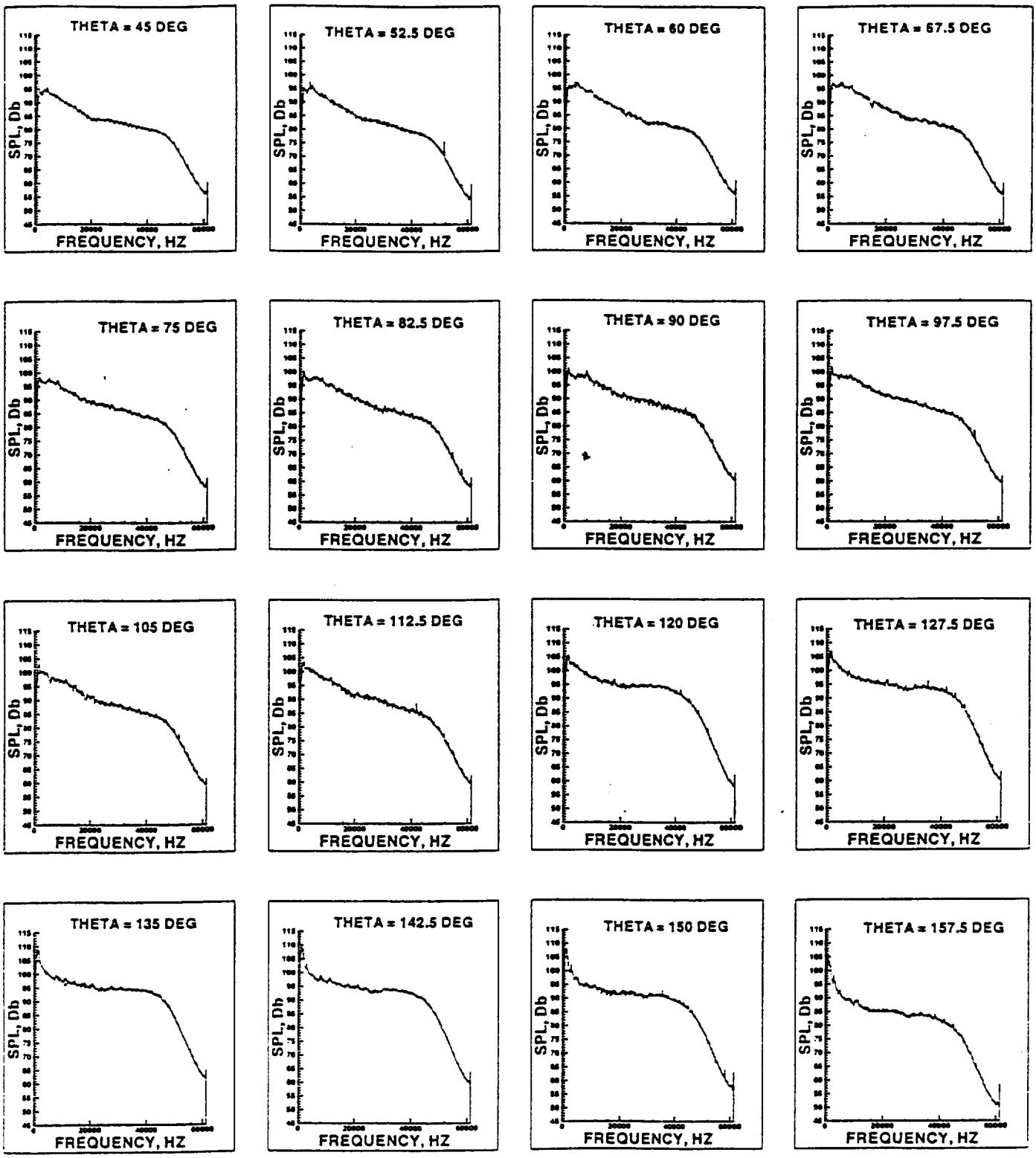

Figure 3 Continued. – Smoothed Narrow Band Spectra at 12 Foot Radius for 0 Degrees Azimuth Angle and 16 Polar Directivity Angles.

d. Nozzle 5, Pexit/Pambient = 1.45

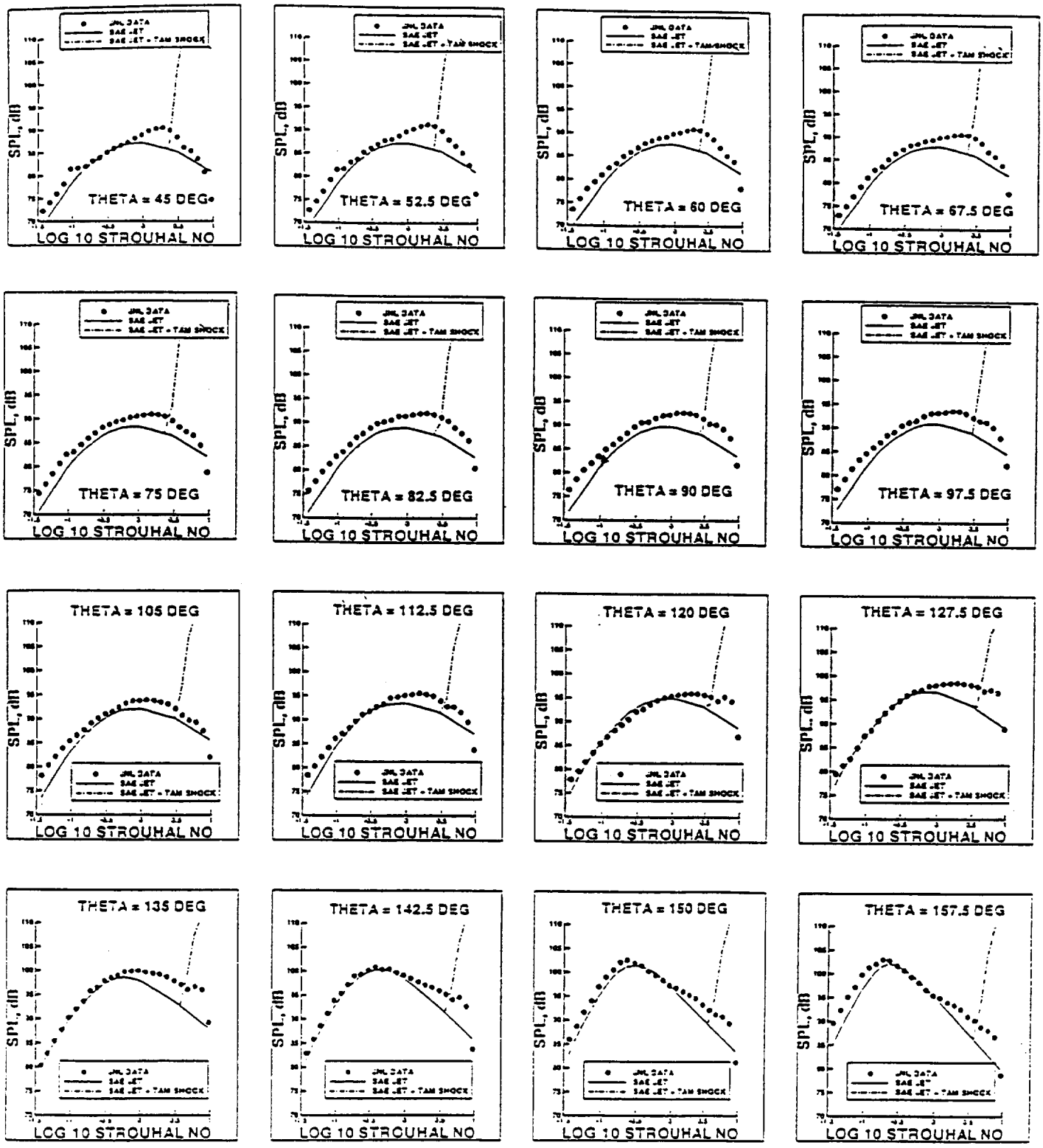

Figure 4. – Comparison of One-Third Octave Band Measured Noise Levels with SAE Circular Jet and Tam Shock Noise Predictions at 12 Foot Radius for 0 Degree Azimuth Angle at 16 Polar Directivity Angles.

a. Nozzle 3, Pexit/Pambient = 0.65

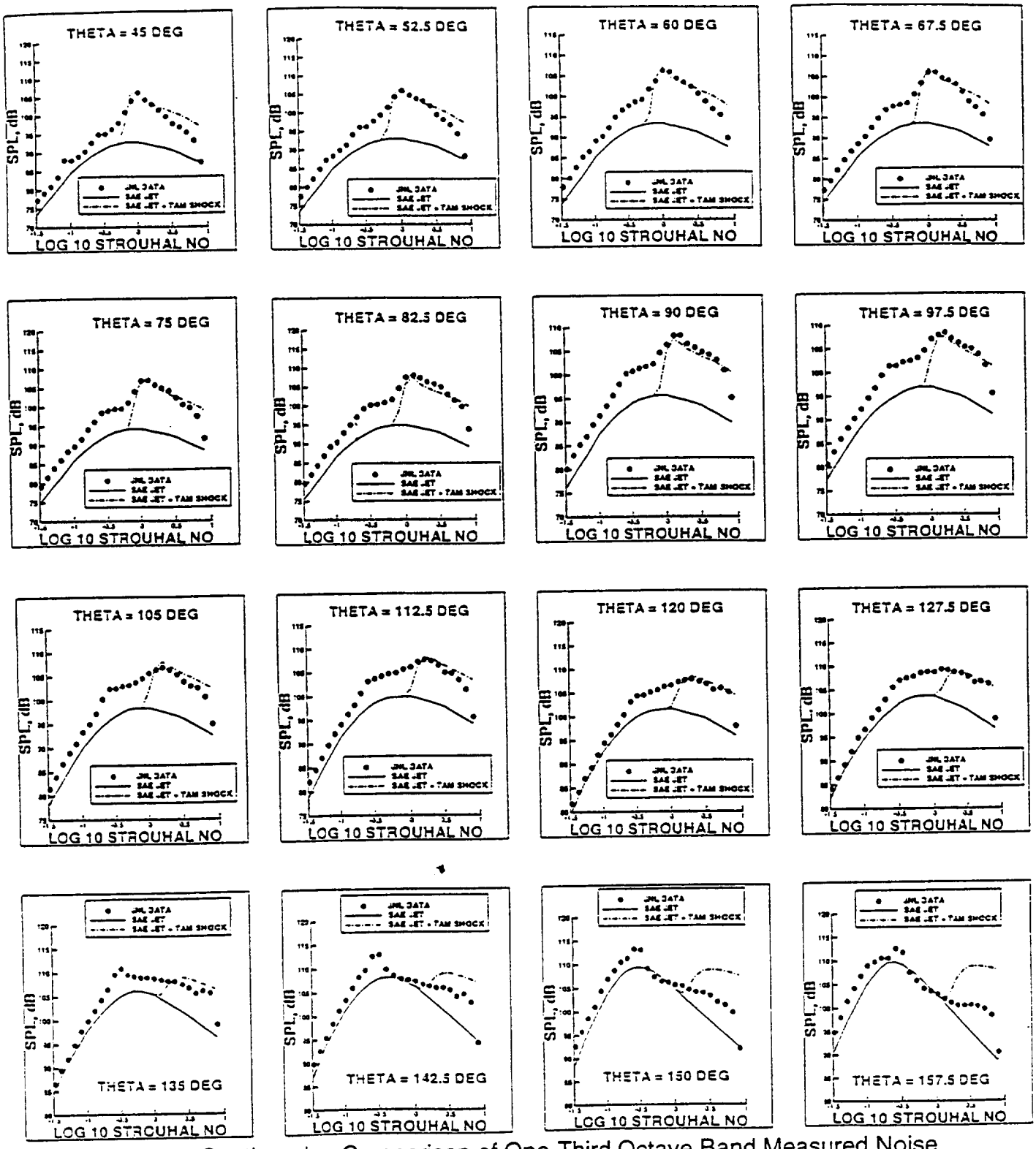

Figure 4 Continued. – Comparison of One-Third Octave Band Measured Noise Levels with SAE Circular Jet and Tam Shock Noise Predictions at 12 Foot Radius for 0 Degree Azimuth Angle at 16 Polar Directivity Angles.

b. Nozzle 3, Pexit/Pambient = 0.85

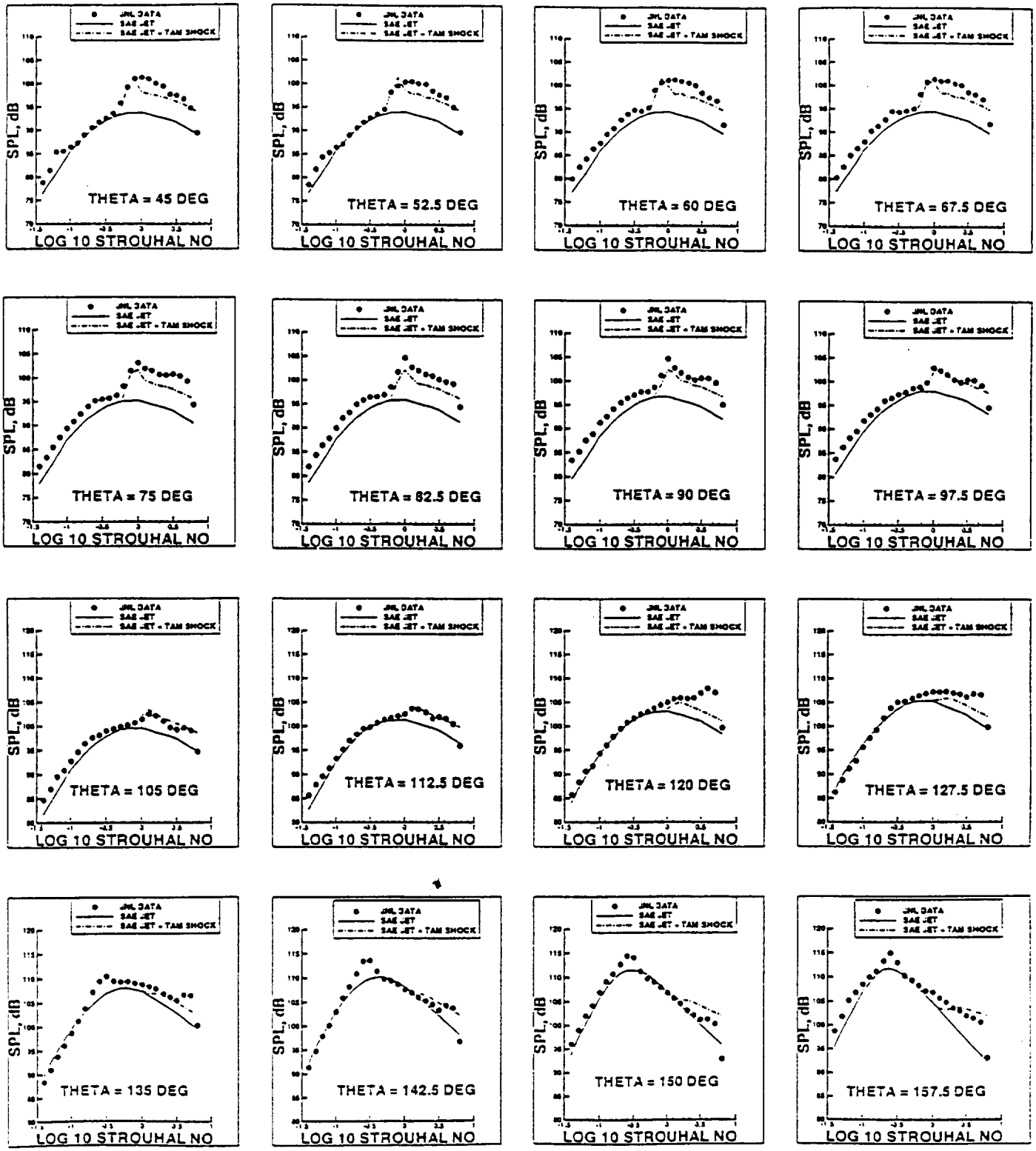

Figure 4 Continued. – Comparison of One-Third Octave Band Measured Noise Levels with SAE Circular Jet and Tam Shock Noise Predictions at 12 Foot Radius for 0 Degree Azimuth Angle at 16 Polar Directivity Angles.

c. Nozzle 4, Pexit/Pambient = 1.00

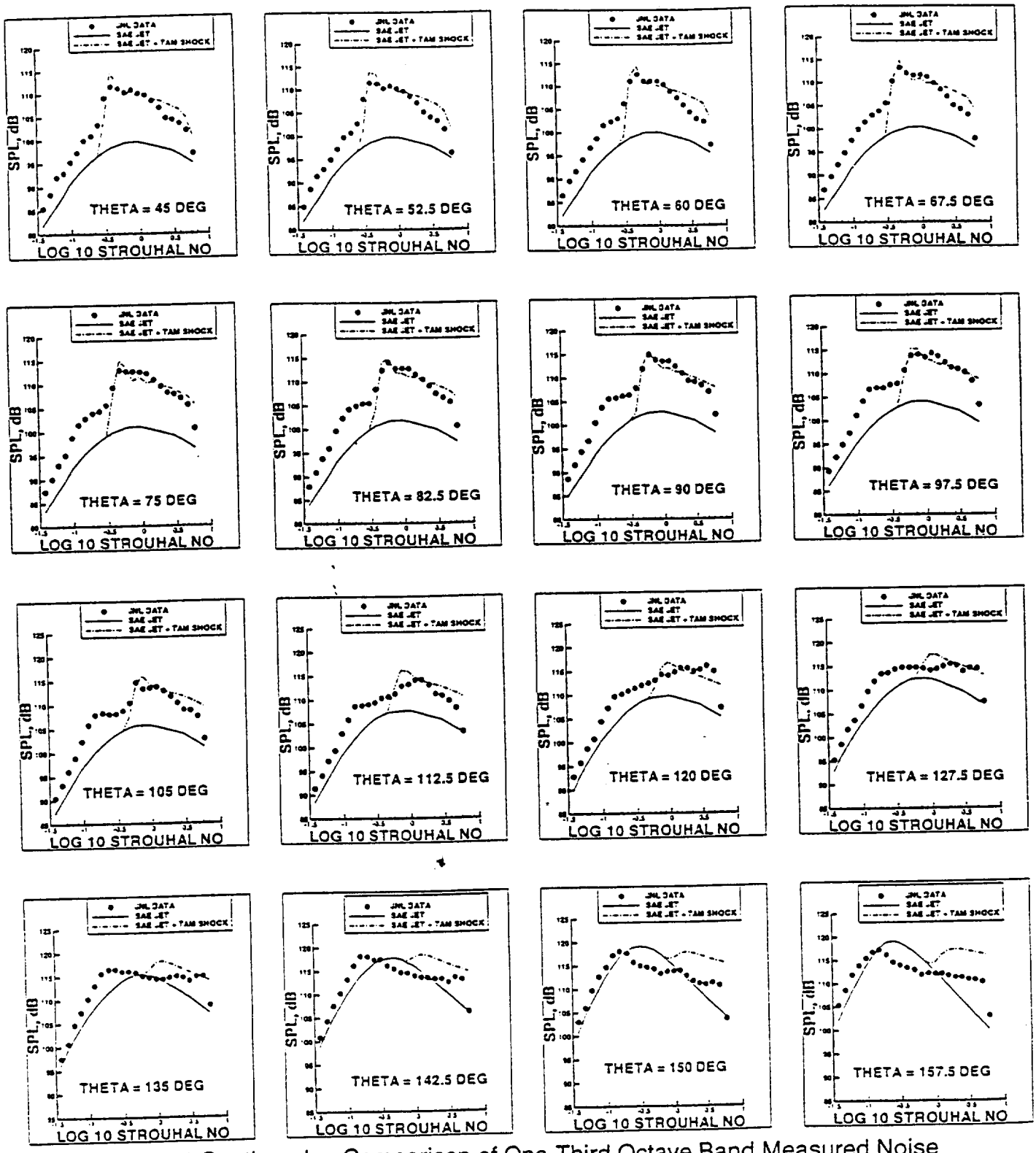

Figure 4 Continued. – Comparison of One-Third Octave Band Measured Noise Levels with SAE Circular Jet and Tam Shock Noise Predictions at 12 Foot Radius for 0 Degree Azimuth Angle at 16 Polar Directivity Angles.

d. Nozzle 4. Pexit/Pambient = 1.45

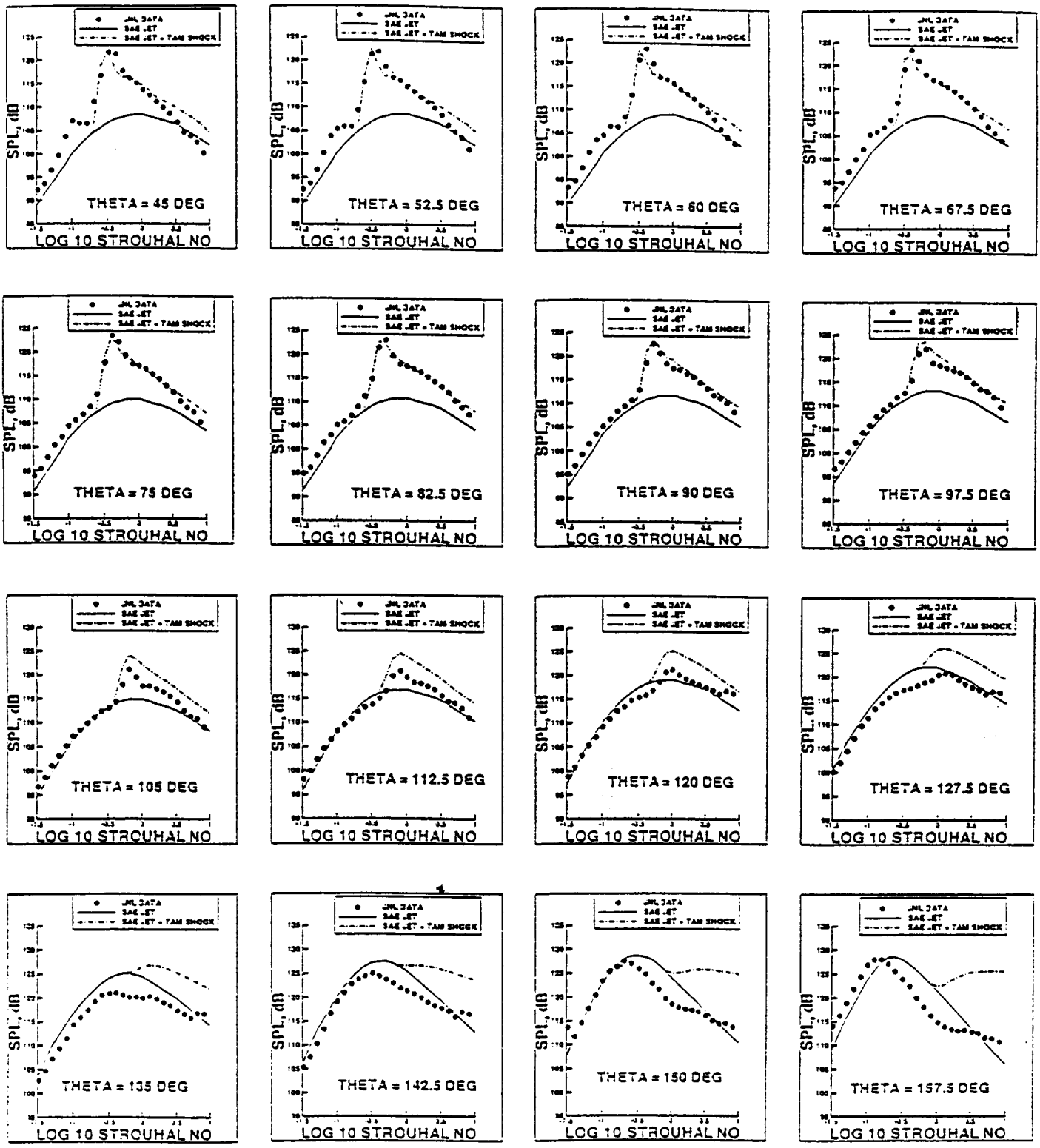

Figure 4 Continued. – Comparison of One-Third Octave Band Measured Noise Levels with SAE Circular Jet and Tam Shock Noise Predictions at 12 Foot Radius for 0 Degree Azimuth Angle at 16 Polar Directivity Angles.

e. Nozzle 1, Pexit/Pambient = 1.25

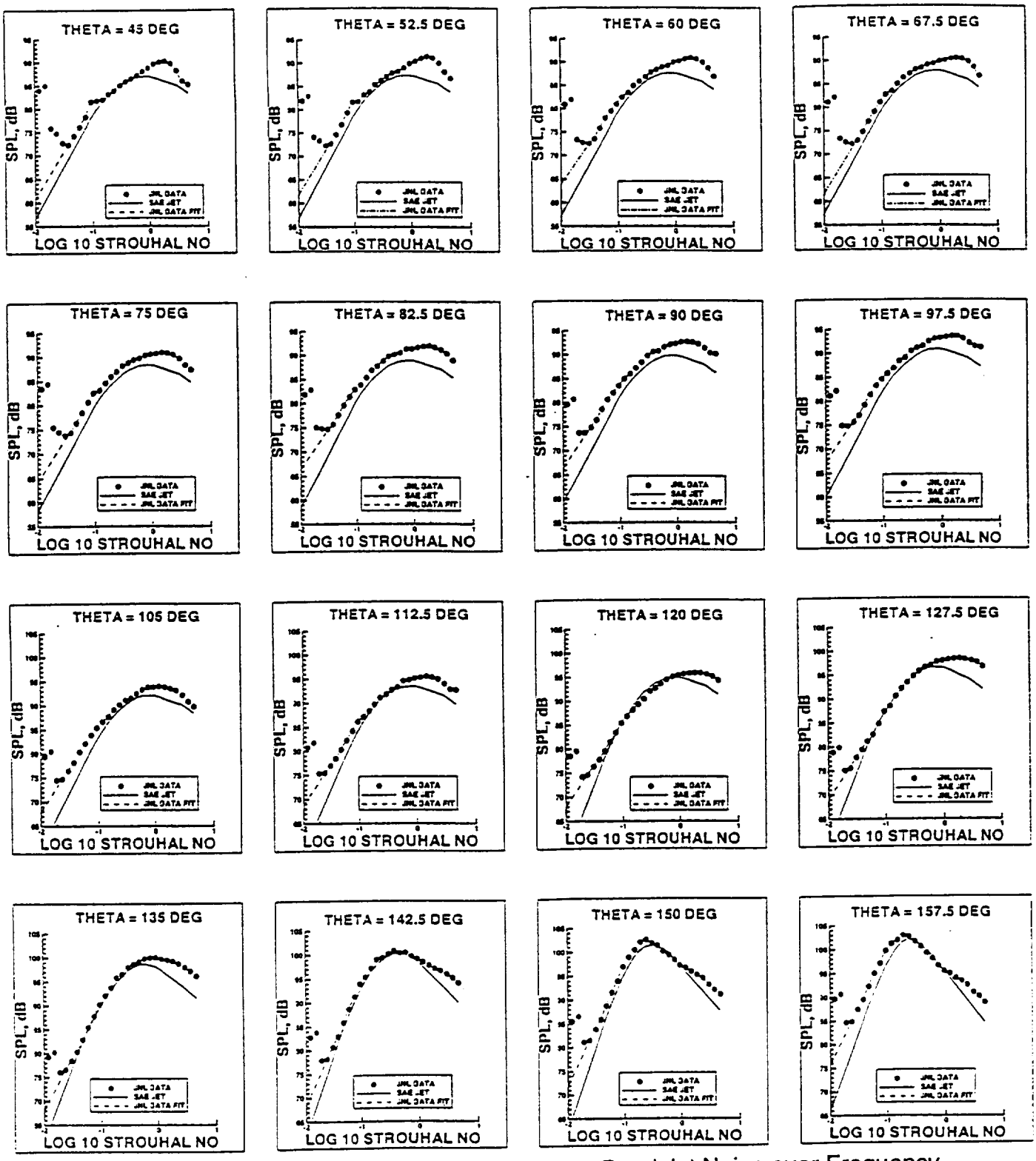

Figure 5. - Extrapolation of One-Third Octave Band Jet Noise over Frequency Range at 12 Foot Radius for 0 Degree Azimuth Angle at 16 Polar Directivity Angles

a. Nozzle 3, Pexit/Pambient = 0.65

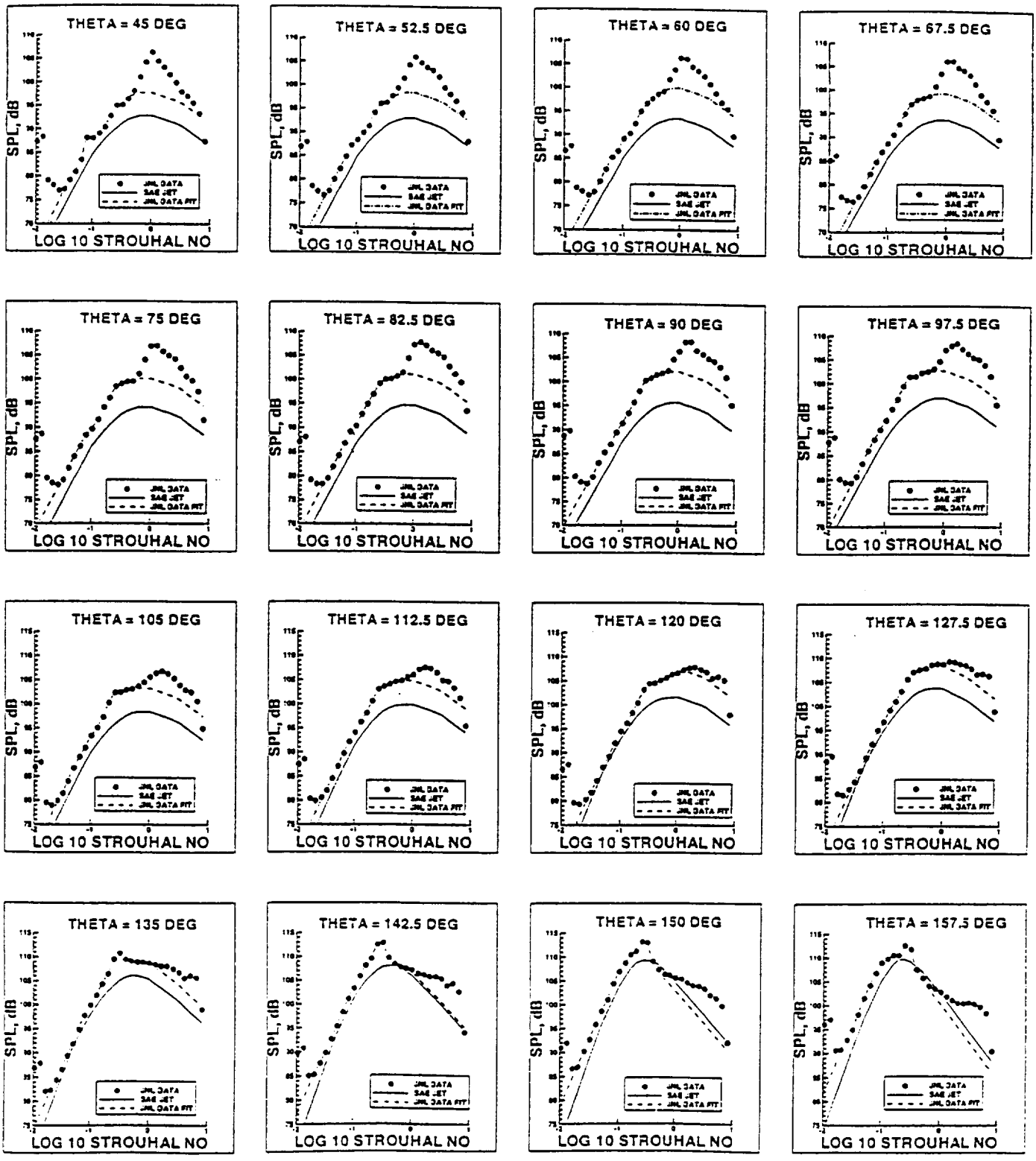

Figure 5 Continued. - Extrapolation of One-Third Octave Band Jet Noise over Frequency Range at 12 Foot Radius for 0 Degree Azimuth Angle at 16 Polar Directivity Angles

b. Nozzle 3, Pexit/Pambient = 0.85

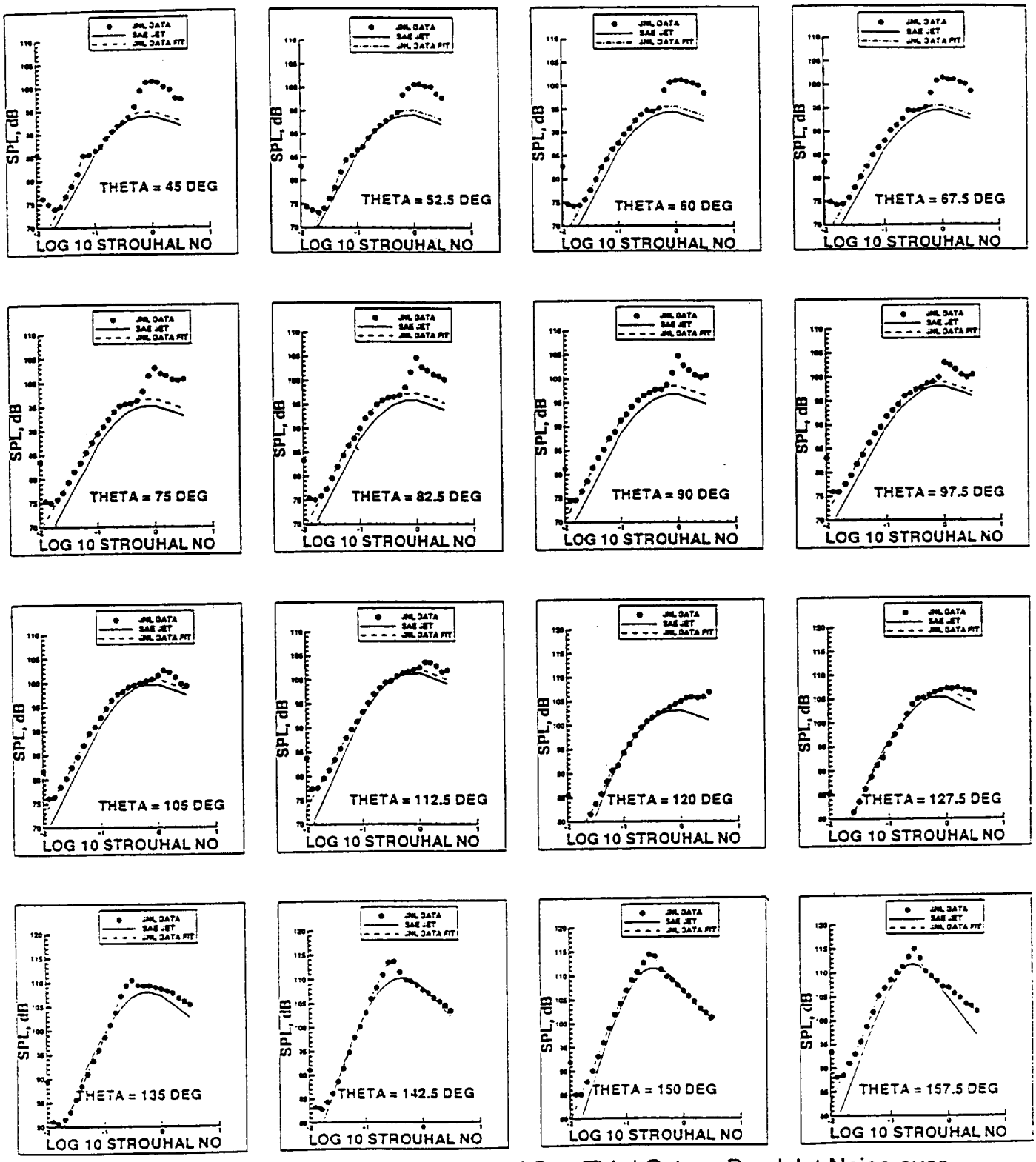

Figure 5 Continued. - Extrapolation of One-Third Octave Band Jet Noise over Frequency Range at 12 Foot Radius for 0 Degree Azimuth Angle at 16 Polar Directivity Angles

c. Nozzle 4, Pexit/Pambient = 1.00

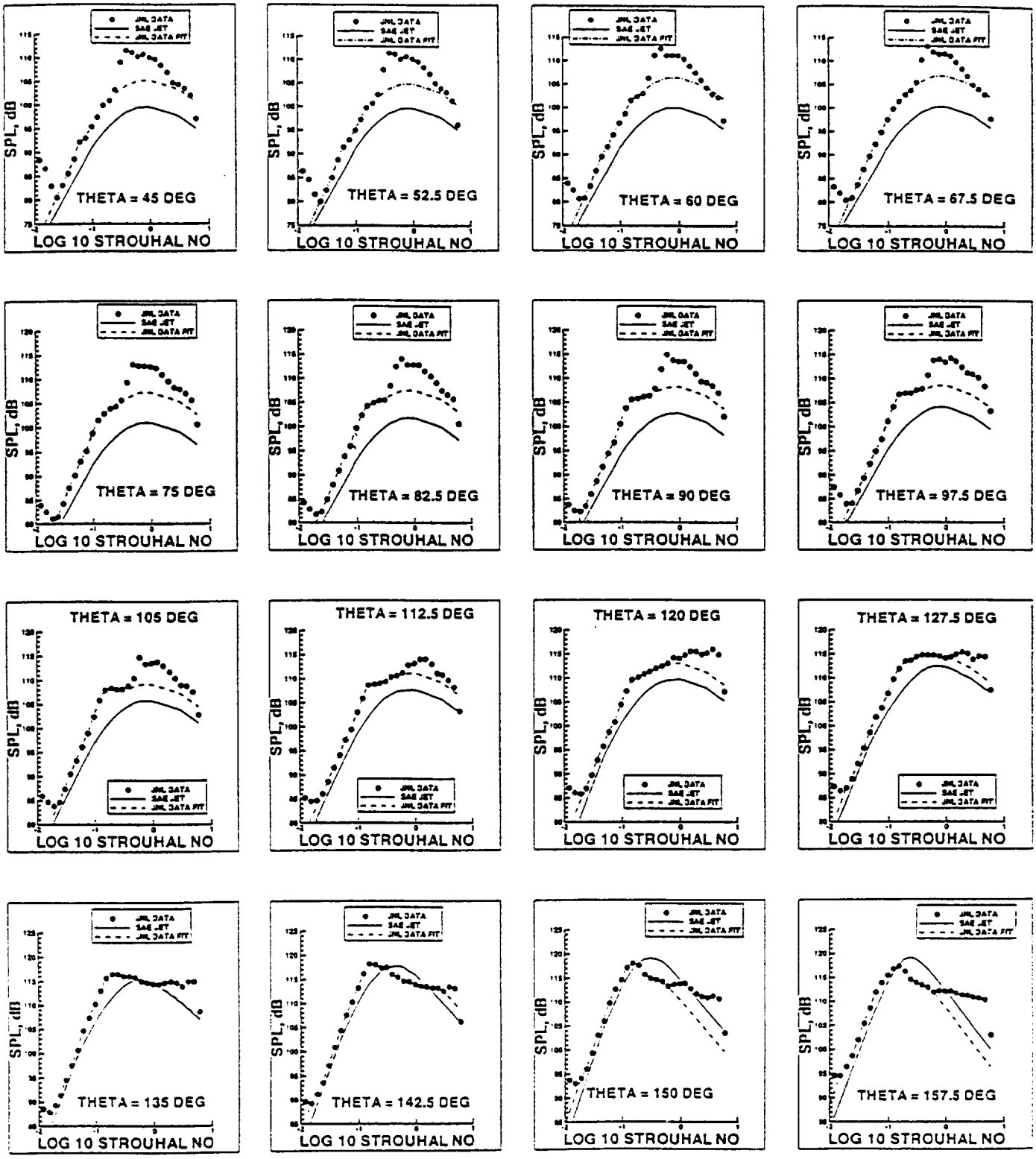

Figure 5 Continued. - Extrapolation of One-Third Octave Band Jet Noise over Frequency Range at 12 Foot Radius for 0 Degree Azimuth Angle at 16 Polar Directivity Angles

d. Nozzle 4, Pexit/Pambient = 1.45

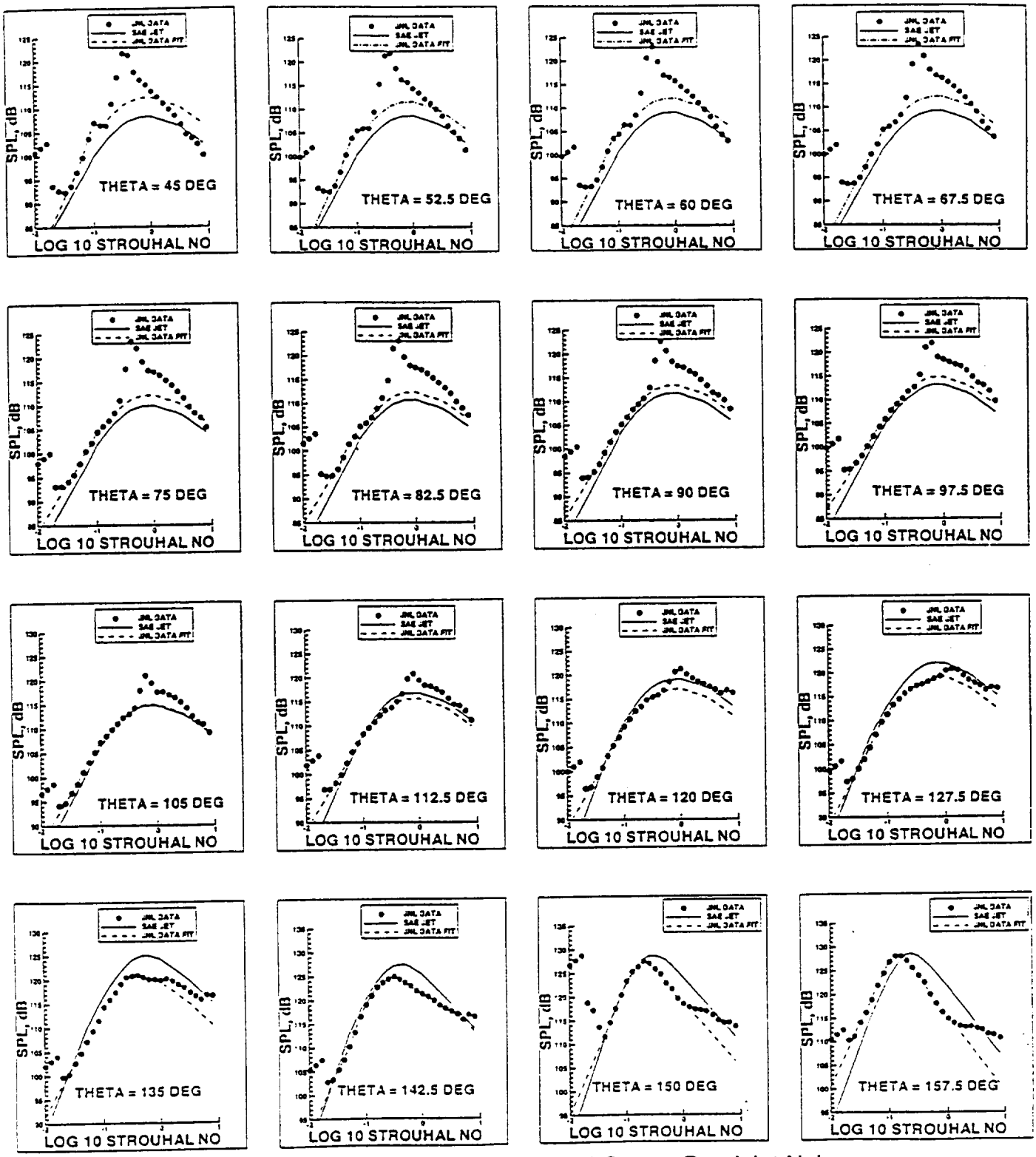

Figure 5 Continued. - Extrapolation of One-Third Octave Band Jet Noise over Frequency Range at 12 Foot Radius for 0 Degree Azimuth Angle at 16 Polar Directivity Angles

e. Nozzle 1, Pexit/Pambient = 1.25

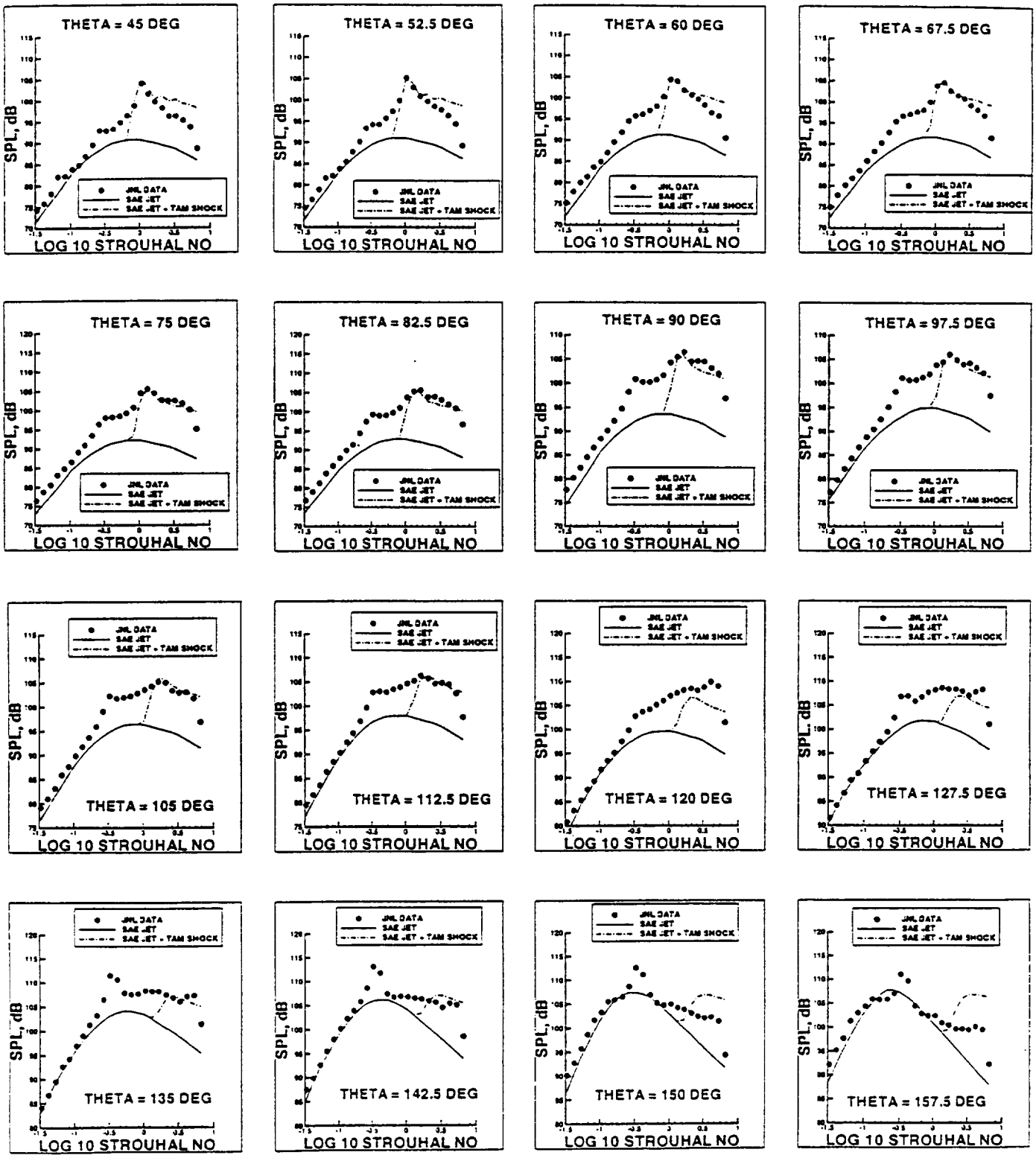

Figure 6. – Comparison of One-Third Octave Band Measured Noise Levels with SAE Circular Jet and Tam Shock Noise Predictions at 12 Foot Radius for 0 Degree Azimuth Angle at 16 Polar Directivity Angles.

a. Nozzle 4, Pexit/Pambient = 0.85

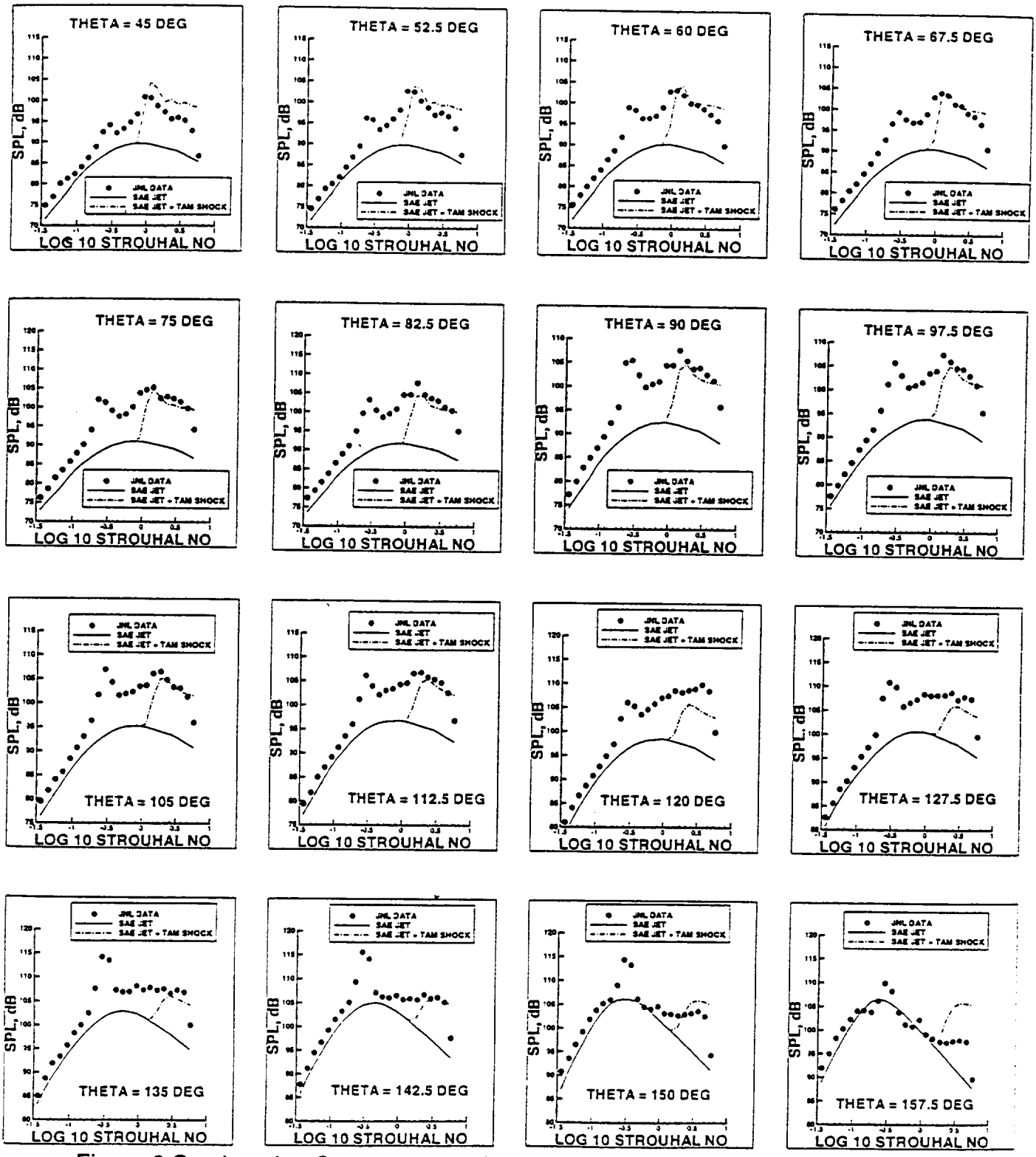

Figure 6 Continued. – Comparison of One-Third Octave Band Measured Noise Levels with SAE Circular Jet and Tam Shock Noise Predictions at 12 Foot Radius for 0 Degree Azimuth Angle at 16 Polar Directivity Angles.

b. Nozzle 5, Pexit/Pambient = 0.85

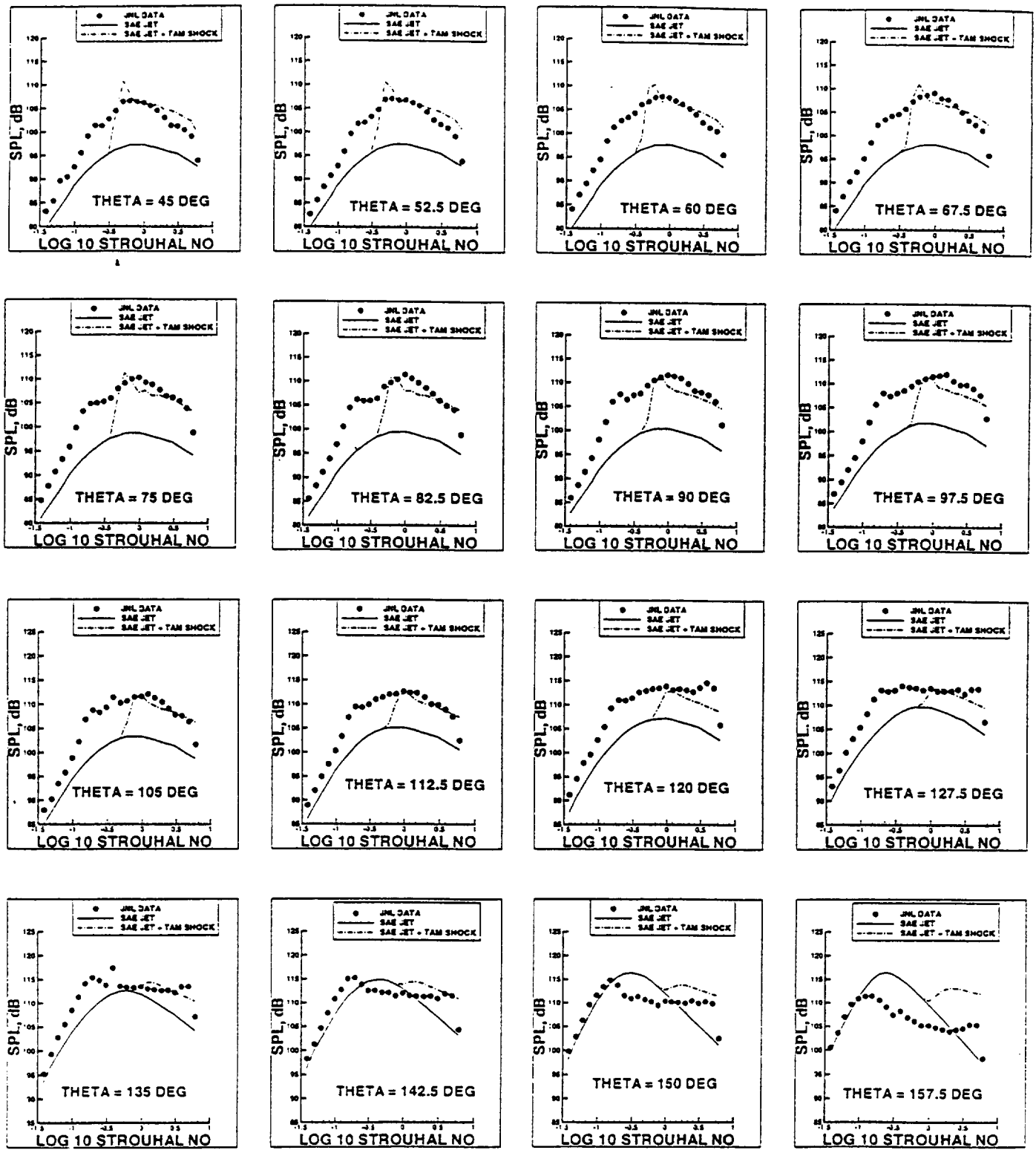

Figure 6 Continued. – Comparison of One-Third Octave Band Measured Noise Levels with SAE Circular Jet and Tam Shock Noise Predictions at 12 Foot Radius for 0 Degree Azimuth Angle at 16 Polar Directivity Angles.

c. Nozzle 4, Pexit/Pambient = 1.25

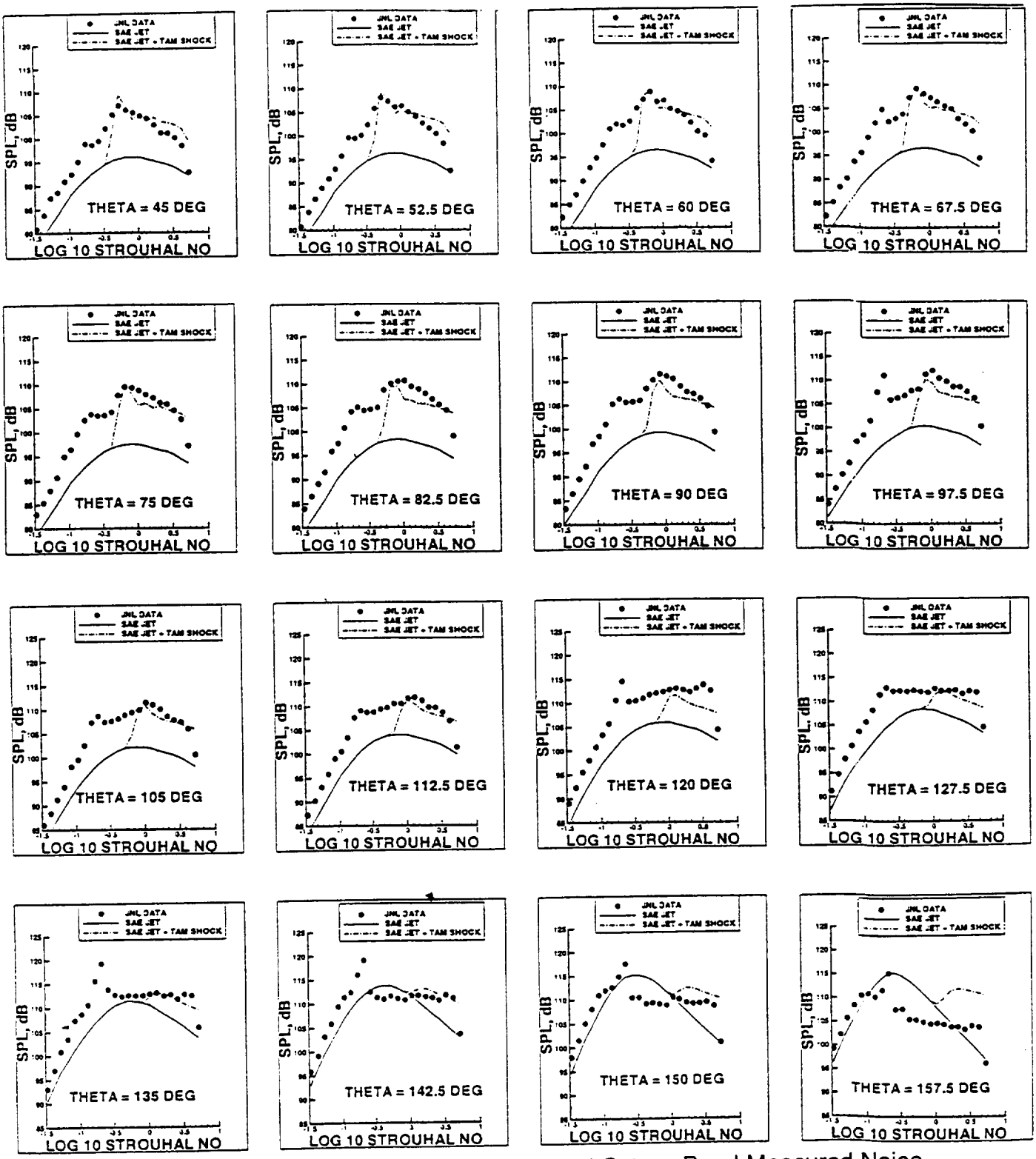

Figure 6 Continued. – Comparison of One-Third Octave Band Measured Noise Levels with SAE Circular Jet and Tam Shock Noise Predictions at 12 Foot Radius for 0 Degree Azimuth Angle at 16 Polar Directivity Angles.

d. Nozzle 5, Pexit/Pambient = 1.25

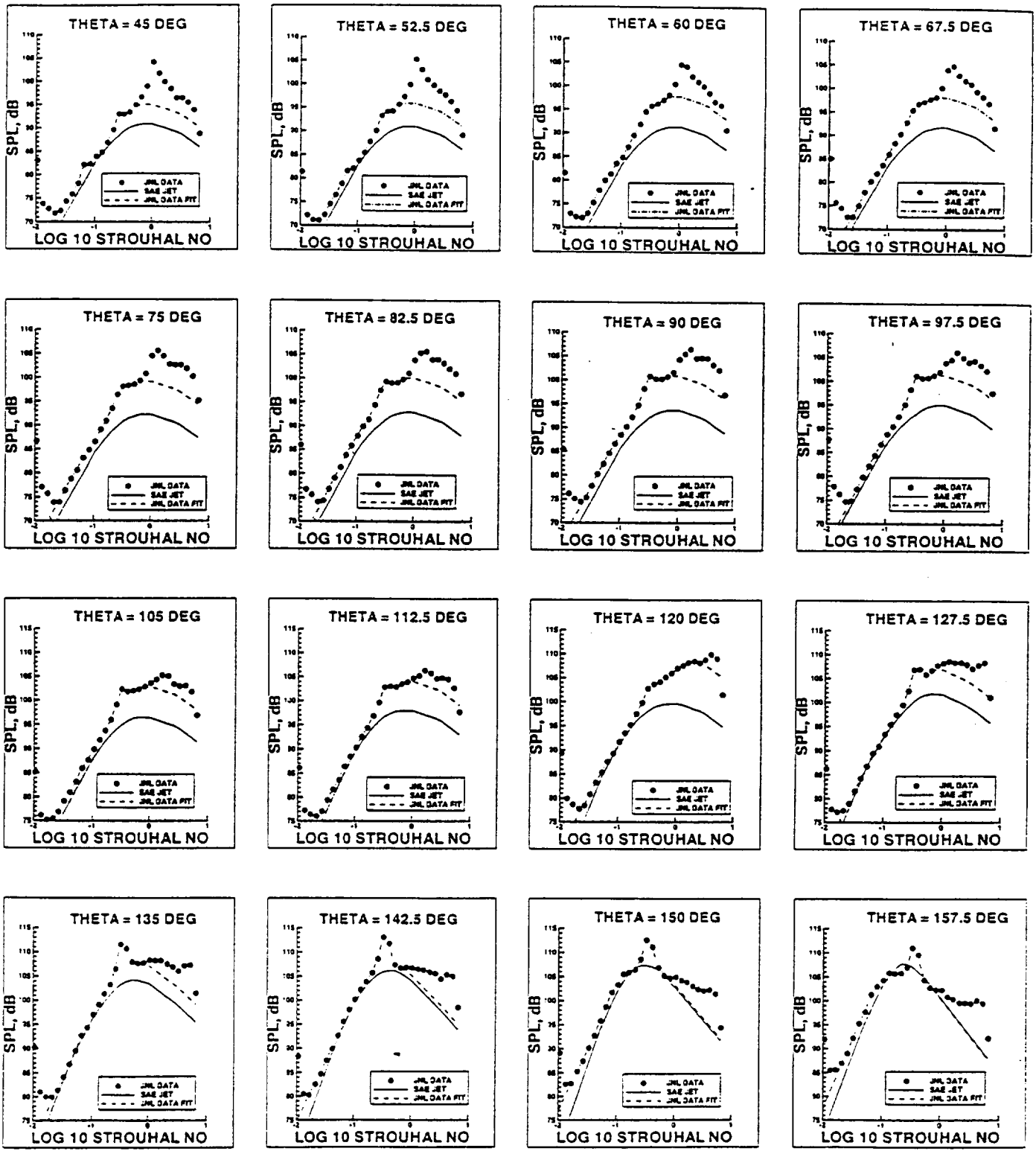

Figure 7. - Extrapolation of One-Third Octave Band Jet Noise over Frequency Range at 12 Foot Radius for 0 Degree Azimuth Angle at 16 Polar Directivity Angles

a. Nozzle 3, Pexit/Pambient = 0.65

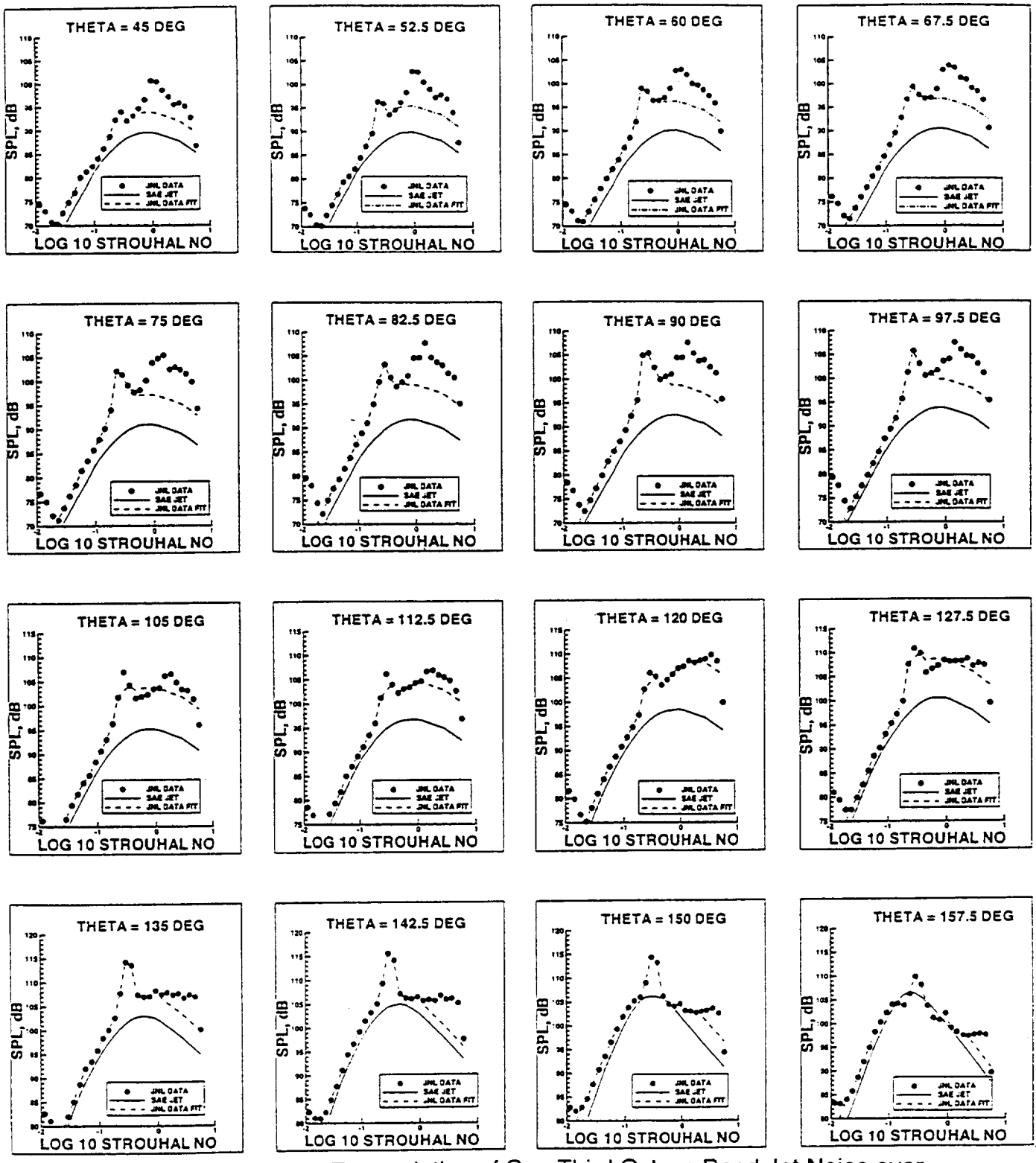

Figure 7 Continued. - Extrapolation of One-Third Octave Band Jet Noise over Frequency Range at 12 Foot Radius for 0 Degree Azimuth Angle at 16 Polar Directivity Angles

b. Nozzle 5, Pexit/Pambient = 0.85

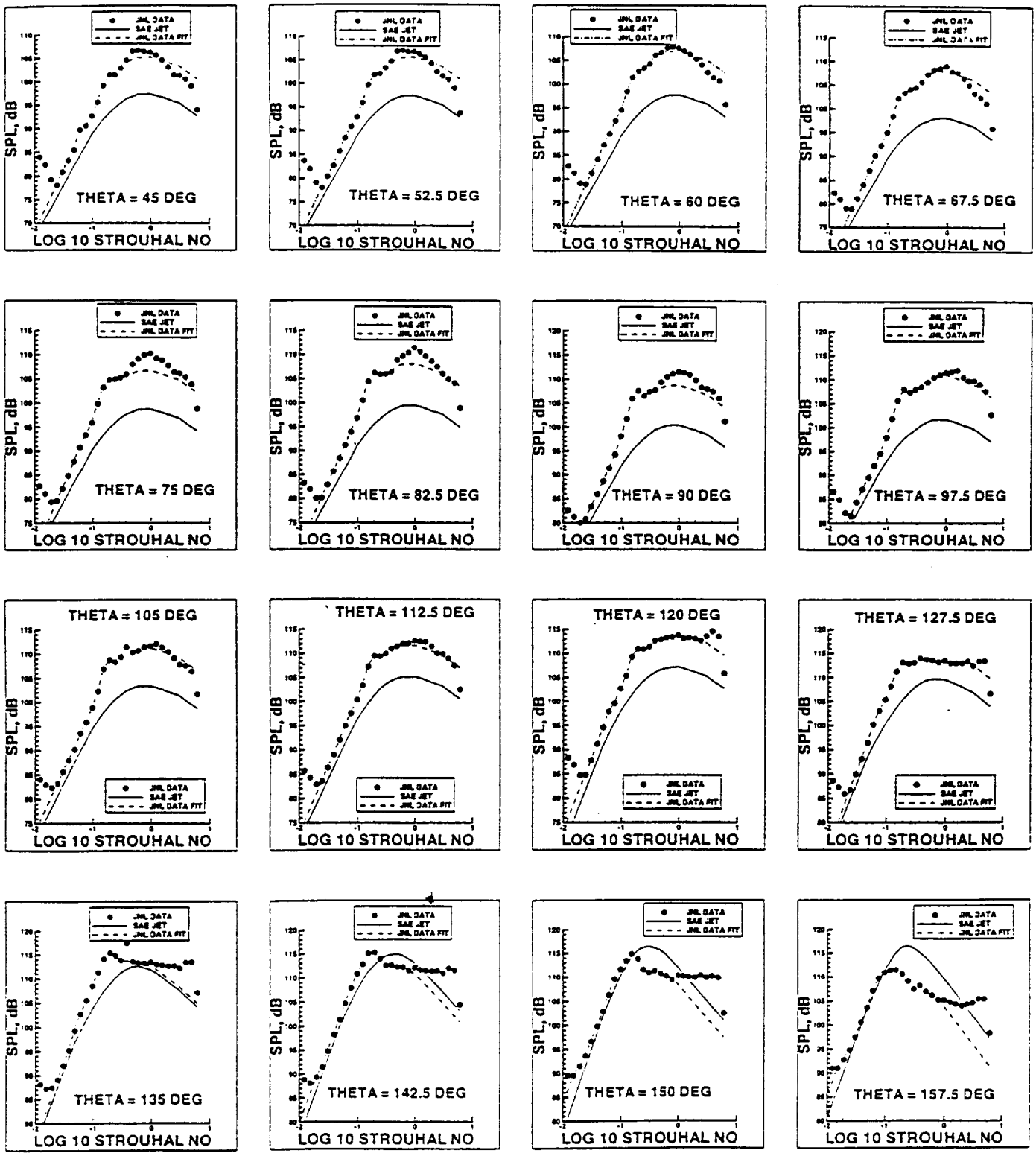

Figure 7 Continued. - Extrapolation of One-Third Octave Band Jet Noise over Frequency Range at 12 Foot Radius for 0 Degree Azimuth Angle at 16 Polar Directivity Angles

c. Nozzle 4, Pexit/Pambient = 1.25

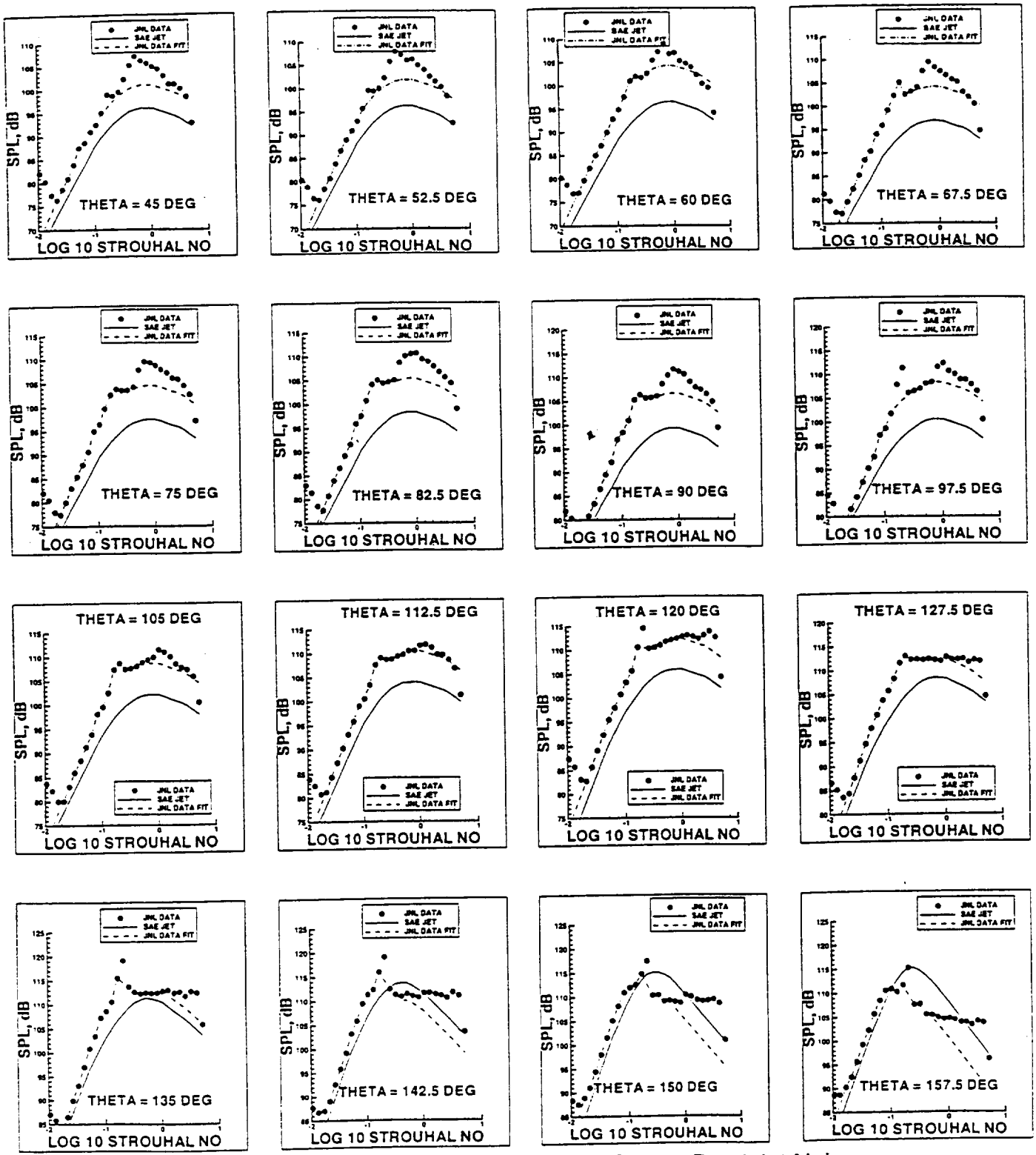

Figure 7 Continued. - Extrapolation of One-Third Octave Band Jet Noise over Frequency Range at 12 Foot Radius for 0 Degree Azimuth Angle at 16 Polar Directivity Angles

d. Nozzle 5, Pexit/Pambient = 1.25

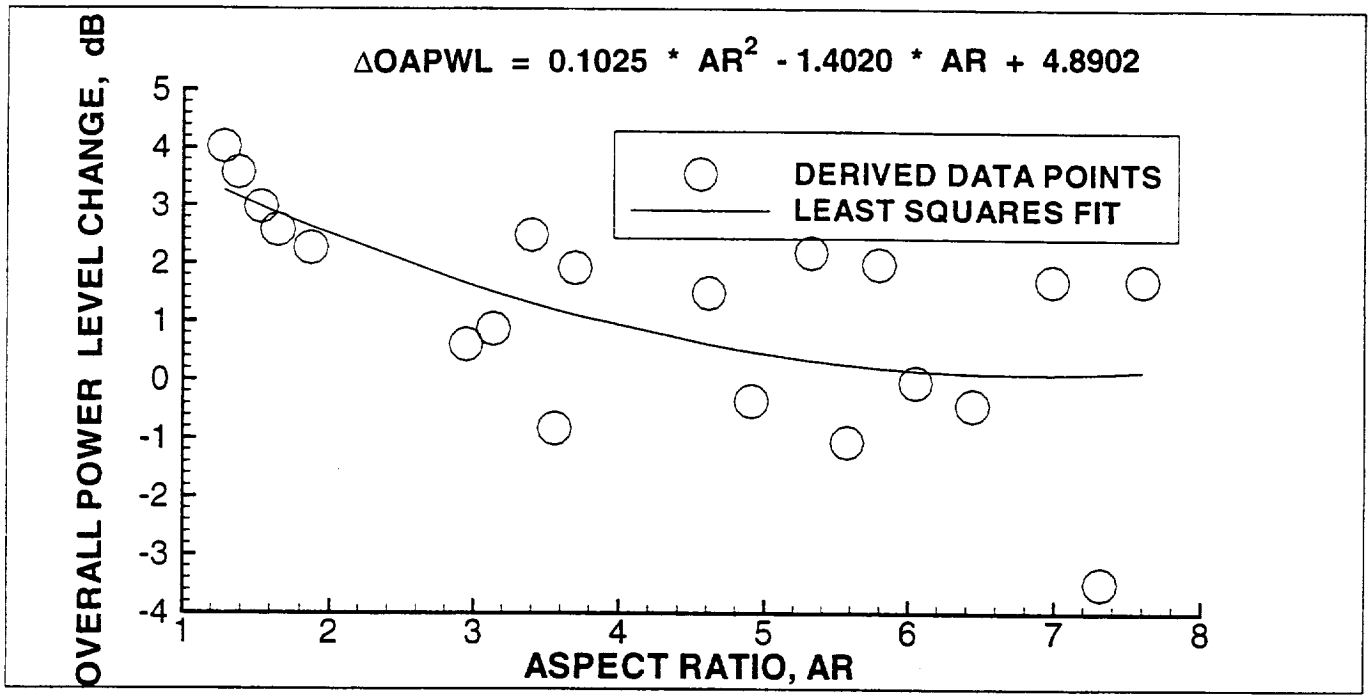

a. Least Squares Fit Based on 20 Test Points

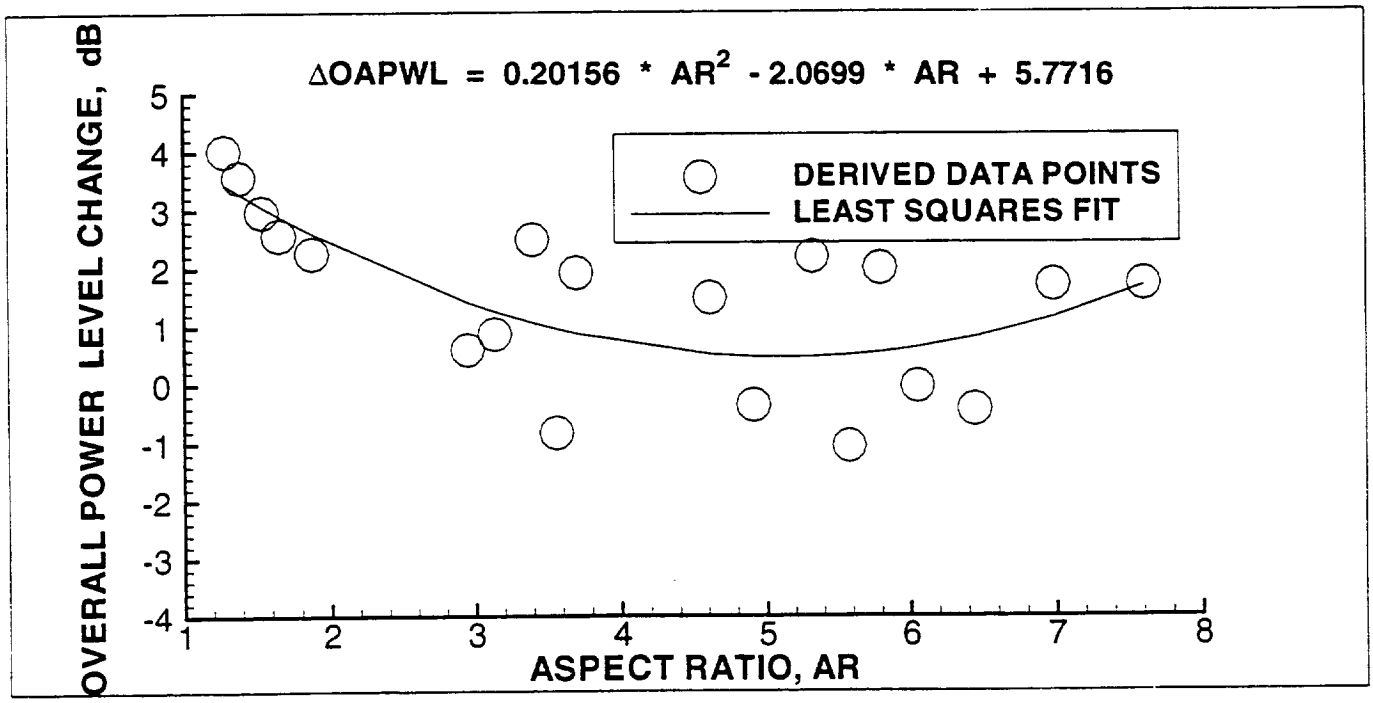

b. Least Squares Fit Based on 19 Test Points

Figure 8. – Variation of Incremental Change in Overall Power Level of Jet Mixing Noise for Rectangular Cold Flow Jets

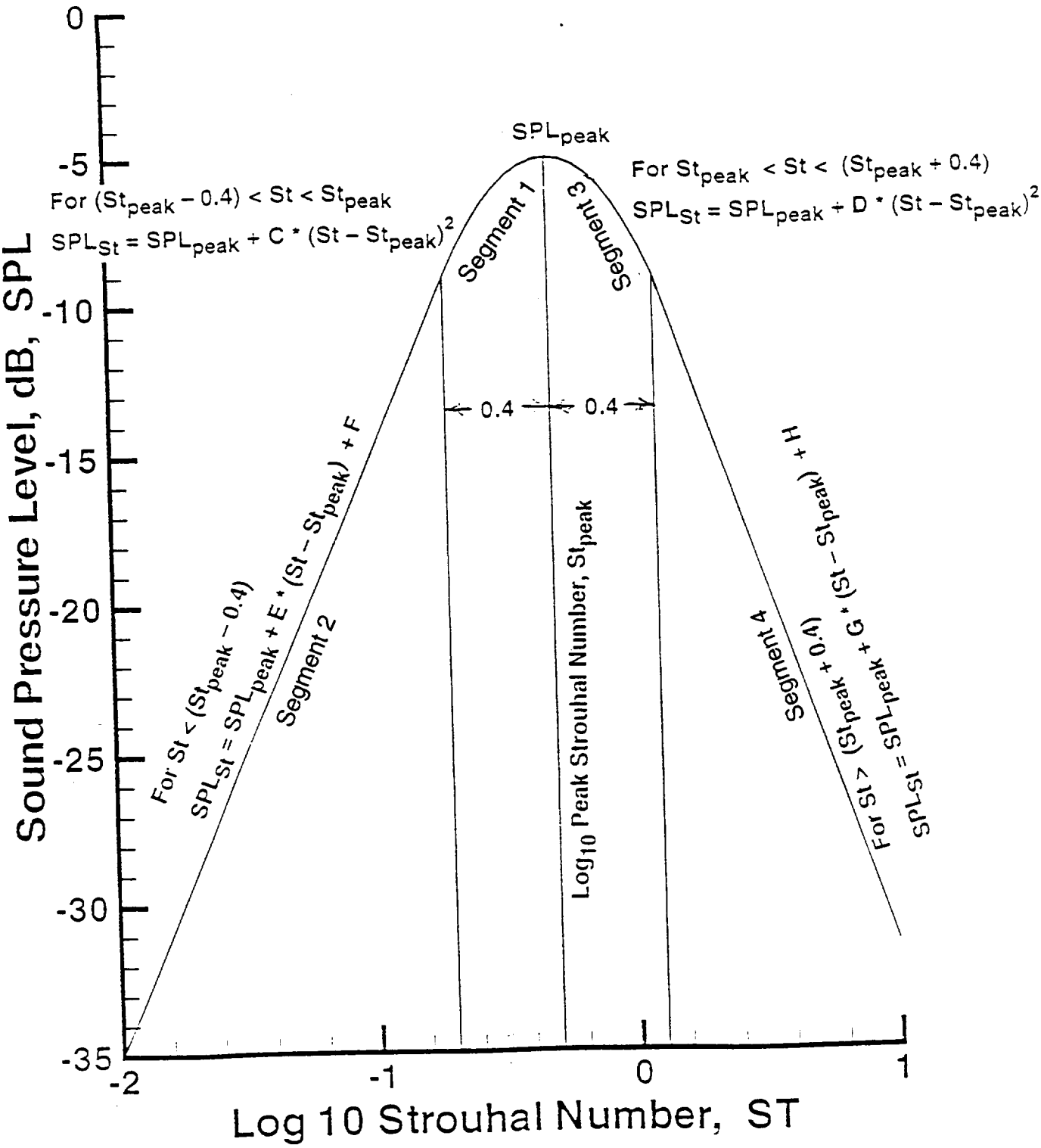

Figure 9. - Spectral Shape Prediction Parameters for Jet Mixing Noise of Cold Flow Rectangular Jets

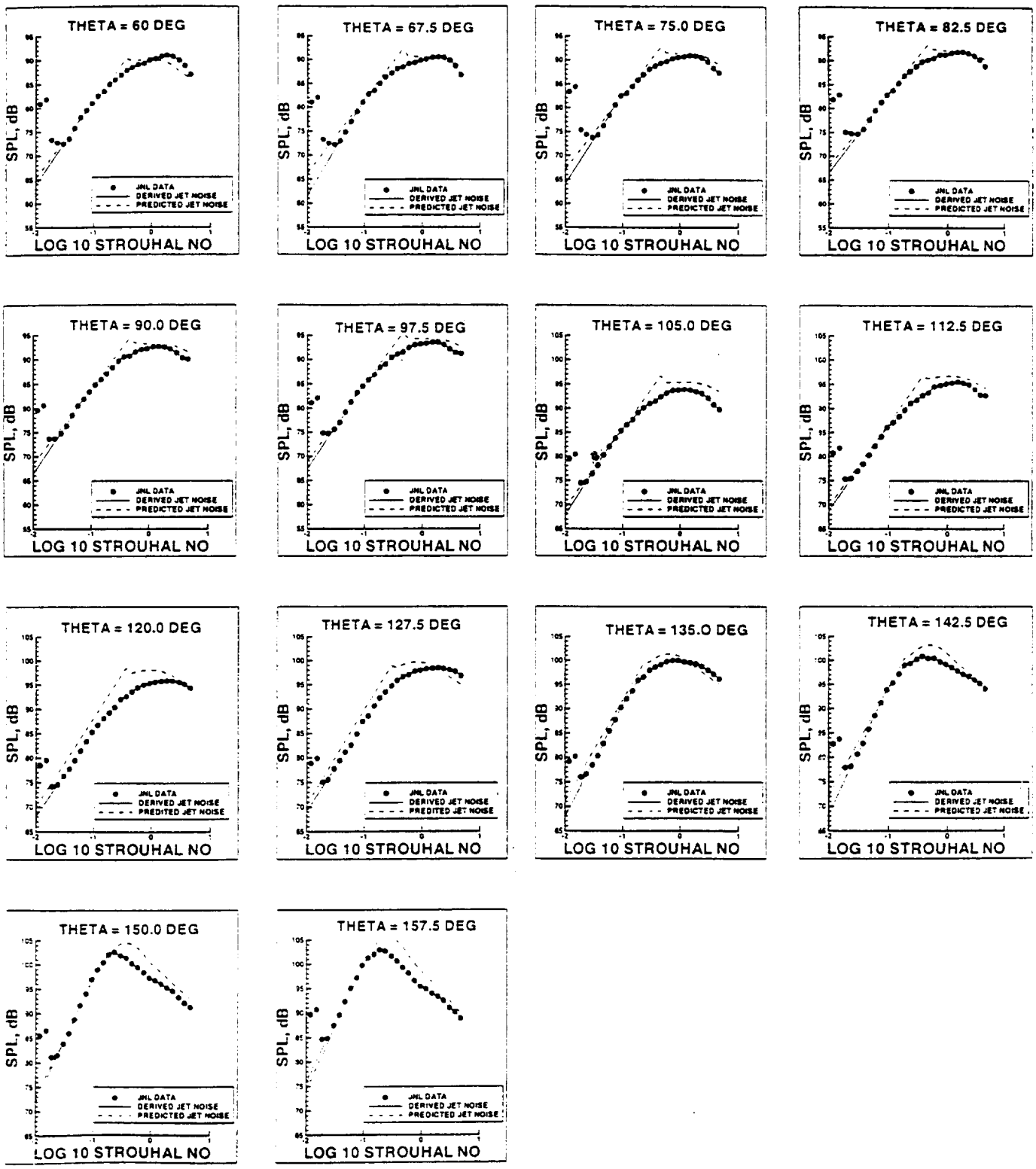

Figure 10. - Comparison of One-Third Octave Band Predicted Jet Mixing Noise with Derived Jet Mixing Noise for 0 degrees Azimuth Angle at 14 Polar Directivity Angles

a. Nozzle 3, Pexit/Pambient = 1.00

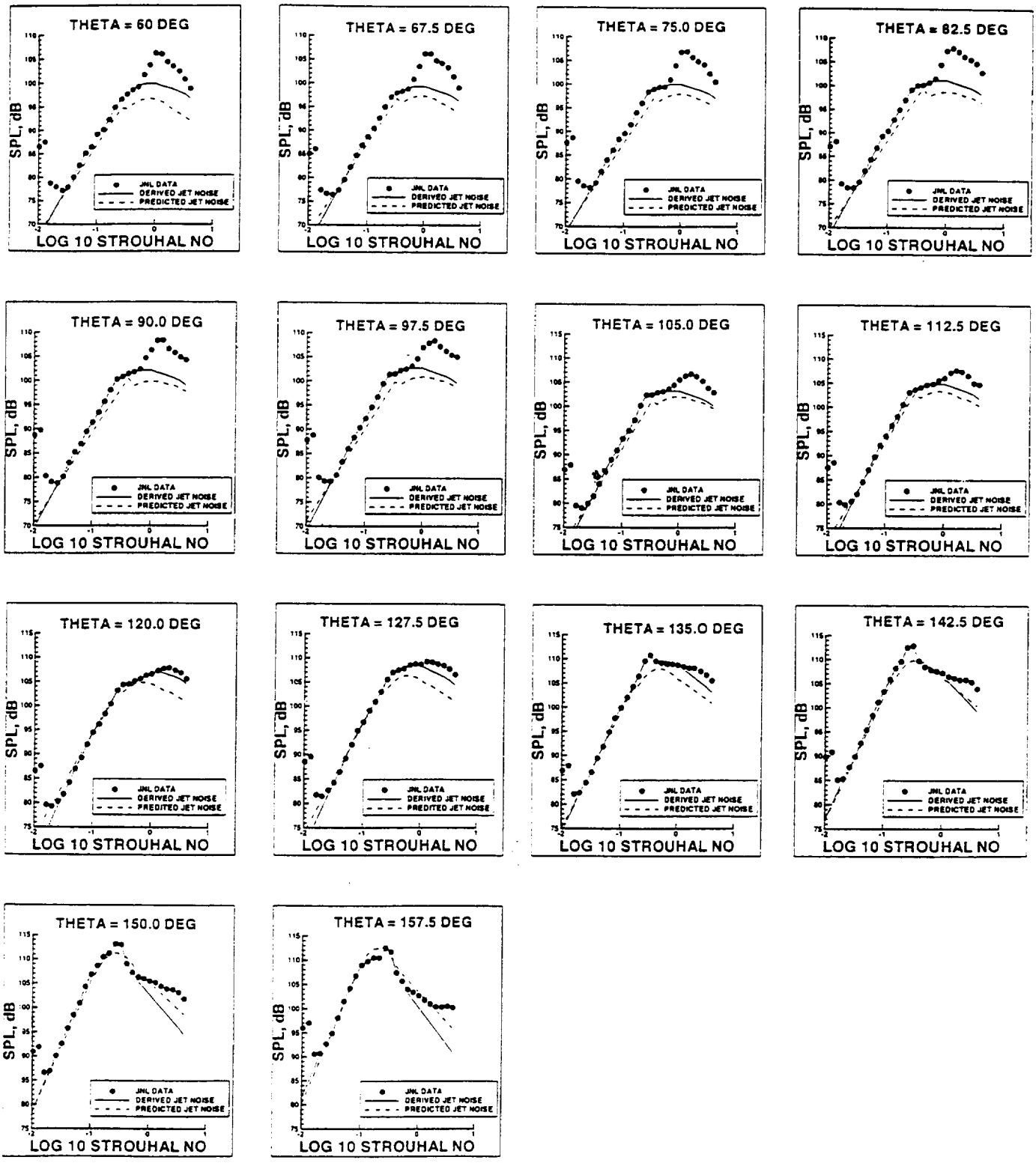

Figure 10 Continued - Comparison of One-Third Octave Band Predicted Jet Mixing Noise with Derived Jet Mixing Noise for 0 degrees Azimuth Angle at 14 Polar Directivity Angles

b. Nozzle 3, Pexit/Pambient = 0.85

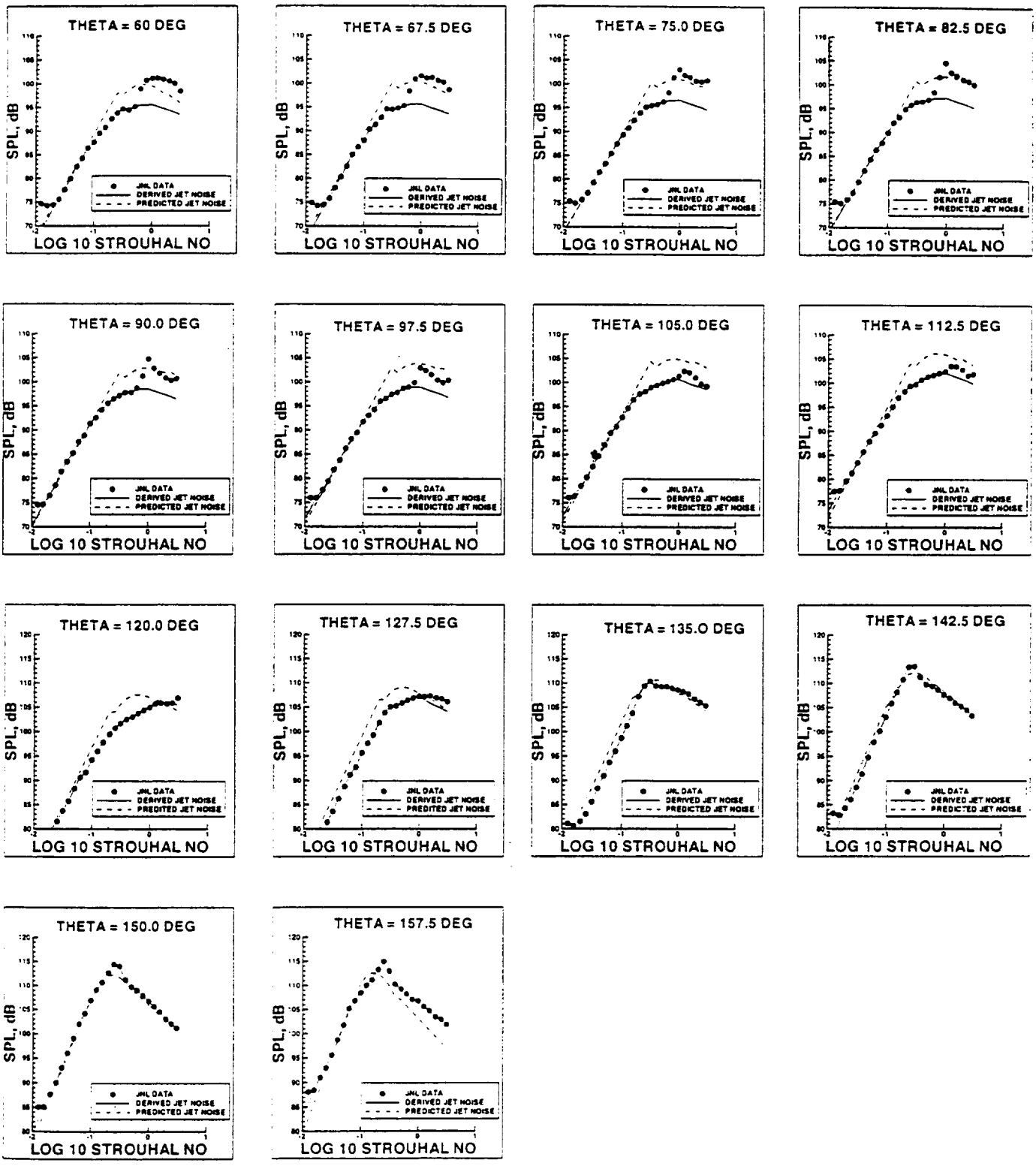

Figure 10 Continued - Comparison of One-Third Octave Band Predicted Jet Mixing Noise with Derived Jet Mixing Noise for 0 degrees Azimuth Angle at 14 Polar Directivity Angles

c. Nozzle 4, Pexit/Pambient = 1.00

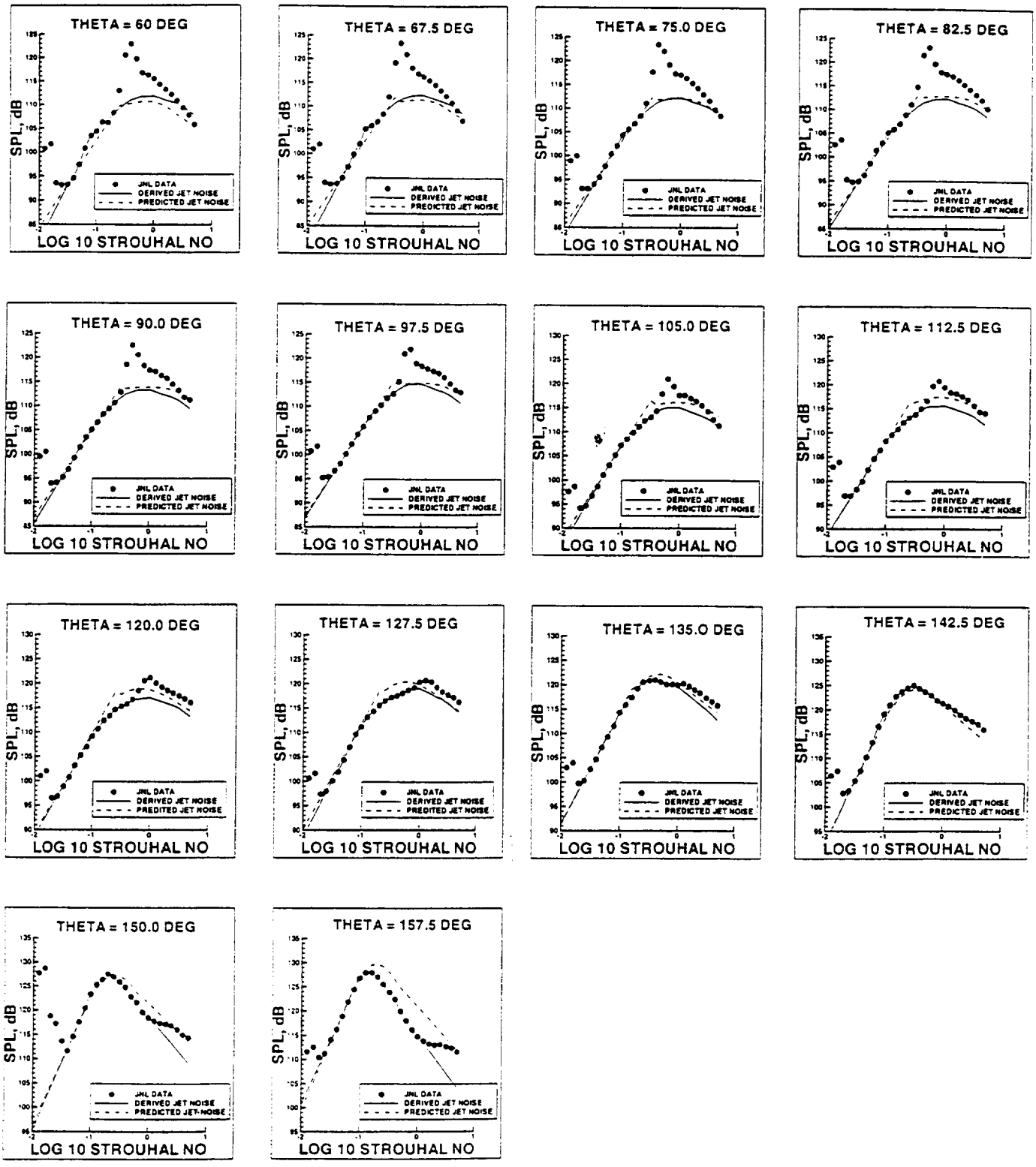

Figure 10 Continued - Comparison of One-Third Octave Band Predicted Jet Mixing Noise with Derived Jet Mixing Noise for 0 degrees Azimuth Angle at 14 Polar Directivity Angles

d. Nozzle 1, Pexit/Pambient = 1.25

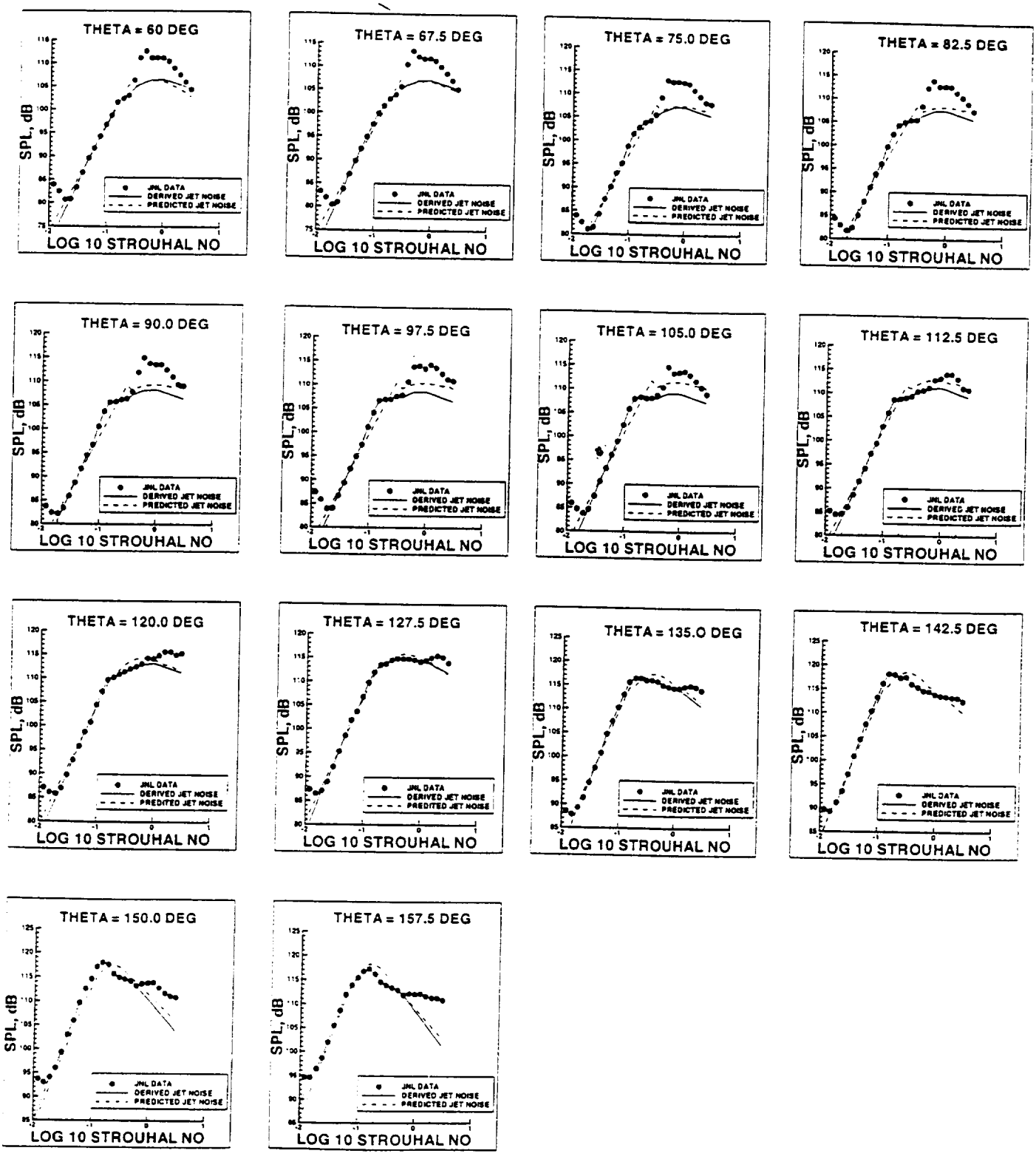

Figure 10 Continued - Comparison of One-Third Octave Band Predicted Jet Mixing Noise with Derived Jet Mixing Noise for 0 degrees Azimuth Angle at 14 Polar Directivity Angles

e. Nozzle 4, Pexit/Pambient = 1.45

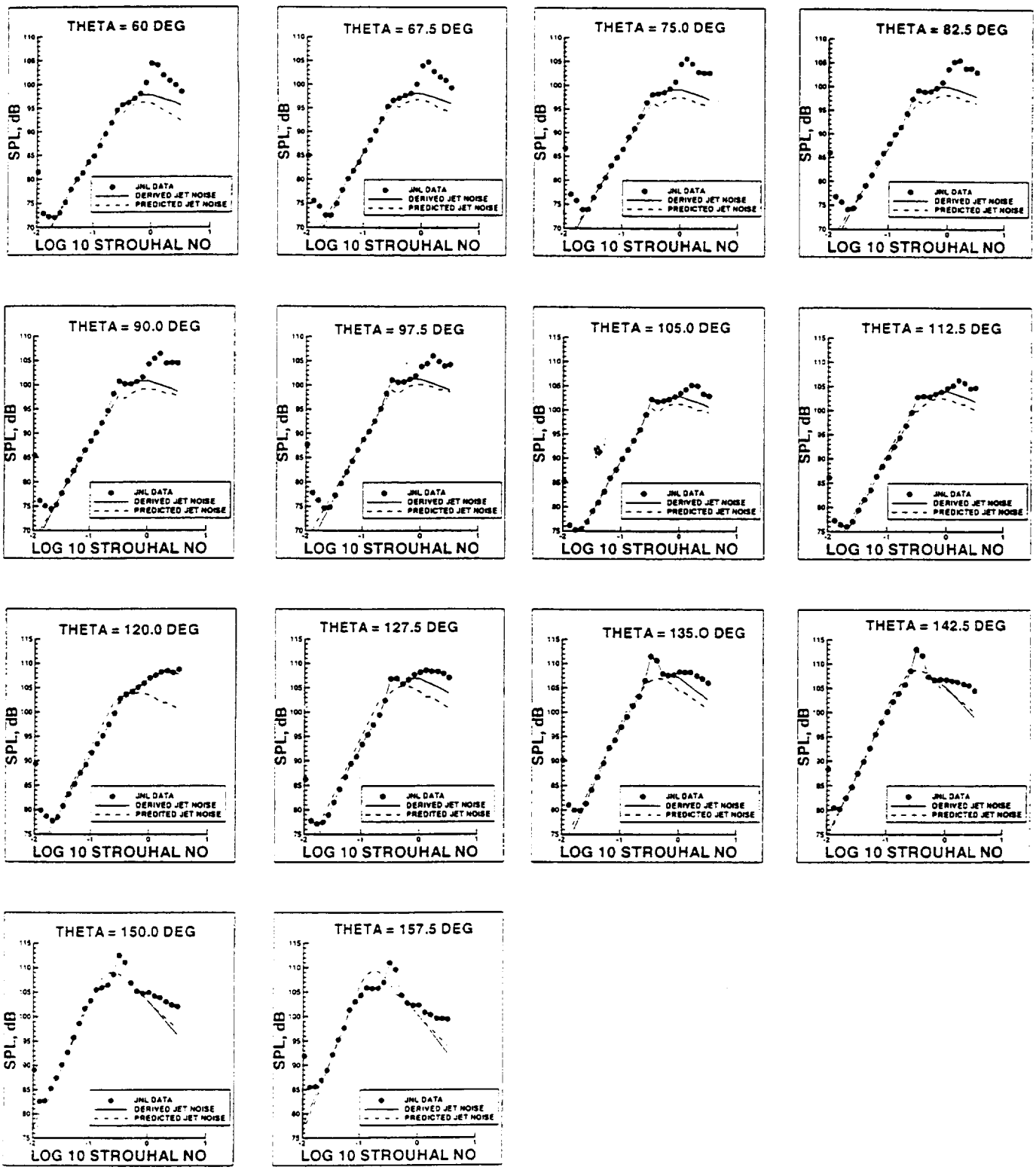

Figure 11. - Comparison of One-Third Octave Band Predicted Jet Mixing Noise with Derived Jet Mixing Noise for 0 degrees Azimuth Angle at 14 Polar Directivity Angles

a. Nozzle 4, Pexit/Pambient = 0.85

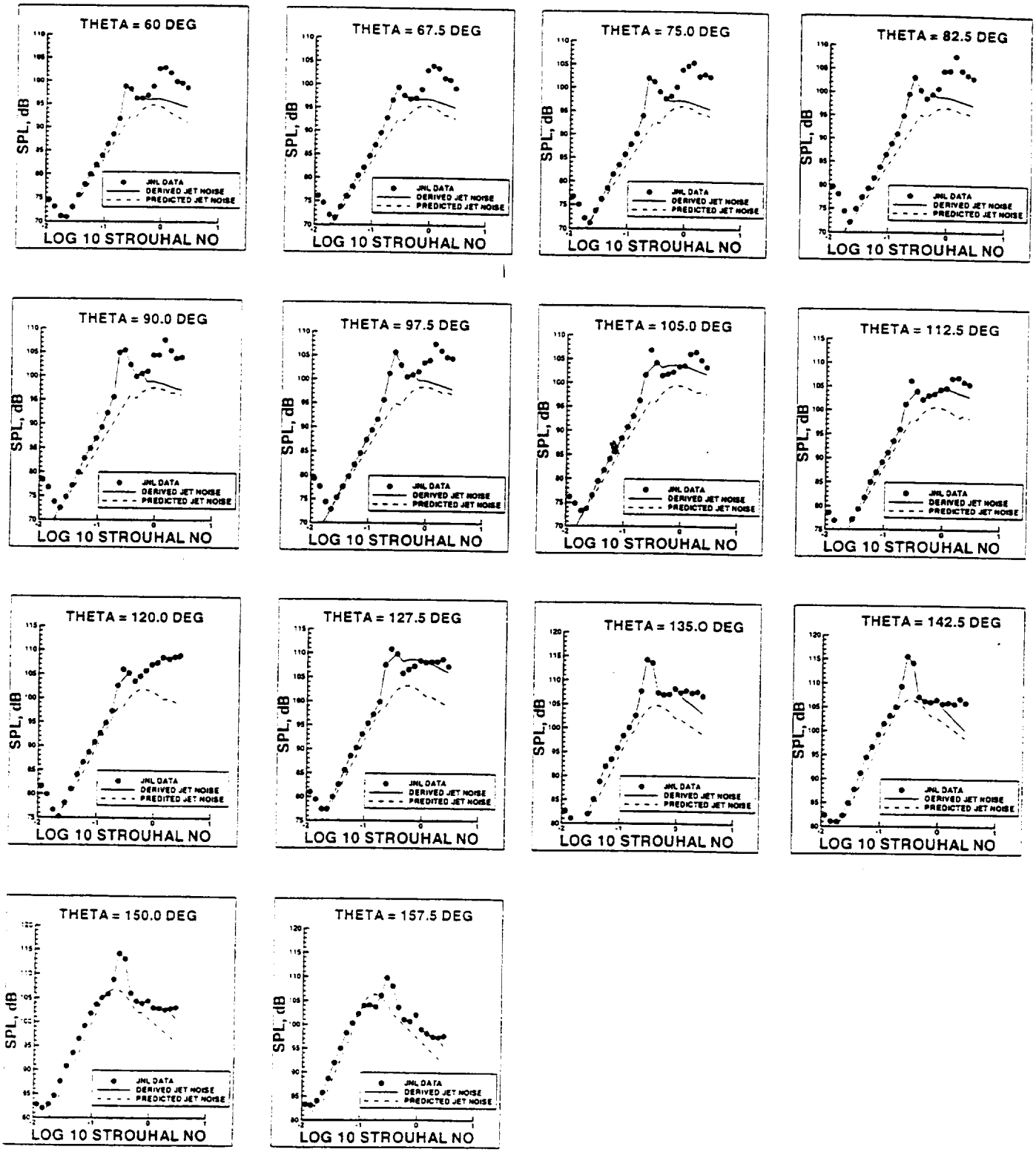

Figure 11 Continued - Comparison of One-Third Octave Band Predicted Jet Mixing Noise with Derived Jet Mixing Noise for 0 degrees Azimuth Angle at 14 Polar Directivity Angles

b. Nozzle 5, Pexit/Pambient = 0.85

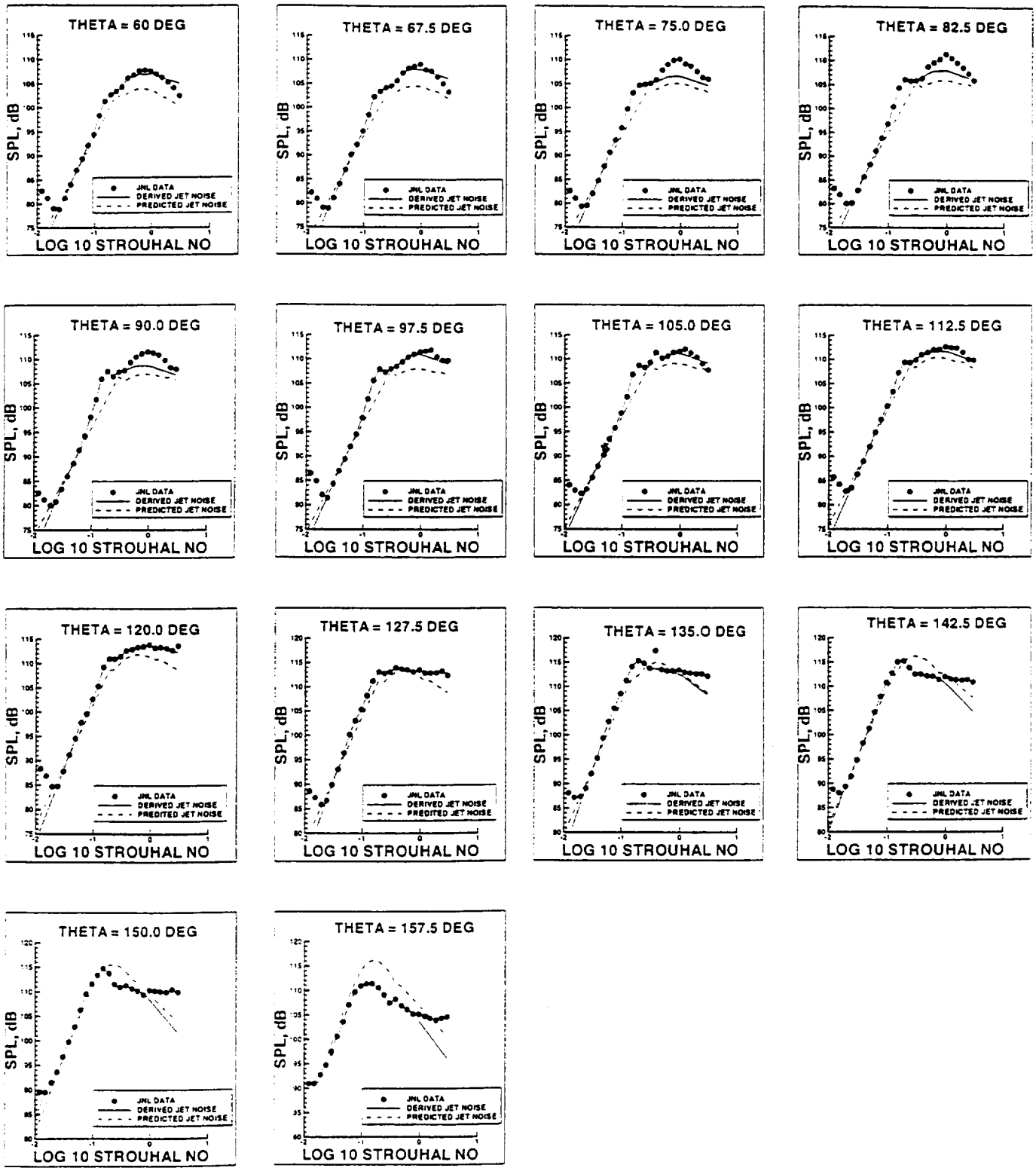

Figure 11 Continued - Comparison of One-Third Octave Band Predicted Jet Mixing Noise with Derived Jet Mixing Noise for 0 degrees Azimuth Angle at 14 Polar Directivity Angles

c. Nozzle 4, Pexit/Pambient = 1.25

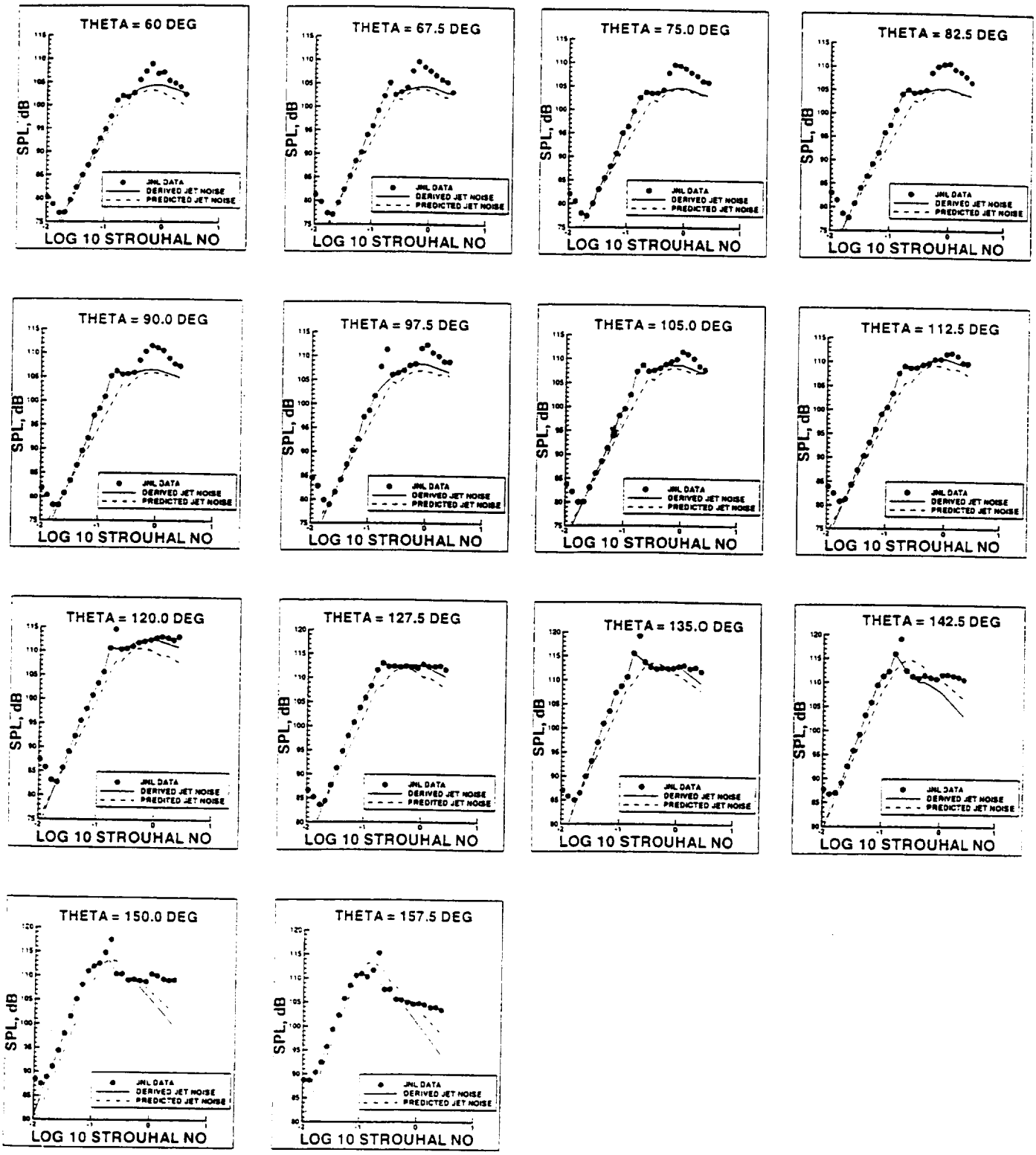

Figure 11 Continued - Comparison of One-Third Octave Band Predicted Jet Mixing Noise with Derived Jet Mixing Noise for 0 degrees Azimuth Angle at 14 Polar Directivity Angles

d. Nozzle 5, Pexit/Pambient = 1.25

REPORT DOCUMENTATION PAGE

Form Approved
OMB No. 0704-0188

1. AGENCY USE ONLY (Leave blank)	2. REPORT DATE	3. REPORT TYPE AND DATES COVERED
	November 1999	Contractor Report

4. TITLE AND SUBTITLE
Development of an Empirical Method for Predicting Jet Mixing Noise of Cold Flow Rectangular Jets

5. FUNDING NUMBERS
NAS1-96014

537-09-42-01

6. AUTHOR(S)
James W. Russell

7. PERFORMING ORGANIZATION NAME(S) AND ADDRESS(ES)
Lockheed Martin Engineering and Sciences
c/o NASA Langley Research Center
Mail Stop 371
Hampton, VA 23681-2199

8. PERFORMING ORGANIZATION REPORT NUMBER

9. SPONSORING/MONITORING AGENCY NAME(S) AND ADDRESS(ES)
National Aeronautics and Space Administration
Langley Research Center
Hampton, VA 23681-2199

10. SPONSORING/MONITORING AGENCY REPORT NUMBER
NASA/CR-1999-209719

11. SUPPLEMENTARY NOTES
Langley Technical Monitor : Robert A. Golub

12a. DISTRIBUTION/AVAILABILITY STATEMENT
Unclassified-Unlimited
Subject Category 71 Distribution: Standard
Availability: NASA CASI (301) 621-0390

12b. DISTRIBUTION CODE

13. ABSTRACT (Maximum 200 words)
This report presents an empirical method for predicting the jet mixing noise levels of cold flow rectangular jets. The report presents a detailed analysis of the methodology used in development of the prediction method. The empirical correlations used are based on narrow band acoustic data for cold flow rectangular model nozzle tests conducted in the NASA Langley Jet Noise Laboratory. There were 20 separate nozzle test operating conditions. For each operating condition 60 Hz bandwidth microphone measurements were made over a frequency range from 0 to 60,000 Hz. Measurements were performed at 16 polar directivity angles ranging from 45 degrees to 157.5 degrees. At each polar directivity angle, measurements were made at 9 azimuth directivity angles. The report shows the methods employed to remove screech tones and shock noise from the data in order to obtain the jet mixing noise component. The jet mixing noise was defined in terms of one third octave band spectral content, polar and azimuth directivity, and overall power level. Empirical correlations were performed over the range of test conditions to define each of these jet mixing noise parameters as a function of aspect ratio, jet velocity, and polar and azimuth directivity angles. The report presents the method for predicting the overall power level, the average polar directivity, the azimuth directivity, and the location and shape of the spectra for jet mixing noise of cold flow rectangular jets.

14. SUBJECT TERMS
jet mixing noiseprediction;
jet mixing noise, rectangular jet

15. NUMBER OF PAGES
97

16. PRICE CODE
A05

17. SECURITY CLASSIFICATION OF REPORT	18. SECURITY CLASSIFICATION OF THIS PAGE	19. SECURITY CLASSIFICATION OF ABSTRACT	20. LIMITATION OF ABSTRACT
Unclassified	Unclassified	Unclassified	UL